

# Technical Report

## TR-10-34

### **Modelling and analysis of canister and buffer for earthquake induced rock shear and glacial load**

Jan Hernelind, 5T Engineering AB

August 2010

**Svensk Kärnbränslehantering AB**

Swedish Nuclear Fuel  
and Waste Management Co

Box 250, SE-101 24 Stockholm  
Phone +46 8 459 84 00



# **Modelling and analysis of canister and buffer for earthquake induced rock shear and glacial load**

Jan Hernelind, 5T Engineering AB

August 2010

*Keywords:* SKBdoc 1229886, Earthquake, Shear, Glacial, Bentonite, Buffer, Copper canister, Cast iron insert, Finite elements.

This report concerns a study which was conducted for SKB. The conclusions and viewpoints presented in the report are those of the author. SKB may draw modified conclusions, based on additional literature sources and/or expert opinions.

A pdf version of this document can be downloaded from [www.skb.se](http://www.skb.se).

# Overview

This report is one in a series of reports that together address the response of the buffer and the canister in a KBS-3 repository to shear movements in fractures intersecting deposition holes.

Rock shear movements to analyse are given as design requirements derived from previous safety assessments. Mechanical properties of the buffer are determined in laboratory tests that are interpreted into a buffer material model with parameter values for the calculations. Mechanical data for the canister insert and copper shell are obtained from laboratory tests yielding canister material models.

The mechanical impact on the buffer and on the canister insert and copper shell by shear movements are determined by finite element modelling. The calculated canister stresses and strains are propagated i) to an assessment of plastic and creep deformation against failure criteria for the copper shell, ii) to an analysis of the damage tolerance of the insert and iii) to an assessment of the margin to global collapse of the insert.

The overall evaluation of whether the calculated impacts result in failures of the canister is made in a design analysis report where impacts are compared to established failure criteria. The design analysis report also summarises the results of the entire series of rock shear analyses as well as several other mechanical load situations of relevance. Furthermore, the design analysis report shows the flow of input data and modelling in the entire shear analysis.

## Abstract

Existing fractures crossing a deposition hole may be activated and sheared by an earthquake. The effect of such a rock shear has been investigated by finite element calculations.

The buffer material in a deposition hole acts as a cushion between the canister and the rock, which reduces the effect of a rock shear substantially. Lower density of the buffer yields softer material and reduced effect on the canister. However, at the high density that is suggested for a repository the stiffness of the buffer is rather high. The stiffness is also a function of the rate of shear, which means that there may be a substantial damage on the canister at very high shear rates. However, the earthquake induced rock shear velocity is lower than 1 m/s which is not considered to be very high.

The rock shear has been modelled with finite element calculations with the code Abaqus. A three-dimensional finite element mesh of the buffer and the canister has been created and simulation of a rock shear has been performed.

The rock shear has been assumed to take place either perpendicular to the canister at the quarter point or at an inclined angle of  $22.5^\circ$  in tension. Furthermore horizontal shear has been studied using a vertical shear plane either at the centre or at  $\frac{1}{4}$ -point for the canister.

The shear calculations have been driven to a total shear of 10 cm.

The canister also has to be designed to withstand the loads caused by a thick ice sheet.

Besides rock shear the model has been used to analyse the effect of such glacial load (either combined with rock shear or without rock shear).

This report also summarizes the effect when considering creep in the copper shell.

## Sammanfattning

Befintliga sprickor som skär deponeringshål kan aktiveras och skjuvas genom ett jordskalv. Inverkan av en sådan bergskjuvning har analyserats med finita element beräkningar.

Bentonitbufferten i ett deponeringshål fungerar som en kudde mellan kapseln och berget, vilken avsevärt reducerar inverkan av en bergskjuvning – ju lägre densitet desto mjukare buffert och desto mindre påverkan på kapseln. Vid de höga densiteter som föreslås för bufferten i ett slutförvar är den däremot ganska styv. Styvheten är också en funktion av skjuvhastigheten, vilket medför att kapseln kan skadas avsevärt vid mycket höga skjuvhastigheter. Dock är skjuvhastigheten pga jordbävning typiskt mindre än 1 m/s vilket ej kan betraktas som mycket hög.

Bergskjuvningen har modellerats och beräknats med finita-element-koden Abaqus. Ett tredimensionellt elementnät som modellerar bufferten och kapseln har skapats och simulering av bergskjuvningar har utförts.

Bergskjuvningen antas ske antingen vinkelrätt mot kapselaxeln eller med 22.5° vinkel mot kapselaxel i drag. Dessutom har horisontell skjuvning studerats med vertikalt skjuvplan antingen i mittplanet eller i ¼-delspunkten för kapseln.

Skjuvberäkningarna har genomförts upp till en total skjuvdeformation av 10 cm.

Kapseln måste också dimensioneras för att bli klara last under en tjock inlandsis.

Förutom bergskjuvning har modellen använts för att analysera effekten av en sådan islast (antingen kombinerad med bergskjuvning eller utan bergskjuvning).

I den här rapporten summeras också effekten när hänsyn tas till krypning i kapseln.

# Contents

<b>1</b>	<b>Introduction</b>	9
1.1	Earthquake induced rock shear	9
1.1.1	Context for this report	9
1.1.2	Earlier investigations	9
1.2	Glacial load	13
<b>2</b>	<b>Geometry definitions and meshes</b>	15
2.1	General	15
2.2	Geometry of parts	16
2.2.1	Deposition hole	16
2.2.2	Insert (BWR)	17
2.2.3	Insert (PWR)	17
2.2.4	Insert lid (BWR and PWR)	17
2.2.5	Copper shell (BWR and PWR)	17
<b>3</b>	<b>Material models</b>	19
3.1	Iron (used by the insert)	19
3.2	Steel (used by the channel tubes in the insert)	19
3.3	Steel (used by the insert lid)	21
3.4	Bentonite model (used for the buffer)	21
3.5	Copper model	23
<b>4</b>	<b>Contact definitions</b>	25
<b>5</b>	<b>Initial conditions</b>	27
<b>6</b>	<b>Boundary conditions</b>	29
<b>7</b>	<b>Calculations</b>	31
7.1	General	31
7.1.1	Rock shear calculation cases	31
7.1.2	Analysis approach	31
7.2	Short term analyses	32
7.3	Hydrostatic pressure	32
7.4	Long term analyses with creep in copper included	32
7.5	Rock shear combined with glacial loads	32
7.6	Glacial loads	33
<b>8</b>	<b>Sensitivity analyses</b>	35
8.1	Rate of rock shear	35
8.2	Choice of coefficient of friction	35
8.3	Uncertainties of the parameters in the creep material model	35
8.4	Buffer thickness	35
8.5	Steel cylinder around the insert	35
<b>9</b>	<b>Results</b>	37
9.1	Results for rock shear	37
9.2	Hot spot regions	44
9.3	Results glacial load	50
<b>10</b>	<b>Uncertainties</b>	59
<b>11</b>	<b>Evaluation and conclusions</b>	61
11.1	Rock shear analysis	61
11.2	Rock shear combined with glacial loads	62
11.3	Glacial load	62
<b>12</b>	<b>References</b>	63

<b>Appendix 1</b>	Short term rock shear perpendicular to canister axis at quarter point 2050ca3	65
<b>Appendix 2</b>	Short term rock shear perpendicular to canister axis at mid point 2050ca3	73
<b>Appendix 3</b>	Short term rock shear inclined 22.5 degrees to canister axis at quarter point 2050ca3 (tension)	79
<b>Appendix 4</b>	Short term rock shear inclined 22.5 degrees to canister axis at mid point 2050ca3 (tension)	85
<b>Appendix 5</b>	Short term rock shear in horizontal direction at a vertical plane (mid section) 2050ca3	91
<b>Appendix 6</b>	Short term rock shear in horizontal direction at a vertical plane (quarter section) 2050ca3	97
<b>Appendix 7</b>	Short term rock shear normal direction at quarter point 2050ca3 for PWR	103
<b>Appendix 8</b>	Short term rock shear normal direction at quarter point 2050ca3 at glacial pressure 30 MPa	109
<b>Appendix 9</b>	Long term rock shear perpendicular to canister axis 2050ca3 (quarter point)	115
<b>Appendix 10</b>	Storage of files	119

# 1 Introduction

The canister has to be designed for earthquake induced rock shear and also for a glacial load.

## 1.1 Earthquake induced rock shear

Earthquake induced rock shear has previously been analyzed, however, more accurate material information and geometry is now available which makes it possible to perform more accurate analyses.

### 1.1.1 Context for this report

One important function of the buffer material in a deposition hole in a repository for nuclear waste disposal is to reduce the damage of rock movements on the canister. The worst case of rock movements is a very fast shear that takes place along a fracture and occurs as a result of an earthquake.

The consequences of such rock shear have been investigated earlier, both by laboratory tests /Börgesson et al. 2004/, laboratory simulations in the scale 1:10 and finite element modelling /Börgesson et al. 2004, Börgesson and Hernelind 2006, Börgesson et al. 1995/.

Those investigations were focussed on a base case with a horizontal shear plane and Na-bentonite as buffer material. Also the influence of the shear angle was studied with 45 and 22.5 degrees inclination between the shear plane and the canister.

Since it is very probable that the Na-bentonite will be transformed to Ca-bentonite or that Ca-bentonite might be used as buffer the calculations now are based on material properties of Ca-bentonite instead of Na-bentonite.

A sequence of analyses has previously been performed for earthquake induced rock shear. The outcome of these analyses is described by /Börgesson and Hernelind 2006/.

The BWR canister has been analyzed with different minor design changes.

In the previous study the material models used for the buffer (bentonite), copper shell, insert (iron) and steel lid (steel) were simplified or not fully tested to have accurate data.

Since the model also has been analyzed with different material definitions a side effect is that the sensitivity on the results has been better understood.

This report summarizes the results for the reference case when the buffer consists of converted Ca-bentonite with density 2,050 kg/m<sup>3</sup> and for comparison also converted Ca-bentonite with density 2,000 kg/m<sup>3</sup> and 1,950 kg/m<sup>3</sup> also have been analyzed.

Both short term response (elastic-plastic material model for copper) and long term response (creep model for copper) has been analyzed.

Also the PWR canister been analyzed but only for the horizontal shear plane.

### 1.1.2 Earlier investigations

The main investigations concerning rock shear through a deposition hole have been the following (in addition to ongoing investigations that will be reported 2010).

#### ***Model shear tests of a canister in a deposition hole***

In this investigation, /Börgesson 1986/ a laboratory model in the scale 1:10 of a deposition hole with bentonite buffer and a canister was sheared with different shear rates. The canister was made of solid copper and it was surrounded by highly compacted water saturated MX-80 bentonite. Before shearing



the swelling pressure was measured by six transducers in order to follow the water uptake process. During shearing pressure, strain, force and deformation were measured in altogether 18 points. The shearing was made at different rates in the various tests.

An extensive sampling after shear was made and the density, water content, degree of saturation, homogenisation and the effect of shear on the bentonite and canister were measured and studied. The results from the shear tests were compared to different calculations. The relevance of the calculations and the need for improved mathematical models could then be studied.

One important conclusion from these tests was that the rate dependence is about 10% increased shear resistance per decade of increased rate of shear. This resulted also in a very clear increase in strain in the canister with increased rate. The results also showed that the saturated bentonite has excellent stress distributing properties. However, the high density of the clay ( $\rho_m = 2,050 \text{ kg/m}^3$ ) made the bentonite produce such a high swelling pressure that the material was rather stiff resulting in a strong deformation of the canister. Since the canister was made of solid copper, it was deformed more than would be expected from a canister with a cast iron insert.

### **Calculations for investigating the influence of shear rate, buffer density, shear displacement and the location of the horizontal shear plane**

The investigation, /Börgesson et al. 2004/ yielded the following main results and conclusions:

The calculations were done with an assumed shear rate of 1.0 m/s at the buffer densities 1,950, 2,000, 2,050 and 2,100  $\text{kg/m}^3$ . At the *reference case* (density 2,000  $\text{kg/m}^3$  and eccentric shear) the plastic strain in the cast iron insert starts after 2 cm shear and increases to 4.4% plastic strain after 20 cm shear displacement. The corresponding maximum plastic strain in the copper is about 8% on the canister shell surface while it is locally much higher at the lid.

The *influence of buffer density* is very strong and an increase in density from the reference case (eccentric shear) 2,000  $\text{kg/m}^3$  to 2,100  $\text{kg/m}^3$  yields an increase in plastic strain after 20 cm displacement from 4.4% to 10%, while a reduction in density to 1,950 yields a reduction in plastic strain to 2.7%.

There is also a surprisingly strong *influence of the shear plane location*. For centric shear at the buffer densities 1,950 and 2,000  $\text{kg/m}^3$  there is practically no plasticization of the cast iron insert, while at the higher densities 2,050 and 2,100  $\text{kg/m}^3$  the plastic strain is 11% and 19% respectively. The influence of buffer density is thus much stronger at centric shear than at eccentric shear. The reason is judged to be that at low density a long part of the canister is needed for keeping it in a firm grip strong enough to prevent tilting, which means that one side of the canister is prevented from tilting at the eccentric shear while the whole canister tilts at centric shear. The reverse is the case at high density where the length of the canister is enough to keep both ends in a firm grip at centric shear and prevent both end from tilting, while the shorter part of the canister still can tilt at the eccentric shear.

The *influence of the magnitude of the shear displacement* logically seems to be rather strong when the canister is prevented from tilting with a plastic strain that usually is more than doubled at an increase in shear displacement from 10 cm to 20 cm. However, when the buffer yields at a shear strength that is not high enough to prevent tilting the magnitude of the shear displacement has no effect, since the canister just continues to tilt as in a liquid with high viscosity.

The *copper shell* has large plastic deformations according to these calculations especially at the high densities. In contrast to the cast iron insert the copper is not affected by the shear plane location. However, the copper is strongly influenced by the tension stresses on the passive sides.

When a more realistic model with contact elements was used the plasticization of the copper was reduced to the same magnitude as in the cast iron insert for the reference case.

The plastic strain in the cast iron was, in contrary to the copper, not affected by *introducing contact elements* around the copper shell due to the slot between the copper and the cast iron, which has the same effect for the cast iron as the contact elements for the copper.

### **Calculations for investigating the influence of shear plane inclination and location as well buffer properties**

The investigation, /Börgesson and Hernelind 2006/, yielded the following main results and conclusions:

The influence of mainly the following factors has been investigated:

- The inclination of the intersection between the shearing fracture and the deposition hole axis.
- Shear direction when the inclination deviates from 90°.
- The location of the shear plane when the inclination is 90°.
- The magnitude of the shear displacement.
- Bentonite type.
- Bentonite density.
- Transformation of the buffer to illite or cemented bentonite.

The results from the calculations show that all these factors have important influence on the damage of the canister but the influence is for most factors not easily described since there are mutual interferences between the different factors. The following general trends regarding the first six factors can be perceived:

- Plastic strain larger than 1% was reached in the copper already at 10 cm shear in all cases with Na- and Ca-bentonite. However, for several cases of Na-bentonite and one case of Ca-bentonite such plastic strain was only reached in the lid.
- The plastic strain in the iron was generally lower than in the copper mainly due to the higher yield stress in the iron. For all cases of Na-bentonite except one and for about half of the Ca-bentonite the plastic strain was lower than 1% after 10 cm shear.
- The shear inclination 45° was more harmful for the copper shell than the shear direction 90° when tension shear is considered. Tension shear at 45° seems to cause a tensile force on the canister shell that exceeds the effect of the bending force. The difference in maximum plastic strain in the copper shell between 45° tension shear and 90° shear with otherwise identical conditions was rather large for all cases except for Ca-bentonite with the density 2,050 kg/m<sup>3</sup>.
- At the shear inclinations 45° and 22.5° tension shear was always more harmful for the copper shell than compression shear. The highest value 19% was reached after 20 cm shear in Ca-bentonite with the density 2,050 kg/m<sup>3</sup>.
- Larger plastic strain in the copper shell was at the shear angle 90° reached at eccentric shear than at centric shear for all cases except the high density Ca-bentonite case. The reason is that at low buffer stiffness the canister tilts if there is not enough canister length (more than half the canister) to keep the canister in a firm grip, but at high buffer stiffness the length of half the canister is enough to prevent tilting.
- The plastic strain increased logically with increasing shear displacement although the influence of the shear displacement is reduced the softer the buffer material is. A doubled shear displacement from 10 cm to 20 cm did not imply a doubling of the plastic strain in the copper shell for any of the cases with Na-bentonite with one or two exceptions. The increase in plastic strain was generally 20–50%. For the cases with Ca-bentonite the influence of the shear displacement was much stronger and a doubled displacement from 10 cm to 20 cm yielded for almost all cases an increase larger than 50% and for more than half of the cases a doubling or more. The main reason for this difference is probably that Na-bentonite has lower stiffness and strength than Ca-bentonite, which means that the Na-bentonite will plasticise earlier and a larger part of the buffer will reach its peak shear resistance earlier. If the entire buffer is ideally plastic the magnitude of the shear displacement has very little influence on the canister damage since the canister “floats around” in the buffer.
- The maximum plastic strain in the copper shell and in the iron insert was for all cases larger for the Ca-bentonite than for the Na-bentonite. In the copper shell it was generally 2–5 times larger but even larger differences occurred. The reason is of course that the Ca-bentonite is stiffer and has higher swelling pressure and strength than the Na-bentonite.
- For the same reason the plastic strain is of course larger the higher the density of the buffer is.

Geochemical transformation of the buffer can lead to a material with quite different properties than the original buffer. The effect of a rock shear through such a buffer may of course have rather different consequences than through the original buffer.

- The analysis of the effect of conversion to illite yielded that the effect on the canister of a rock shear is insignificant compared to when no transformation has taken place since the strength of the illitic clay is only a tenth of the strength of MX-80. The reason for the low strength is of course the low swelling pressure of the illite. All cases of partly illitization can be concluded to lead to consequences of a rock shear that are less severe than if no transformation takes place due to the loss in swelling pressure.
- Cementation of bentonite with the thickness 8.75 cm around the canister yields that the effect of a rock shear is more severe than if the original bentonite is kept due to the increased stiffness of the buffer. However, the properties of cemented bentonite are not known so the calculation must be regarded as an example rather than as a prediction.

The calculations are associated with several uncertainties that should be considered when the consequences of a rock shear are analyzed.

- Besides the fact that the properties of the cemented buffer are not known there are some uncertainties regarding the material models of the unaffected buffer. The prime one is the model of Ca-bentonite. The properties of Ca-bentonite have not been investigated to such extent as the properties of Na-bentonite. The model is based on the knowledge of Na-bentonite and a limited amount of tests on Ca-bentonite.
- The properties of the copper and iron are taken from earlier tests and information. Since the yield properties are of major importance for magnitude of the plastic strain the results of the calculations should be re-evaluated if new data emerge.
- The contact elements surrounding the buffer are assumed to have no cohesion at tensile stress.
- The element mesh could be too coarse to reveal local stress concentrations, especially in the lids. The geometry of the lids does not agree with the present design. If these matters are important some checks should be made by using a more refined mesh and updated lid geometry.
- The buffer is assumed to be completely homogeneous with a density corresponding to the expected average density of the buffer. In reality the buffer has a slightly lower density close to the canister and close to the rock and thus a slightly higher density in the rest of the buffer due to the slots that exist from start. However, the influence of this difference is judged to be small.

### **Calculations for investigating the effect of creep in the copper shell**

The investigation, /Hernelind 2006/, yielded the following main results and conclusions:

- The calculations were made with an assumed shear rate of 1.0 m/s at the buffer density 2,000 kg/m<sup>3</sup>. The creep effect has been analyzed by using a creep theory suggested by Kjell Pettersson.
- The *influence of the magnitude of the shear displacement* logically seems to be rather strong when the canister is prevented from tilting with a plastic strain that usually is more than doubled at an increase in shear displacement from 10 cm to 20 cm. However, the effect on the global deformation when creep is taken into consideration is rather minor.
- The *copper shell* is strongly plasticized according to these calculations, especially at the high densities and including creep implies that the peak stress is reduced but the total strain increases due to creep. For this case the maximum creep strain occurs close to the top cover where the maximum creep strain is 11.5%. Close to the centre of the copper shell maximum creep strain is about 0.9% and the equivalent plastic strain (PEEQ) is 2.4% when shearing for 20 cm. For the mid part it seems as the total strain is not affected by creep (plastic plus creep strain is almost constant).
- The plastic strain in the cast iron was, in contrary to the copper, not affected significantly by *introducing creep in the copper shell*.
- According to these calculations the creep seems to have minor influence on the results except for the neighbourhood of the lid in the copper shell where the creep strains are rather high.
- However, the correct creep material data was not available when these calculations were made and thus also the creep effect has been re-analyzed using the latest available experimental results.

## 1.2 Glacial load

The canister has to survive at least one glacial period within the design time of 100,000 years. The copper shell thus has to be designed for a maximum total load consisting of the glacial load combined with the swelling pressure within the buffer. The magnitude of the swelling pressure depends on the bentonite being used which for the reference case is based on Na-bentonite converted to Ca-bentonite with density 2,050 kg/m<sup>3</sup>.

The relevant loading processes are then taken from the updated design premises report /SKB 2009/.

The load is assumed to be applied for a long time which implies that creep of the copper has to be considered.

A previous study /Dillström et al. 2009/ has been performed both as 2D- and 3D-analyses but without considering creep in the copper and no results were reported for the copper shell.

Also the material model for the insert is now built on more accurate data.

Furthermore, there have been design changes, especially at the bottom and at the top of the canister, and the changes are taken into account in the re-analyses.

This report summarizes results for the BWR-canister when the effect of the glacial load is simulated considering creep in the copper shell.

## 2 Geometry definitions and meshes

### 2.1 General

The geometry used for the earthquake induced rock shear consists of the insert (made of iron), the insert lid (made of steel) and the copper shell surrounded by buffer material (bentonite). The geometry is based on CAD-geometries received from SKB /SKBdoc 1203875/ and should therefore correspond to the current design.

Due to symmetry only one half has been modelled, except for the case of horizontal shear at a vertical plane (either at the mid section or at the quarter point). The mesh is then generated by 3-dimensional solid elements, mainly 8-noded hexahedral (most of them using full integration technique) and a few 6-noded wedge.

The model size is defined by about 123,000 elements and 160,000 nodes (total number of variables about 550,000).

For the full model (used for horizontal shear at a vertical plane) about 350,000 elements and 490,000 nodes (total number of variables about 1,170,000).

For the glacial load analyses the model does not include the buffer and thus the model will contain fewer elements and nodes (about 110,000 elements, 150,000 nodes and 390,000 variables).

A sequence of static analyses has been performed studying the effect of changes in the design both for the copper shell, insert and insert lid.

Material properties have also been defined more accurately based on recent available data from experiments.

Compared to previous analyses also the used mesh has been improved.

For the buffer two different meshes were used; one is used for rock shear perpendicular to the axis of the canister and another mesh (essentially the bentonite) for rock shear inclined at 22.5 degrees, Figures 2-1–2-3.

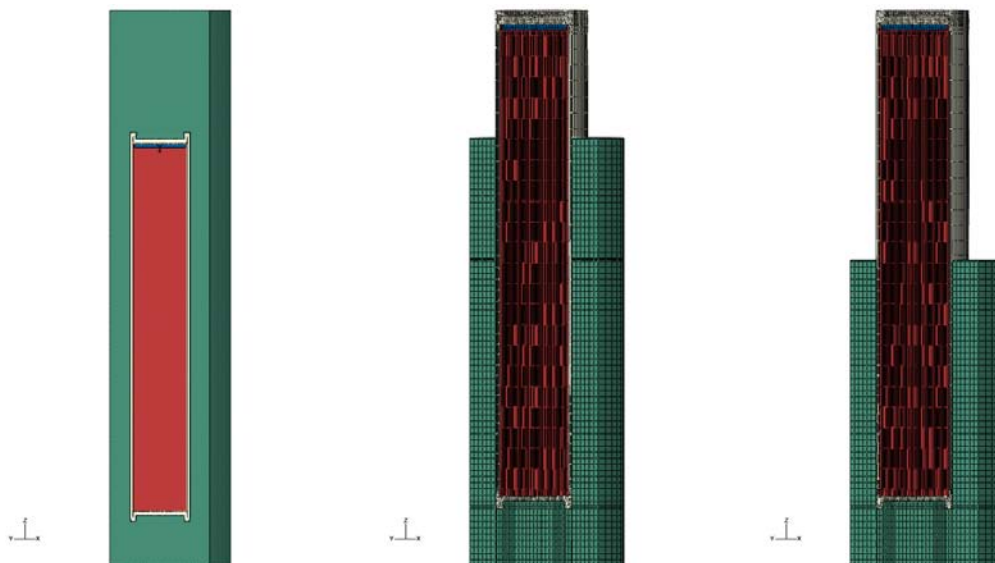


**Figure 2-1.** Plot of geometry for rock shear perpendicular to axis of canister (left),  $\frac{1}{4}$  shearing part removed (mid) and  $\frac{1}{2}$  shearing part removed (right).

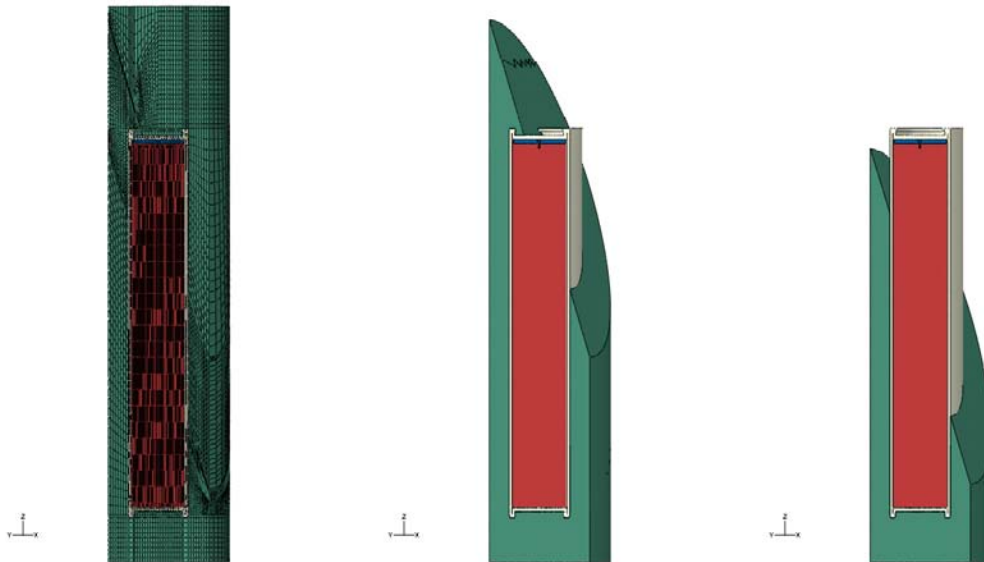


**Figure 2-2.** Plot of geometry for rock shear inclined 22.5 degrees to axis of canister (left),  $\frac{1}{4}$  shearing part removed (mid) and  $\frac{1}{2}$  shearing part removed (right).

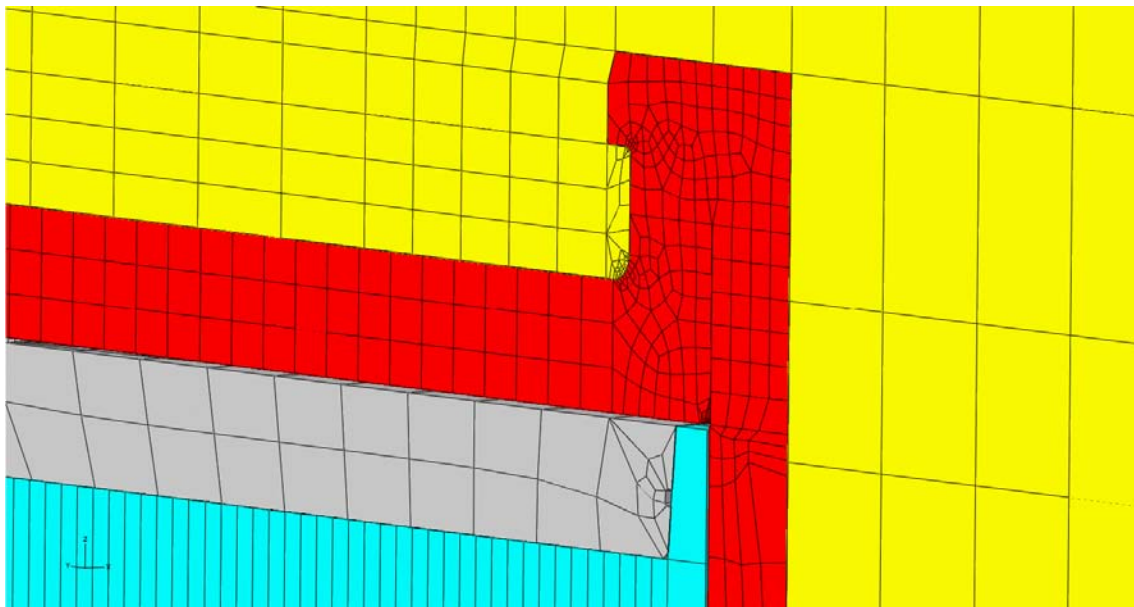


**Figure 2-3.** Detail of upper corner showing bentonite (yellow), copper shell (red), insert lid (grey) and insert (cyan).

## 2.2 Geometry of parts

### 2.2.1 Deposition hole

The model of the deposition hole has a diameter of 1.75 m and a length of 6.9 m. The canister is placed about 0.5 m above the bottom and about 1.5 m below the top of the deposition hole. Buffer material (bentonite) surrounds the canister and will fill out the deposition hole. The rock shear is then simulated by prescribing boundary conditions at the buffer envelope.

### 2.2.2 Insert (BWR)

The insert is made of iron and has been simplified regarding the square tubes which are assumed to be tied to the cast iron insert and thus these contribute as added material to the insert. This simplification will probably overestimate stresses and strains in this region.

The insert is modeled as a homogeneous part with 3D solids, see Figure 2-4.

### 2.2.3 Insert (PWR)

The insert is made of iron and has been simplified regarding the square tubes which are assumed to be tied to the cast iron insert and thus these contribute as added material to the insert. This simplification will probably overestimate stresses and strains in this region.

The insert is modeled as a homogeneous part with 3D solids, see Figure 2-5.

### 2.2.4 Insert lid (BWR and PWR)

The insert lid is made of steel and is modelled with 3D solids, see Figure 2-6.

### 2.2.5 Copper shell (BWR and PWR)

The copper shell surrounds the insert and interacts with the buffer and the insert. The canister has been modelled rather accurately in order to catch “hot spots” where large strains are expected, e.g. the fillets at the bottom and top (the lid). The lid is welded to the flange and lid and canister will act as one part, see Figure 2-7.

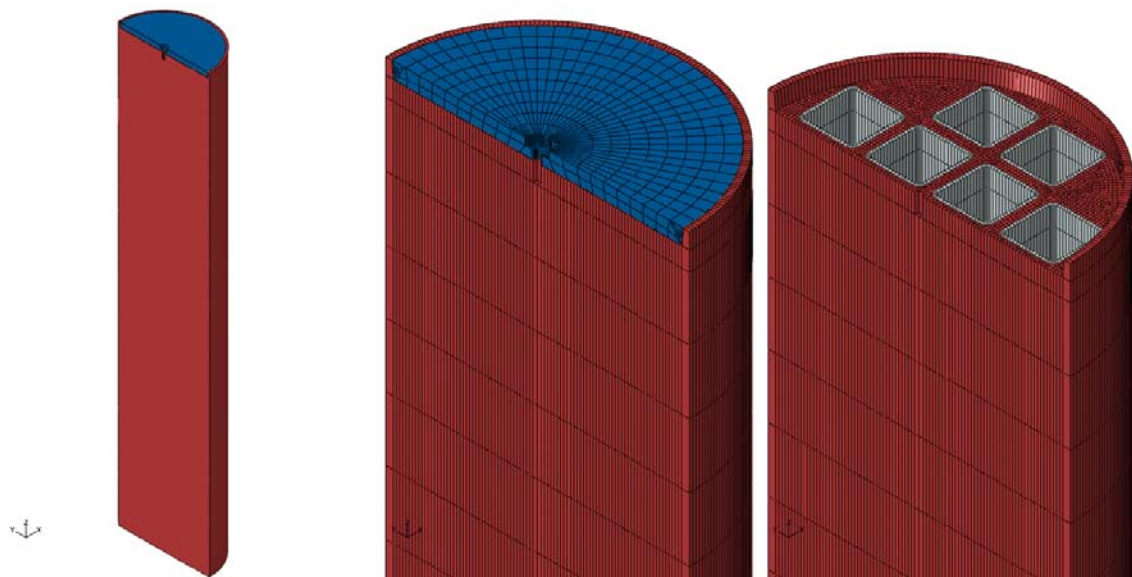


**Figure 2-4.** Insert BWR geometry (left), mesh with lid (mid) and without lid (right).

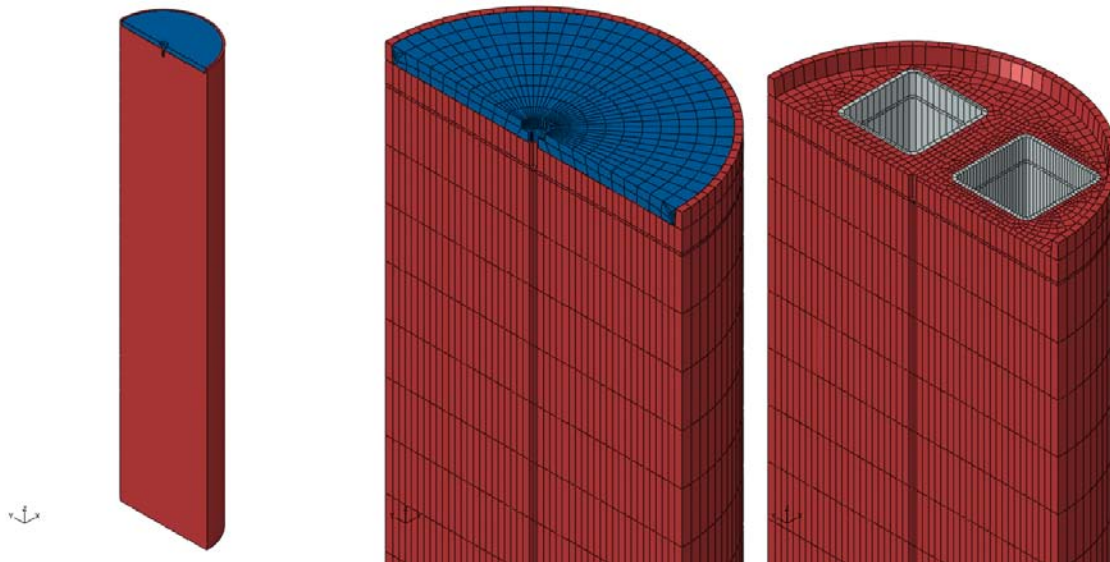


**Figure 2-5.** Insert PWR geometry (left), mesh with lid (mid) and without lid (right).

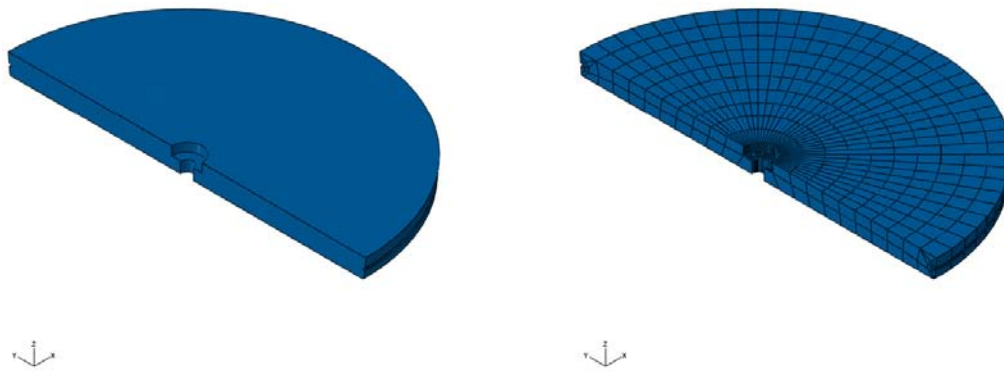


**Figure 2-6.** Insert lid geometry (left) and mesh (right).

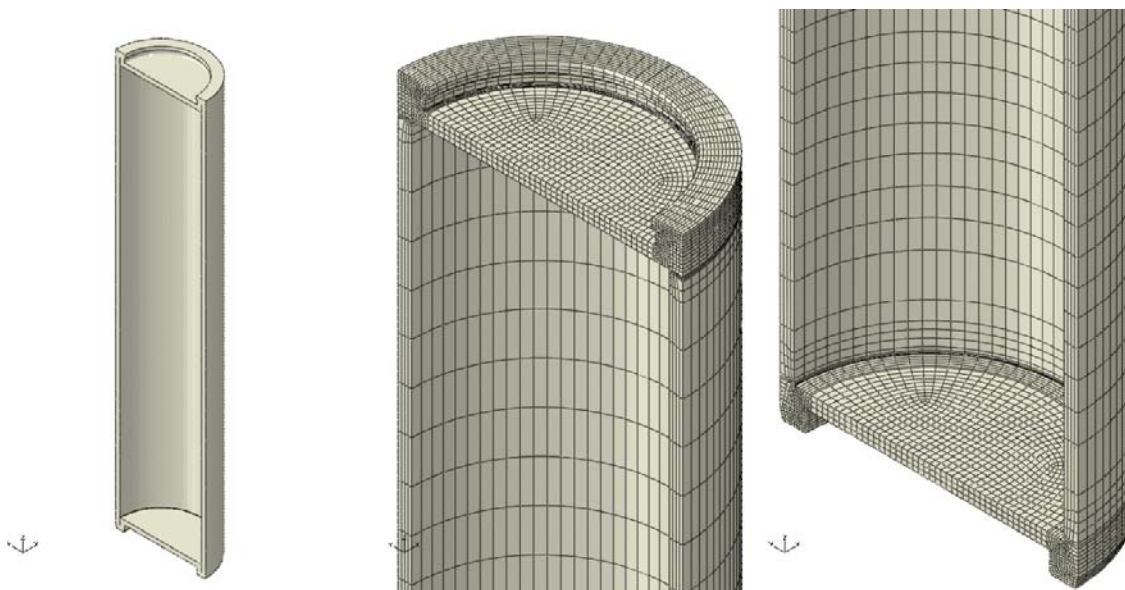


**Figure 2-7.** Copper shell geometry (left), mesh top (mid) and mesh bottom (right).



### 3 Material models

The finite element code Abaqus was used for the calculations. The materials have been modelled as elastic-plastic with stress-strain properties that correspond to each material and the applied shear load induced strain rate, when applicable.

#### 3.1 Iron (used by the insert)

The material model for the insert is based on a von Mises' material model with elastic behaviour defined by Young's modulus and the Poisson's ratio and the plastic behaviour defined through yield surface (true stress) versus plastic strain (defined as logarithmic strain), see Table 3-1 and Figure 3-1 /SKBdoc 1201865/.

The experiments were performed at 0°C.

The strain rate dependency is defined by assuming that the yield surface is proportional to the strain rate factor (at the strain rate 0.5 1/s the factor 1.08 has been chosen and at strain rate 0 1/s the factor is 1.0). The instantaneous strain rate factor is then linearly interpolated between 1 and 1.08 using the instantaneous strain rate.

Furthermore, Young's modulus  $E = 166$  GPa and Poisson's ratio  $\nu = 0.32$ .

#### 3.2 Steel (used by the channel tubes in the insert)

The material model for the channel tubes in the insert is based on a von Mises' material model with elastic behaviour defined by Young's modulus and the Poisson's ratio. The plastic behaviour is defined through yield surface (true stress) versus plastic strain (using logarithmic strain).

**Table 3-1. Stress-strain definition for insert.**

Plastic Strain (%)	Stress (MPa)			Strain rate factor at strain rate = 0.5
	Strain rate = 0	Strain rate = $2 \times 10^{-4}$	Strain rate = 0.5	
0	293	293	348	1.19
1	324	324	367	1.13
2	349	349	385	1.10
3	370	370	406	1.10
4	389	389	423	1.09
5	404	404	438	1.09
6	418	418	451	1.08
7	428	428	464	1.08
8	438	438	474	1.08
9	447	447	483	1.08
10	456	456	490	1.07
11	465	465	498	1.07
12	472	472	504	1.07
13	478	478	510	1.07
14	484	484	516	1.07
15	488	488	520	1.07
16	491	491	521	1.06

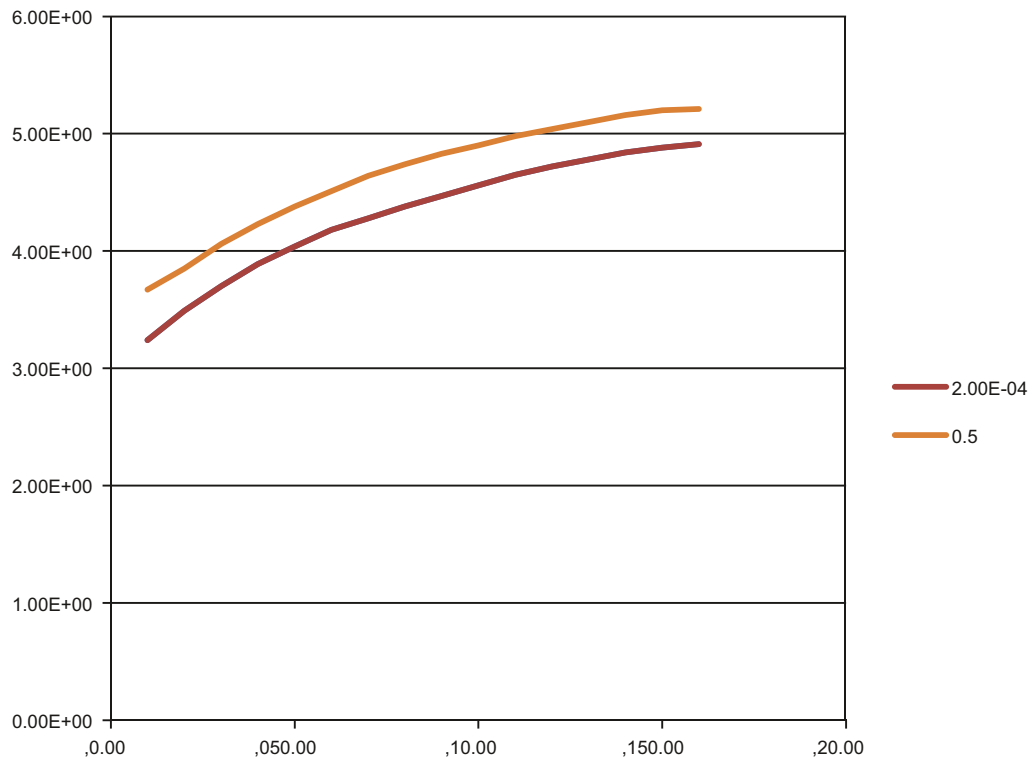


**Figure 3-1.** Yield surface [MPa] versus plastic strain [%] for different plastic strain rates. Note that the base (plastic) is defined to coincide with strain rate =  $2 \times 10^{-4}$ .

The steel cassette tubes are manufactured by steel S355J2H, for example Domex 355 MC B. SKB has earlier supplied test data for the yield point of their material, however no stress-strain data to be used in a plastic analysis. The stress-strain curve for Domex 355 MC B /SSAB 2008/ can be scaled using the yield stress and tensile ultimate strength measured by SKB,  $R_e = 412$  MPa and  $R_m = 511$  MPa. With this procedure a simplified stress-strain curve is obtained and described by Table 3-2.

Furthermore, Young's modulus  $E = 210$  GPa and Poisson's ratio  $\nu = 0.3$ .

The data with lowest value from the experiment has been chosen for the yield surface. However, the plasticity definition for the steel channel tubes has very minor influence on the overall results.

**Table 3-2. Stress-strain definition for channel tubes used in the insert.**

Strain (%)	Stress (MPa)	Log Strain (%)	True Stress (MPa)
0	0	0	0
0.196	411	0.196	412
15	509	14.3	587
20	510	18.5	613

### 3.3 Steel (used by the insert lid)

The material model for the insert lid is based on a von Mises' material model with elastic behaviour defined by Young's modulus and the Poisson's ratio. The plastic behaviour is defined through yield surface (true stress) versus plastic strain (calculated as logarithmic strain).

Manufacturing drawings for the lid specify steel S355J2G3. Strain versus stress for steel. Domex 355 MC B with  $Re = 389$  MPa and  $Rm = 484$  MPa can be found from /SSAB 2008/. According to /SS-EN 10025-2:2004/ the material S355 with nominal thickness 40–63 mm has  $Re = 335$  MPa and  $Rm = 470–630$  MPa. Scaling stress-strain curves for Domex 355 by the minimum values given in SS-EN 10025-2:2004 implies the simplified material definition (engineering data) given in Table 3-3.

Furthermore, Young's modulus  $E = 210$  GPa and Poisson's ratio  $\nu = 0.3$ .

The data with lowest value from the experiments /SS-EN 10025-2:2004/ has been chosen for the yield surface. However, the plasticity definition for the insert lid has very minor influence on the overall results.

### 3.4 Bentonite model (used for the buffer)

The bentonite is modelled based on recent experiments, see /Börgesson et al. 2010/ and adapted to the actual density of the bentonite. The bentonite buffer is modelled using only total stresses that do not include the pore water pressure, the reason being the very fast compression and shear.

The most important properties of the bentonite for the rock shear are the stiffness and the shear strength. These properties vary with bentonite type, density and rate of strain. Ca-bentonite has higher shear strength than Na-bentonite and the shear strength increases with increasing density and strain rate. Since it cannot be excluded that the Na-bentonite MX-80 will be ion-exchanged to Ca-bentonite the properties of Ca-bentonite is used in the modelling. The acceptable density at saturation of the buffer material is 1,950–2,050 kg/m<sup>3</sup> which is covered by the models below.

The material model is in Abaqus expressed with the von Mises' stress  $\sigma_j$  that describes the "shear stress" in three dimensions according to Equation 3-1.

$$\sigma_j = (((\sigma_1 - \sigma_3)^2 + (\sigma_1 - \sigma_2)^2 + (\sigma_2 - \sigma_3)^2)/2)^{1/2} \quad 3-1$$

where

$\sigma_1$ ,  $\sigma_2$  and  $\sigma_3$  are the principal stress components.

The material model defines the relation between the stress and the strain and is partitioned in elastic and plastic parts. For details regarding definition of the shear strength and the influence of density, pressure and rate of shear see (/Börgesson et al. 1995, Börgesson et al. 2004/).

#### **Rate dependent elastic-plastic stress-strain relation**

The elastic-plastic stress strain relations used for the three different densities are derived according to the description above in an identical way as the relations used in all previous calculations.

The bentonite is modelled as linear elastic combined with the von Mises plastic hardening – Table 3-4 shows the elastic constants. The plastic hardening curve is made a function of the strain rate of the material. The reason for the latter relation is that the shear strength of bentonite is rather sensitive to the strain rate. It increases with about 10% for every 10 times increase in strain rate. Since the rock shear at an earthquake is very fast (1 m/s) the influence is strong and the resulting shear strength will be different at different parts of the buffer. Figure 3-2 shows the material model. The stress-strain relation is plotted at different strain rates.

The experiments /Börgesson et al. 2010/ show that also Young's modulus ( $E$ ) is dependent on strain rate but in the calculations this has been neglected and a representative stiffness has been chosen (sensitivity analyses did show minor changes of the results when varying Young's modulus between maximum and minimum values achieved from the experiments).

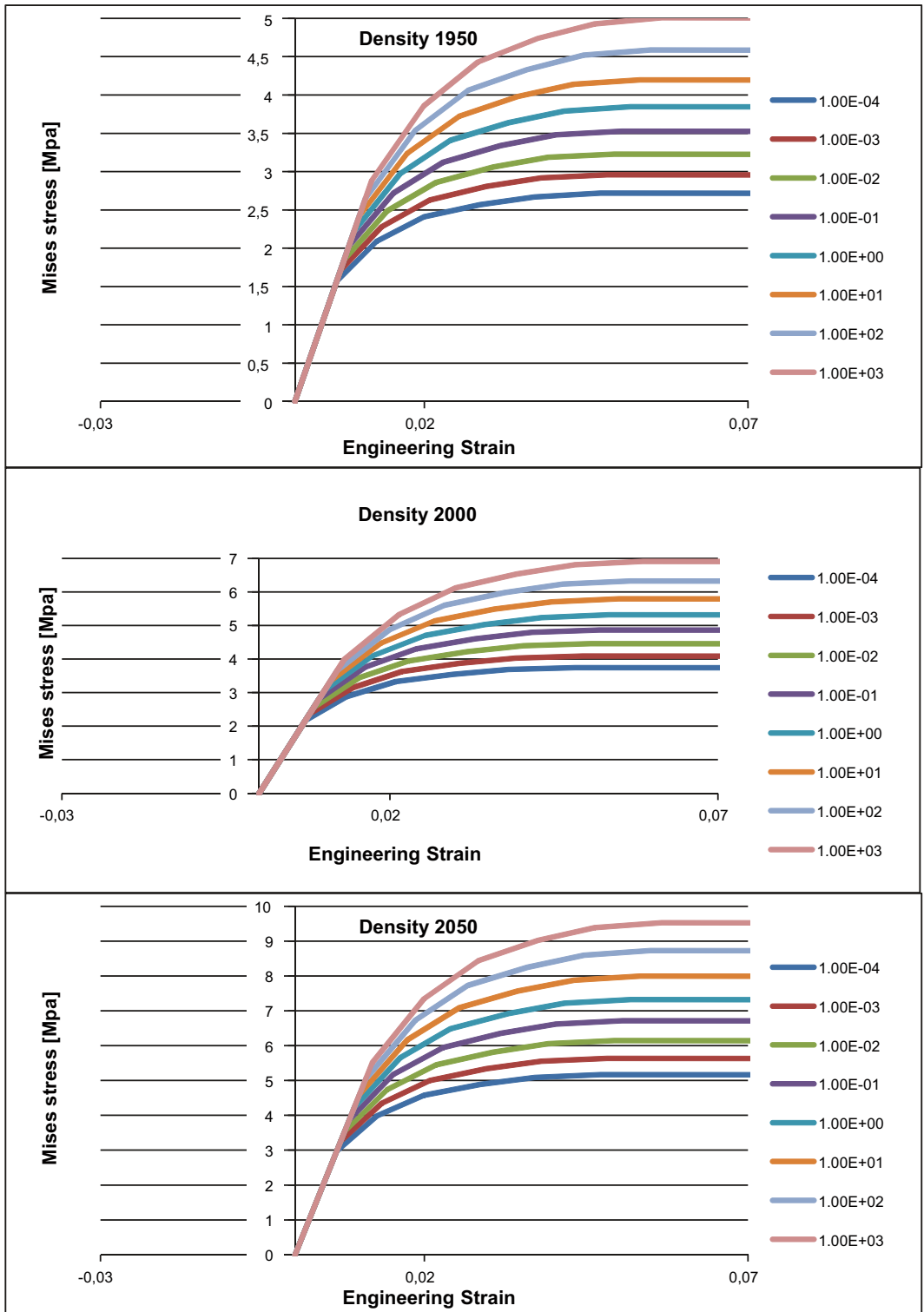


Figure 3-2. Plot of material definition for the bentonite buffer for different densities and strain rates (Mises stress versus engineering strain).

**Table 3-3. Stress-strain definition for the insert lid.**

Strain (%)	Stress (MPa)	Log Strain (%)	True Stress (MPa)
0	0	0	0
0.1595	335	0.1593	335
15	470	13.98	540
20	470	18.2	564

**Table 3-4. Elastic material data for the bentonite buffer Na converted to Ca.**

Density/Swelling pressure	Elastic part E (MPa) $\nu$
1,950/5.3	243 0.49
2,000/8	307 0.49
2,050/12.3	462 0.49

**Material model when using pore pressure elements**

The material model has been tuned especially for fast shearing analysis but for consolidation analysis a pressure dependent elastic stiffness is required (in Abaqus the model is named Porous Elastic) which cannot be combined with von Mises plasticity when using Abaqus.

For this case the Porous Elastic is combined with the DruckerPrager model, which has been defined corresponding to the von Mises model (friction angle zero and the same rate dependent yield surface). Furthermore a few additional properties have to be defined as shown below:

```
* Porous Bulk Moduli (keyword in Abaqus)
** Defines bulk modulus for skeleton and water [MPa]
2.1e+6, 2.1e3
* Permeability, specific=1e-5 (keyword in Abaqus)
** specific defines specific weight [N/mm3]
** permeability [mm/s]
1e-13
```

**3.5 Copper model**

The stress-strain properties of the copper in the copper shell were investigated by the Corrosion and metals research institute Kimab and the results are then represented by a creep material model developed by Rolf Sandström, see /Sandström and Andersson 2008, Jin and Sandström 2008, Sandström et al. 2009/.

The material model for the short duration rock shear analysis is based on a simplified elastic-plastic material model, see Table 3-5 using data from the creep model assuming a strain rate of 0.005/s which is considered as conservative.

**Table 3-5. Elastic-plastic material data for the copper at strain rate 0.005/s.**

Elastic part	Plastic part: von Mises stress $\sigma_i$ (MPa) at the following plastic strains ( $\epsilon_p$ )						
E (MPa) $\nu$	0	0.10	0.20	0.30	0.40	0.50	
1.2·10 <sup>5</sup> 0.308	72	178	235	269	288	300	

The flow curve data has been calculated from /Sandström et al. 2009/ wherein Equation (17) has been used together with the parameter values defined in the corresponding Table 4-2 /Sandström et al. 2009/ as well as  $m = 3.06$ ,  $\alpha = 0.19$ ,  $\omega = 14.66$ .

The copper model data is shown in Figure 3-3.

Also long term duration has been simulated using the creep model implemented in Abaqus as a user supplied subroutine (CREEP) which is essentially based on Equation 10-6 in /Andersson-Östling and Sandström 2009/.

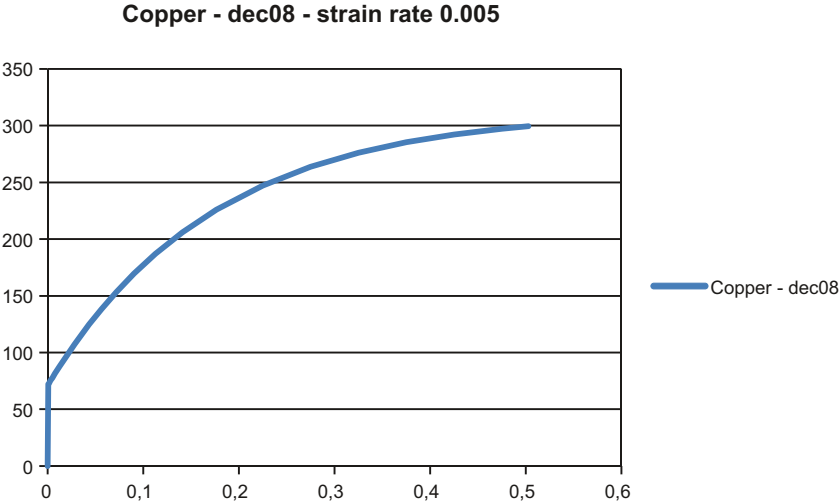


Figure 3-3. Copper shell material model gives the Mises stress as a function of the engineering strain.

## 4 Contact definitions

All the boundaries of the buffer, the copper shell, the insert and the insert lid interact through contact surfaces allowing finite sliding. All contact surfaces have friction at sliding with no cohesion and the friction coefficient 0.1, i.e. the friction angle and cohesion are:

$$\phi = 5.7^\circ$$

$$c = 0 \text{ kPa}$$

Since the actual value for the coefficient of friction is uncertain, a sensitivity analysis has been performed by also using the values 0.05 and 0.2.

The contact is released when the contact pressure is lost.

A few contact pairs are tied together (tied means that the surfaces are constrained together and will not allow for opening/closing or sliding) in order to improve the numerical convergence rate. This applies at the contact pairs between the insert and insert lid and also at the bottom of insert and copper shell bottom.

The interaction between the buffer and the rock (not modelled) is assumed to be tied through prescribed boundary conditions and will not allow for opening/closing or sliding.

## 5 Initial conditions

Initial conditions are defined as:

- Temperature for all nodes in the model as 300 K (only used for the creep analysis and is used by the user defined creep material). The temperature is assumed not to change during the analysis.
- Total pressure for the buffer to simulate the swelling pressure plus 500 meter water pressure (5 MPa) when using elastic-plastic material model without pore pressure. The magnitude depends on the density of the bentonite (22, 28 and 40.2 MPa used for 1,950, 2,000 respectively 2,050 kg/m<sup>3</sup>) and the stiffness of canister and buffer.
- Effective pressure (12.3 MPa for bentonite with density 2,050 kg/m<sup>3</sup>) and pore pressure –12.3 MPa when doing the hydrostatic analysis to simulate the effect of the glacial pressure. The total stress is equal to effective stress plus pore pressure which implies that the buffer initially is in a state of equilibrium. In the second step the pore pressure is increased to 5 MPa to include the ground water pressure.
- Internal solution dependent variables (SVAR) have been initialized to zero when using the user defined creep material.



## 6 Boundary conditions

Symmetry conditions have been specified for the symmetry plane (displacements in the normal direction to the symmetry plane prescribed to zero), see Figure 6-1. Furthermore, when the effect of only glacial load is analyzed, the rigid body motion has been constrained by prescribing the displacements to zero at the axis of symmetry at one point in the axial direction and at two points in the horizontal direction, see Figure 6-2.

The surrounding rock has been simulated by prescribing the corresponding displacements at the outer surface of the buffer and depends also on type of simulation.

Pore pressure corresponding to the glacial pressure has been defined for the bentonite when doing the hydrostatic pressure analysis.

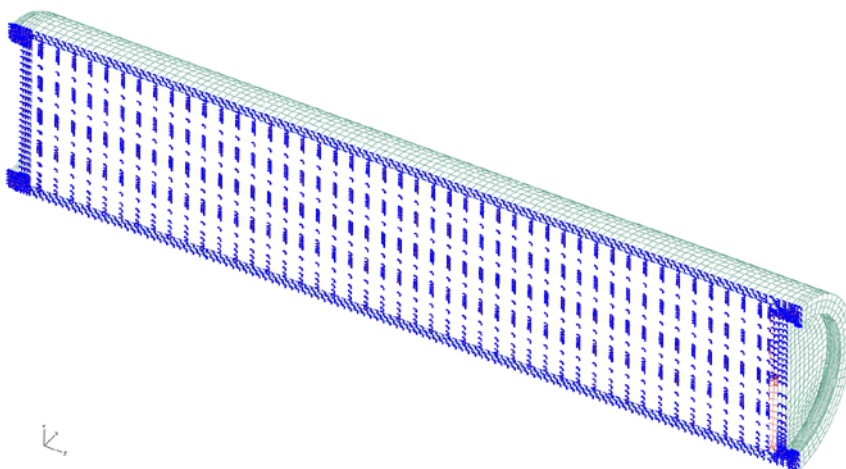


**Figure 6-1.** Prescribed symmetry conditions.

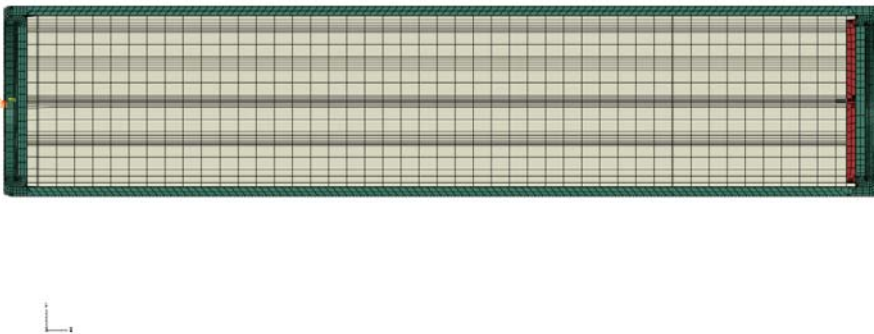


**Figure 6-2.** Boundary conditions (red dots) to avoid the rigid body motion, when the buffer is not modelled at all.

## 7 Calculations

### 7.1 General

#### 7.1.1 Rock shear calculation cases

The reference case for BWR is based on Na-bentonite converted to Ca-bentonite with density 2,050 kg/m<sup>3</sup>. For comparison reasons Ca-bentonite with densities 2,000 kg/m<sup>3</sup> and 1,950 kg/m<sup>3</sup> have also been analyzed.

Three cases of rock shear directions have been analyzed – these directions have been chosen based on the results from previous analysis:

##### **rock shear perpendicular to the axis of the canister**

- at  $\frac{3}{4}$  of the height from the bottom (model6g\_normal\_quarter\_2050ca3/2000ca3/1950ca3)
- at  $\frac{1}{2}$  of the height (model6g\_normal\_half\_2050ca3/2000ca3/1950ca3)

##### **rock shear in tension inclined with 22.5 degrees to the axis of the canister**

- at  $\frac{3}{4}$  of the height from the bottom (model6g\_22\_quarter\_tension\_2050ca3/2000ca3/1950ca3)
- at  $\frac{1}{2}$  of the height (model6g\_22\_mid\_tension\_2050ca3/2000ca3/1950ca3)

##### **rock shear in the horizontal direction through a vertical plane (full model)**

- at the symmetry plane (model6g\_full\_hori\_mid\_2050ca3)
- at  $\frac{3}{4}$  vertical plane (model6g\_full\_hori\_quarter\_2050ca3).

The long term scenario has also been analyzed where creep effects are included for the copper shell.

The PWR has been analyzed with rock shear perpendicular to the axis of the canister at  $\frac{3}{4}$  of the height from the bottom using Na-bentonite converted to Ca-bentonite with density 2,050 kg/m<sup>3</sup> (model6g\_PWR\_normal\_quarter\_2050ca3).

#### 7.1.2 Analysis approach

The numerical calculations are performed using the FE-code Abaqus (Dassault Systèmes Simulia Corp. version 6.8) assuming non-linear geometry and material definitions. This means that all non-linearities defined by the input will be considered such as large displacements, large deformations, non-linear interactions (contact) and non-linear materials.

All non-linear contributions will be used when forming the equations to be solved for each equilibrium iteration.

Short term analysis is based on static response and the results will not depend on the time used for the simulation except if rate-dependent material data is used.

Long term analysis is based on static response and the results will depend on the time used for the simulation.

The code will choose suitable time-increments for the loading based on (in most cases) default convergence tolerances.

The long term analysis (100,000 years) is performed with the applied glacial load – a more realistic time period is in the order of 1,000 to 10,000 years and thus the creep effect will be overestimated.

## 7.2 Short term analyses

The short term analyses (few seconds) consist of three steps where the shearing is prescribed by boundary conditions. In the first step initial stresses corresponding to the swelling pressure plus the 5 MPa hydrostatic pressure (the deposition is made about 500 meters below the surface) in the bentonite is applied. However, since the canister deforms when the initial stresses are applied the actual magnitude of the swelling pressure will decrease. For that reason the initial pressure for bentonite with density 2,050 kg/m<sup>3</sup> (and measured swelling pressure of 12.3+5 MPa) is given as 40.2 MPa. For bentonite with density 2,000 kg/m<sup>3</sup> (and measured swelling pressure of 8 MPa) the initial pressure is given as 28 MPa and for bentonite with density 1,950 (and measured swelling pressure of 5.25 MPa) the initial pressure is given as 22 MPa. As expected the loss of initially defined pressure increases with increased stiffness of the bentonite. Another observation is that the swelling pressure will vary both in the axial and radial direction which means that it's not possible to have the correct swelling pressure without using elements with pore pressure as a degree of freedom (Abaqus have those elements but the material model is tuned to total stresses and not effective stresses).

In the second step 5 cm is used for the shearing magnitude followed by further 5 cm shearing magnitude in the third step.

The results for BWR are shown in Appendix 1–6 for density 2,050 kg/m<sup>3</sup>.

The PWR results are shown in Appendix 7 for density 2,050 kg/m<sup>3</sup>.

## 7.3 Hydrostatic pressure

The hydrostatic pressure caused by the ice sheet (30 MPa) has been simulated by one analysis where pore-pressure elements have been used for the bentonite. For all nodes in the bentonite the pore pressure has been prescribed to 30 MPa. The swelling pressure for bentonite with density 2,050 kg/m<sup>3</sup> has been defined by initial conditions for the effective stress (12.3 MPa). The analysis consists of 4 steps, where gravity load is applied in the first step and in the second step the pore pressure is prescribed to 30 MPa after 13,000 years followed by two steps where the shearing magnitude is ramped up to 5 respectively 10 cm.

The material model for bentonite has been tuned for total stress theory but in this case an effective stress theory is used which needs a modification to handle the swelling process. The model for effective stress analysis is available but has not been tuned for the fast shearing analyzed in this report and therefore the material model for this case is DruckerPrager model with definitions corresponding to the von Mises plasticity model used in the other analyses combined with a non-linear pressure dependent elastic model (porous elastic).

Model name is model6g\_normal\_quarter\_glacial3\_2050ca3.

The results are shown in Appendix 8.

## 7.4 Long term analyses with creep in copper included

The long term analyses (100,000 years) are performed by using the full symmetric model.

The results for the reference case are shown in Appendix 9 (model6g\_normal\_quarter\_creep\_2050ca3).

## 7.5 Rock shear combined with glacial loads

Two scenarios are of interest:

- A thick layer of ice has been developed during about 13,000 years corresponding to a load of 30 MPa followed by an earthquake.
- An earthquake occurs followed by a time period of about 13,000 years where a thick layer of ice is built up corresponding to a load of 30 MPa.

However, due to convergence difficulties only the second scenario has been successfully analyzed using a strategy where the buffer is replaced by corresponding reaction forces before applying a pressure of 30 MPa on the copper shell outer surface (model6g\_normal\_quarter\_pressure1a/1b/2a/2b\_2050ca3).

## 7.6 Glacial loads

The total pressure acting on the copper shell consists of swelling pressure (15 MPa) and glacial load (30 MPa) and thus 45 MPa has been applied to the outer surface of the copper shell (the buffer is excluded from the model in this case). Figure 7-1 shows normal directions for the outer surface where the pressure is applied.

The creep material model requires extremely small time increments if the model contains singularities. The analysis will run much faster if instead a plasticity model is used in these regions and to check if such simplification can be justified three different models have been used, Figure 7-2:

Model6g\_glacier\_creep\_2050ca3 (creep model used for all elements in the copper shell).

Model6g\_glacier\_creep2\_2050ca3 (plasticity model used around the welds).

Model6g\_glacier\_creep3\_2050ca3 (plasticity around all singularities and creep model in the rest of the copper shell).

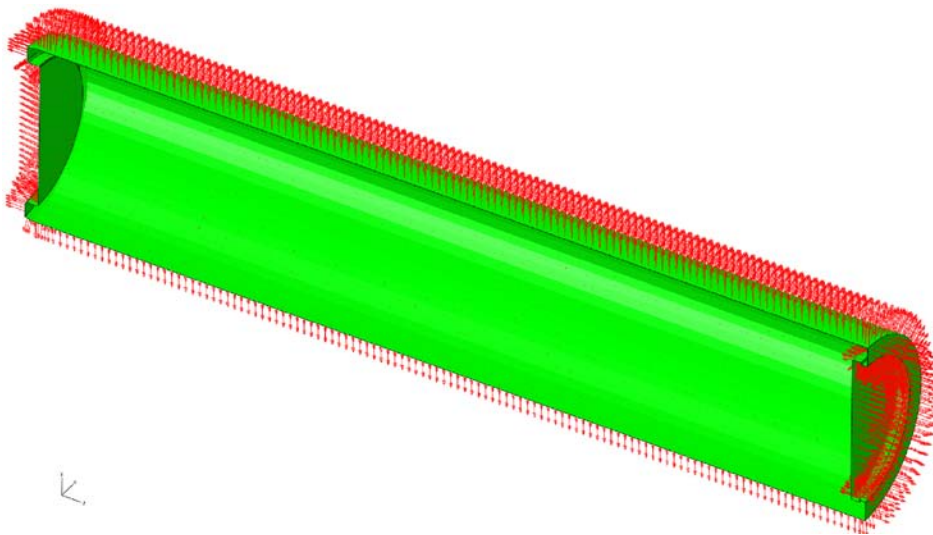


**Figure 7-1.** The total pressure load is applied opposite to the normal direction.

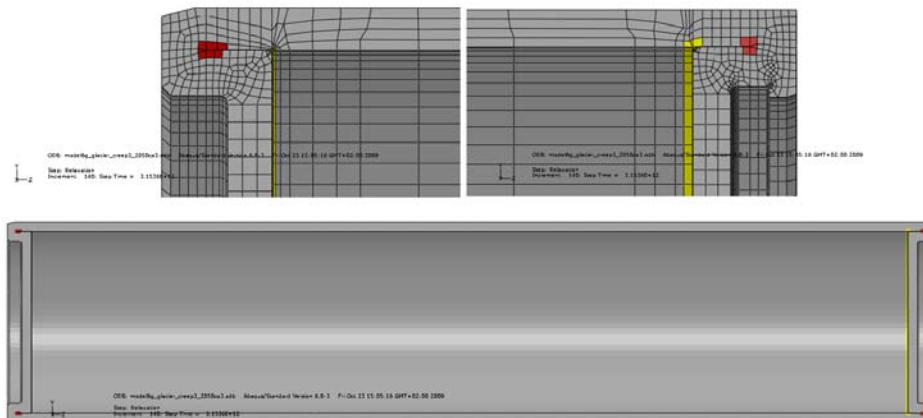


**Figure 7-2.** Material definition regions for the copper shell. Red region using plasticity for modelxx\_creep2\_xx above and modelxx\_creep3\_xx is using plasticity for both red and yellow region.

## 8 Sensitivity analyses

Some sensitivity analyses are performed to study the influence of the uncertainty in description of shear movement (8.1), modelling parameters (8.2–8.3) and possible alternative designs (8.4–8.5).

### 8.1 Rate of rock shear

For the reference case the rock shear displacement is assumed to have a velocity of 1 m/s and the sensitivity of this choice has been checked by using a velocity of 0.1 m/s (model6g\_normal\_quarter\_slow\_2050ca3), which will slightly decrease the maximum strain and stress magnitudes, see Tables 9-1–9-5.

### 8.2 Choice of coefficient of friction

In most analyses a contact coefficient of 0.1 has been used to define interaction between different parts. To check the sensitivity of this assumption one analysis has been made by instead using 0.2 (model6g\_normal\_quarter\_doublefrict\_2050ca3) and one analysis using 0.05 (model6g\_normal\_quarter\_halffrict\_2050ca3). As can be seen in Tables 9-1–9-5 there is a small change of the results, especially when using the highest value but still the maximum strains are rather low.

### 8.3 Uncertainties of the parameters in the creep material model

Since there are some uncertainties in the creep material definition one additional analysis (model6g\_normal\_quarter\_creep\_ggr5\_2050ca3) has been performed where the creep strain rate is magnified by a factor of 5, see /Andersson-Östling and Sandström 2009/ but this seems to only slightly increase the maximum creep magnitude, see Tables 9-1–9-5.

### 8.4 Buffer thickness

The effect of the buffer thickness is studied by a model where the buffer thickness has been doubled to 70 cm (model6g\_thick\_normal\_quarter\_2050ca3). Tables 9-1–9-5 show minor influence of the buffer thickness.

### 8.5 Steel cylinder around the insert

The effect of reinforcement of the cast iron insert with a surrounding steel cylinder (thickness about 2.4 cm) has been studied (model6g\_normal\_quarter\_steel\_2050ca3). Tables 9-1–9-5 show a decrease of maximum strains except for the copper shell top/bottom at 10 cm shearing.

## 9 Results

For each analysis a large amount of results are available and to have an indication only a few values are reported.

### 9.1 Results for rock shear

For the short term rock shear analyses the peak values for Mises' stress and plastic strain (PEEQ) are summarized in Tables 9-1–9-5.

#### Reference cases – insert

The highest value for PEEQ in the cast iron insert, 1.6% and in the steel channels, 2.9% occurs when the rock shear is perpendicular to the axis of the canister at the quarter point.

For the cast iron insert the failure criteria is based on stress level (maximum axial tension stress, S33) and thus Table 9-1 also contains the corresponding global stresses. As can be seen the highest value is 361 MPa and it occurs also when the rock shear is perpendicular to the axis of the canister at the quarter point.

**Table 9-1. Summary of results for the insert.**

Model name Model6g_xx	1 – iron insert 2 – steel channel tubes		PEEQ/CEEQ [%]				Mises [MPa]				S33 [MPa] maximum tension		Comment
	Shearing [cm] Insert material		5		10		5		10		5	10	
	1	2	1	2	1	2	1	2	1	1			
normal_quarter_2050ca3	0.5	0.9	1.6	2.9	321	470	351	678	333	361			
normal_quarter_creep_2050ca3	0.4	0.4	1.5	1.9	314	455	347	651	336	365			
normal_quarter_creep_ggr5_2050ca3	0.4	0.4	1.5	1.9	314	455	320	652	336	365			
normal_quarter_glacial3_2050ca3	0	0.003	0.09	0.2	335	475	345	486	102	257			
normal_quarter_pressure_2050ca3	1.0	1.9	2.3	4.4	340	551	357	688	295	328		After glacial load	
normal_quarter_halffrict_2050ca3	0.5	0.5	1.6	2.1	319	463	350	674	333	362			
normal_quarter_doublefrict_2050ca3	0.7	1.5	1.9	3.9	336	468	356	678	332	359			
normal_quarter_slow_2050ca3	0.5	0.8	1.7	2.6	312	462	344	678	327	354			
normal_quarter_steel_2050ca3	0.3	0.4	0.6	0.9	305	476	370	539	330	357			
thick_normal_quarter_2050ca3	0.1	0.1	0.9	0.9	301	455	339	517	304	340			
normal_half_2050ca3	0.1	0.3	0.7	1.5	299	464	315	469	212	265			
normal_half_creep_2050ca3	0.01	0.1	0.1	0.4	292	441	298	460	192	235			
22_quarter_tension_2050ca3	0	0.2	0.09	0.3	290	495	297	499	126	219		Stops after 9.2 cm	
22_quarter_tension_creep_2050ca3	0	0	–	–	139	287	–	–	119	–		Stops after 5.1 cm	
22_mid_tension_2050ca3	0.03	0.2	0.2	0.6	295	491	301	489	177	258			
22_mid_tension_creep_2050ca3	0	0.1	–	–	259	493	–	–	197	–		Stops after 5.5 cm	
full_hori_quarter_2050ca3	0.4	0.3	0.4	0.5	300	545	303	559	64	83			
full_hori_quarter_creep_2050ca3	0.3	0.3	–	–	301	550	–	–	80	–		Stops after 6.4 cm	
full_hori_mid_2050ca3	0.5	0.7	0.6	0.8	309	558	311	550	82	93			
full_hori_mid_creep_2050ca3	0.5	0.7	0.6	0.9	312	551	314	549	100	112			
normal_quarter_2000ca3	0.2	0.3	1.2	1.3	309	457	340	600	324	354			
22_mid_tension_2000ca3	0	0.04	0	1.7	213	488	287	490	130	207			
22_quarter_tension_2000ca3	0	0	0	0.03	199	474	227	485	98	120		Stops after 6.6 cm	
normal_quarter_1950ca3	0.1	0.1	0.7	0.7	301	452	320	487	310	336			
22_mid_tension_1950ca3	0	0	0	0	155	392	192	486	98	134		Stops after 8.9 cm	
22_quarter_tension_1950ca3	0	0	0	0	149	342	175	389	95	100		Stops after 7.1 cm	
PWR_normal_quarter_2050ca3	0.5	0.3	1.5	1.2	318	416	350	426	325	356			
PWR_normal_quarter_creep_2050ca3	0.3	0.2	1.3	1.0	313	414	342	425	324	354		Copper shell – creep only	

### Reference cases – copper shell

The peak values for plastic strain occur at a few “hot spots” and therefore the results for the copper shell are reported for nine regions (in the cylindrical part, in areas containing the welds (top and bottom), in areas containing geometric discontinuity (top and bottom), the fillet regions (top and bottom) and finally the remaining regions (top and bottom), see Figure 9-1. The summary of results is listed in Tables 9-2–9-5.

The highest value for PEEQ in the copper shell, 29%, occurs when the rock shear is perpendicular to the axis of the canister at the midpoint. However, the largest values are at the welds and at regions where the geometry is discontinuous and these are regions where maximum values strongly depend on the mesh density. The peak values occurs already when the initial conditions are applied (swelling pressure and pore pressure) and are assumed to not cause any severe damage since they mainly are in a compressive state. Besides the singular regions the highest value occurs at the top fillet, 9.6%, and occurs when the rock shear is perpendicular to the axis of the canister at the midpoint.

The peak value occurs for 10 cm shearing and are of course lower for the design case (5 cm shearing).

### Additional results

The tables also contain results when the hydrostatic pressure caused by the glacial and the hydrostatic pressure from the depth of 500 m is added by using pore pressure elements which indicates a reduction in maximum stresses and strains.

The tables furthermore contain results when using the creep material model instead of plasticity for the copper shell – in this case the effective creep strain (CEEQ) is reported – also the strain rate effect from the creep model reduces (most regions) the maximum strain magnitudes but the maximum stress will increase in the copper shell. The results after long time (100,000 years) are listed in Tables 9-6–9-8.

For the case “Rock shear combined with a following glacial load (30 MPa)” the results listed in Tables 9-1–9-5 (normal\_quarter\_pressure\_2050ca3) show an increase in most regions compared to the corresponding reference case (normal\_quarter\_2050ca3). However, plastic strains in copper shell and steel channels are still rather small and furthermore the axial stress (S33) which is used when estimating allowed crack size actually decrease compared to the reference case.

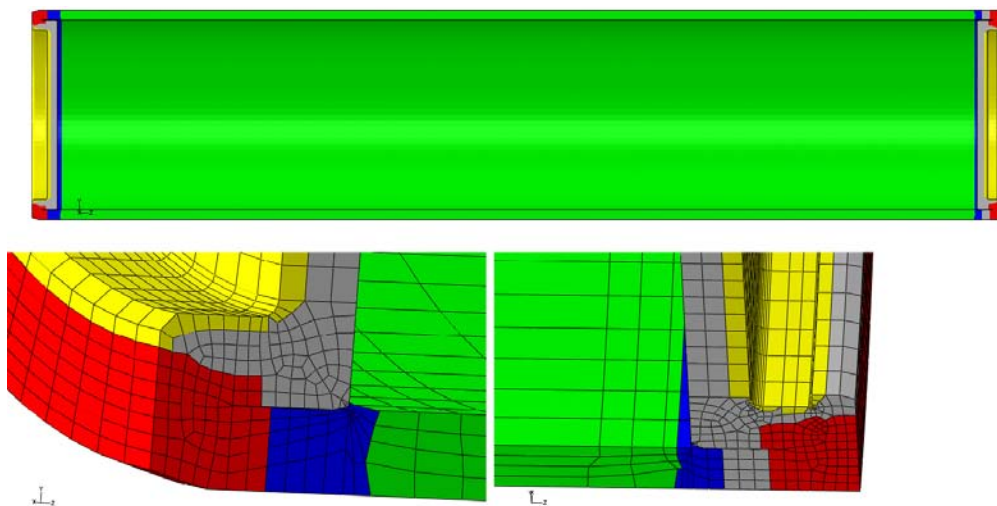


**Figure 9-1.** Output regions for copper shell. Region 1 – mid canister (green). Region 2 – top weld (red, lower right). Region 3 – bottom weld (red, lower left). Region 4 – top discontinuous geometry (blue, lower right). Region 5 – bottom discontinuous geometry (blue, lower left). Region 6 – top fillet (yellow, lower right). Region 7 – bottom fillet (yellow, lower left). Region 8 – top remaining (grey, lower right). Region 9 – bottom remaining (grey, lower left).

**Table 9-2. Summary of strain results for copper shell at 5 cm shearing.**

Model name Model6g_xx	1 – mid shell 2, 3 – top/bot welds 4, 5 – top/bot discontinuous 6, 7 – top/bot fillets 8, 9 – top/bot reminding Copper shell region	PEEQ/CEEQ [%] 5 cm shearing								
		1	2	3	4	5	6	7	8	9
normal_quarter_2050ca3		1.0	3.6	2.7	1.5	16	0.4	0.05	2.6	0.8
normal_quarter_creep_2050ca3		0.7	2.6	5.5	1.8	7.2	0.09	0	0.2	0.3
normal_quarter_creep_ggr5_2050ca3		0.7	2.6	5.4	1.8	7.5	0.09	0	0.2	0.3
normal_quarter_glacial3_2050ca3		1.3	12.3	3.1	3.2	16	1.9	0.08	1.9	1.0
normal_quarter_pressure_2050ca3		1.4	3.6	2.8	2.1	23	0.9	0.1	3.1	1.3
normal_quarter_halffrict_2050ca3		1.0	4.0	2.7	1.4	16	0.4	0.8	2.6	0.9
normal_quarter_doublefrict_2050ca3		1.1	2.3	2.6	2.0	17	0.4	0.3	0.7	0.7
normal_quarter_slow_2050ca3		1.0	3.6	2.7	1.5	16	0.4	0.05	2.4	0.8
normal_quarter_steel_2050ca3		0.8	3.4	2.7	1.5	16	0.4	0.2	1.9	1.0
thick_normal_quarter_2050ca3		0.8	3.0	2.8	1.7	12	0.8	1.0	0.8	1.2
normal_half_2050ca3		1.9	4.5	3.3	6.3	21	4.7	1.4	3.0	1.7
normal_half_creep_2050ca3		0.8	4.3	4.5	2.3	6.7	0.2	0.1	0.3	0.4
22_quarter_tension_2050ca3		1.5	14	9.5	2.4	15	9.3	0.9	5.5	1.2
22_quarter_tension_creep_2050ca3		0.1	0.4	6.2	0.1	1.2	0.1	0.1	0	0.09
22_mid_tension_2050ca3		0.7	4.3	5.1	1.8	15	0.9	1.0	0.9	1.2
22_mid_tension_creep_2050ca3		0.6	3.1	9.6	2.1	2.0	0.8	0.1	0.3	0.2
full_hori_quarter_2050ca3		0.7	4.2	5.0	1.1	4.3	2.7	1.4	1.6	1.3
full_hori_quarter_creep_2050ca3		0.6	7.2	10.1	3.3	2.5	0.6	0.1	0.7	0.3
full_hori_mid_2050ca3		0.9	4.1	3.5	1.1	6.9	3.6	1.3	1.7	1.7
full_hori_mid_creep_2050ca3		0.4	6.0	7.3	3.1	2.1	0.5	0.1	1.0	0.2
normal_quarter_2000ca3		0.8	2.8	2.5	1.1	14	0.5	0.1	0.6	1.0
22_mid_tension_2000ca3		0.5	5.0	5.3	1.2	8.1	0.5	0.5	0.8	0.6
22_quarter_tension_2000ca3		0.7	17	9.6	2.1	8.1	4.4	0.7	2.4	0.8
normal_quarter_1950ca3		0.6	2.3	2.6	0.9	12	0.8	0.2	0.5	1.0
22_mid_tension_1950ca3		0.5	4.3	5.3	0.6	3.4	0.4	0.2	0.5	0.3
22_quarter_tension_1950ca3		0.6	18	9.3	1.6	4.0	2.0	0.5	1.2	0.5
PWR_normal_quarter_2050ca3		1.1	3.2	2.7	1.3	17	0.5	0.1	0.8	0.8
PWR_normal_quarter_creep_2050ca3		0.7	2.5	5.3	0.2	9.4	0.2	0	0.2	0.5



**Table 9-3. Summary of strain results for copper shell at 10 cm shearing.**

Model name Model6g_xx	PEEQ/CEEQ [%] 10 cm shearing									
	1	2	3	4	5	6	7	8	9	
1 – mid shell										
2, 3 – top/bot welds										
4, 5 – top/bot discontinuous										
6, 7 – top/bot fillets										
8, 9 – top/bot reminding										
Copper shell region										
normal_quarter_2050ca3	2.0	4.3	2.7	1.6	16	0.5	0.05	3.1	0.8	
normal_quarter_creep_2050ca3	1.8	2.9	5.5	1.9	8.8	0.09	0	0.2	0.4	
normal_quarter_creep_ggr5_2050ca3	1.9	3.0	5.5	1.8	9.2	0.09	0	0.2	0.4	
normal_quarter_glacial3_2050ca3	1.4	13	3.1	3.3	17	2.2	0.5	1.9	1.4	
normal_quarter_pressure_2050ca3	2.7	4.3	2.8	2.1	23	1.7	0.2	3.5	1.3	
normal_quarter_halffrict_2050ca3	1.9	5.2	2.7	1.5	16	0.5	0.1	3.2	0.1	
normal_quarter_doublefrict_2050ca3	2.2	2.3	2.6	2.1	17	0.5	0.03	0.7	0.7	
normal_quarter_slow_2050ca3	2.0	4.1	2.7	1.6	16	0.5	0.05	2.9	0.8	
normal_quarter_steel_2050ca3	1.2	3.9	2.9	1.9	21	0.7	1.3	1.9	1.8	
thick_normal_quarter_2050ca3	1.4	3.8	2.8	1.8	12	0.8	1.6	0.8	1.5	
normal_half_2050ca3	4.4	8.8	7.5	15	29	9.6	2.9	6.0	2.5	
normal_half_creep_2050ca3	0.8	5.7	4.7	4.0	7.6	0.5	0.2	0.4	0.7	
22_quarter_tension_2050ca3	1.8	27	12	2.4	15	13	1.6	7.1	1.6	
22_quarter_tension_creep_2050ca3	–	–	–	–	–	–	–	–	–	
22_mid_tension_2050ca3	0.9	14	5.9	2.3	16	3.5	2.5	1.9	2.3	
22_mid_tension_creep_2050ca3	–	–	–	–	–	–	–	–	–	
full_hori_quarter_2050ca3	0.9	6.9	5.4	1.1	6.0	3.3	1.6	1.6	1.5	
full_hori_quarter_creep_2050ca3	–	–	–	–	–	–	–	–	–	
full_hori_mid_2050ca3	1.1	5.4	3.7	1.5	9.1	4.8	1.6	1.7	1.9	
full_hori_mid_creep_2050ca3	0.5	6.2	7.6	3.1	2.2	0.5	0.1	1.0	0.3	
normal_quarter_2000ca3	1.8	3.1	2.5	1.2	14	0.5	0.3	0.6	1.1	
22_mid_tension_2000ca3	0.6	16	5.7	1.5	9.2	1.4	1.4	1.0	1.4	
22_quarter_tension_2000ca3	0.7	30	9.9	2.1	8.1	4.3	0.8	2.5	0.9	
normal_quarter_1950ca3	1.2	2.6	3.0	1.3	12	1.0	0.5	0.5	1.2	
22_mid_tension_1950ca3	0.5	12	5.6	0.7	4.5	0.6	0.6	0.5	0.6	
22_quarter_tension_1950ca3	0.6	29	9.4	1.6	4.2	2.0	0.6	1.2	0.6	
PWR_normal_quarter_2050ca3	2.1	3.7	2.7	1.4	17	0.7	0.1	1.1	0.8	
PWR_normal_quarter_creep_2050ca3	1.8	2.6	5.5	0.2	10	0.2	0	0.2	0.6	

**Table 9-4. Summary of stress results for copper shell at 5 cm shearing.**

Model name Model6g_xx	1 – mid shell 2, 3 – top/bot welds 4, 5 – top/bot discontinuous 6, 7 – top/bot fillets 8, 9 – top/bot reminding Copper shell region	Mises [MPa] 5 cm shearing								
		1	2	3	4	5	6	7	8	9
normal_quarter_2050ca3		103	145	147	121	201	81	85	109	103
normal_quarter_creep_2050ca3		237	206	223	308	304	178	141	206	283
normal_quarter_creep_ggr5_2050ca3		233	205	220	309	298	173	139	200	278
normal_quarter_glacial3_2050ca3		102	210	152	121	216	100	87	113	88
normal_quarter_pressure_2050ca3		116	149	142	118	262	85	84	141	119
normal_quarter_halffrict_2050ca3		102	146	97	117	198	82	84	111	88
normal_quarter_doublefrict_2050ca3		111	88	99	115	202	81	85	113	108
normal_quarter_slow_2050ca3		102	146	147	121	201	80	85	109	104
normal_quarter_steel_2050ca3		94	104	144	120	201	81	81	127	88
thick_normal_quarter_2050ca3		102	141	102	109	207	94	92	98	89
normal_half_2050ca3		139	99	149	134	254	130	94	112	95
normal_half_creep_2050ca3		241	227	230	317	310	236	242	228	279
22_quarter_tension_2050ca3		128	268	185	112	133	174	96	179	93
22_quarter_tension_creep_2050ca3		221	181	200	99	174	104	202	115	187
22_mid_tension_2050ca3		92	178	144	128	118	112	94	115	91
22_mid_tension_creep_2050ca3		212	325	259	322	271	235	244	216	218
full_hori_quarter_2050ca3		128	146	146	116	145	108	101	129	94
full_hori_quarter_creep_2050ca3		294	239	256	407	262	223	242	326	220
full_hori_mid_2050ca3		107	98	142	121	171	118	99	115	98
full_hori_mid_creep_2050ca3		239	241	266	400	267	217	235	315	233
normal_quarter_2000ca3		123	131	100	105	187	84	82	117	111
22_mid_tension_2000ca3		94	173	144	109	105	109	88	107	84
22_quarter_tension_2000ca3		93	260	186	112	109	122	93	115	96
normal_quarter_1950ca3		107	121	101	100	174	85	83	120	88
22_mid_tension_1950ca3		82	152	142	100	127	86	88	108	87
22_quarter_tension_1950ca3		95	247	183	120	114	99	91	142	88
PWR_normal_quarter_2050ca3		103	145	144	110	206	103	89	111	90
PWR_normal_quarter_creep_2050ca3		238	212	234	211	301	195	178	206	275

**Table 9-5. Summary of stress results for copper shell at 10 cm shearing.**

Model name Model6g_xx	1 – mid shell 2, 3 – top/bot welds 4, 5 – top/bot discontinuous 6, 7 – top/bot fillets 8, 9 – top/bot reminding Copper shell region	Mises [MPa] 10 cm shearing								
		1	2	3	4	5	6	7	8	9
normal_quarter_2050ca3		126	106	139	120	196	83	84	117	88
normal_quarter_creep_2050ca3		260	335	220	315	298	176	145	198	276
normal_quarter_creep_ggr5_2050ca3		257	321	216	310	292	172	144	192	270
normal_quarter_glacial3_2050ca3		103	212	151	122	220	103	85	115	102
normal_quarter_pressure_2050ca3		116	104	142	117	263	98	85	125	94
normal_quarter_halffrict_2050ca3		127	108	97	116	190	82	84	148	86
normal_quarter_doublefrict_2050ca3		125	88	98	114	198	81	86	122	105
normal_quarter_slow_2050ca3		127	104	139	121	197	91	84	113	88
normal_quarter_steel_2050ca3		118	128	146	106	254	83	93	109	105
thick_normal_quarter_2050ca3		119	156	103	110	214	103	99	105	93
normal_half_2050ca3		137	119	166	223	259	177	112	144	106
normal_half_creep_2050ca3		238	224	230	357	307	234	237	250	279
22_quarter_tension_2050ca3		145	348	206	128	253	191	98	164	95
22_quarter_tension_creep_2050ca3		–	–	–	–	–	–	–	–	–
22_mid_tension_2050ca3		104	272	149	123	189	119	109	135	104
22_mid_tension_creep_2050ca3		–	–	–	–	–	–	–	–	–
full_hori_quarter_2050ca3		125	199	135	119	164	115	106	120	97
full_hori_quarter_creep_2050ca3		–	–	–	–	–	–	–	–	–
full_hori_mid_2050ca3		131	155	141	103	189	131	104	109	100
full_hori_mid_creep_2050ca3		234	243	260	400	275	220	228	314	220
normal_quarter_2000ca3		130	139	99	101	188	83	81	108	87
22_mid_tension_2000ca3		92	271	121	110	147	90	95	114	93
22_quarter_tension_2000ca3		91	319	188	117	121	126	93	109	91
normal_quarter_1950ca3		113	93	101	100	180	86	83	119	89
22_mid_tension_1950ca3		88	217	150	118	118	83	87	93	102
22_quarter_tension_1950ca3		95	229	185	109	153	91	91	118	93
PWR_normal_quarter_2050ca3		133	104	137	112	208	94	87	116	90
PWR_normal_quarter_creep_2050ca3		263	327	238	224	295	195	182	222	267

**Table 9-6. Summary of results for long term rock shear analyses after 10 cm shearing.**

Model name Model6g_xx	1 – iron insert 2 – steel channel tubes  Shearing [cm] Insert material	PEEQ/CEEQ [%]		Mises [MPa]		S33 [MPa] maximum tension	Comment
		10		10		10	
		1	2	1	2	1	
normal_quarter_creep_2050ca3		1.5	1.9	319	645	331	
normal_quarter_creep_ggr5_2050ca3		1.5	1.9	320	647	332	
normal_half_creep_2050ca3		0.1	0.4	245	370	190	
22_quarter_tension_creep_2050ca3		–	–	–	–	–	Stops after 5.1 cm
22_mid_tension_creep_2050ca3		–	–	–	–	–	Stops after 5.5 cm
full_hori_quarter_creep_2050ca3		–	–	–	–	–	Stops after 6.2 cm
full_hori_mid_creep_2050ca3		0.6	0.9	252	506	82	
PWR_normal_quarter_creep_2050ca3		1.3	1.4	311	310	323	Copper shell – creep only

**Table 9-7. Summary of strain results for long term rock shear analyses after 10 cm shearing.**

Model name Model6g_xx	1 – mid shell 2, 3 – top/bot welds 4, 5 – top/bot discontinuous 6, 7 – top/bot fillets 8, 9 – top/bot reminding Copper shell region	PEEQ/CEEQ [%] 10 cm shearing								
		1	2	3	4	5	6	7	8	9
normal_quarter_creep_2050ca3		1.9	3.2	5.9	1.9	14	0.2	0.03	0.4	0.9
normal_half_creep_2050ca3		0.9	6.9	6.1	4.3	9.9	0.9	0.5	0.6	1.2
22_quarter_tension_creep_2050ca3		–	–	–	–	–	–	–	–	–
22_mid_tension_creep_2050ca3		–	–	–	–	–	–	–	–	–
full_hori_quarter_creep_2050ca3		–	–	–	–	–	–	–	–	–
full_hori_mid_creep_2050ca3		1.1	8.5	8.1	3.1	2.8	0.8	0.2	1.5	0.5
PWR_normal_quarter_creep_2050ca3		1.9	3.0	6.3	0.7	14	0.3	0.07	0.4	1.1

**Table 9-8. Summary of stress results for long term rock shear analyses after 10 cm shearing.**

Model name Model6g_xx	1 – mid shell 2, 3 – top/bot welds 4, 5 – top/bot discontinuous 6, 7 – top/bot fillets 8, 9 – top/bot reminding Copper shell region	Mises [MPa] 10 cm shearing								
		1	2	3	4	5	6	7	8	9
normal_quarter_creep_2050ca3		177	154	146	208	191	133	145	150	166
normal_quarter_creep_ggr5_2050ca3		170	147	155	205	188	128	139	160	159
normal_half_creep_2050ca3		159	139	162	217	193	134	141	186	183
22_quarter_tension_creep_2050ca3		–	–	–	–	–	–	–	–	–
22_mid_tension_creep_2050ca3		–	–	–	–	–	–	–	–	–
full_hori_quarter_creep_2050ca3		–	–	–	–	–	–	–	–	–
full_hori_mid_creep_2050ca3		137	146	197	281	165	135	134	198	137
PWR_normal_quarter_creep_2050ca3		174	189	158	161	228	148	142	185	144

### PWR canister

The PWR canister, Tables 9-1–9-5, shows very small plastic strains (except for the bottom geometric discontinuity in the copper shell) and using the creep material model (in this case the creep model is used for all regions in the copper shell) shows the same tendency – decreased maximum strains and increased stresses, especially in the copper shell.

### Output regions

The numbers in Tables 9-2–9-5 are for copper shell shown at nine regions, Figure 9-1 and should be used with care and in combination with the corresponding plots in the enclosed appendices.

Since the creep model also contains plastic deformation the main part of creep strains are reached already at the shearing phase (after 0.1 second). Thereafter only small changes of the creep strains are observed.

The creep strain after long time (100,000 years) shows similar behavior for all listed results – the strains (CEEQ/PEEQ) increases with time and the stresses decreases, compare Tables 9-1–9-5 with Tables 9-6–9-8.

Maximum creep strain is 1.9% (neglecting singular regions) compared to 2.0% when elastic-plastic material is used at 10 cm shearing (normal shearing direction for density 2,050), comparing Tables 9-3 and 9-7.

Mises' stress relaxes linearly with time in a lin-log diagram, see Appendix 9.

## 9.2 Hot spot regions

The location of hot spots depends on type of analysis but in most cases there are a few hot spots occurring at fillets, corners or discontinuous geometries such as welds or sudden change of geometry. A few hot spots are shown in Figures 9-2–9-7 where the selection is done for cases having the hot spots most visible.

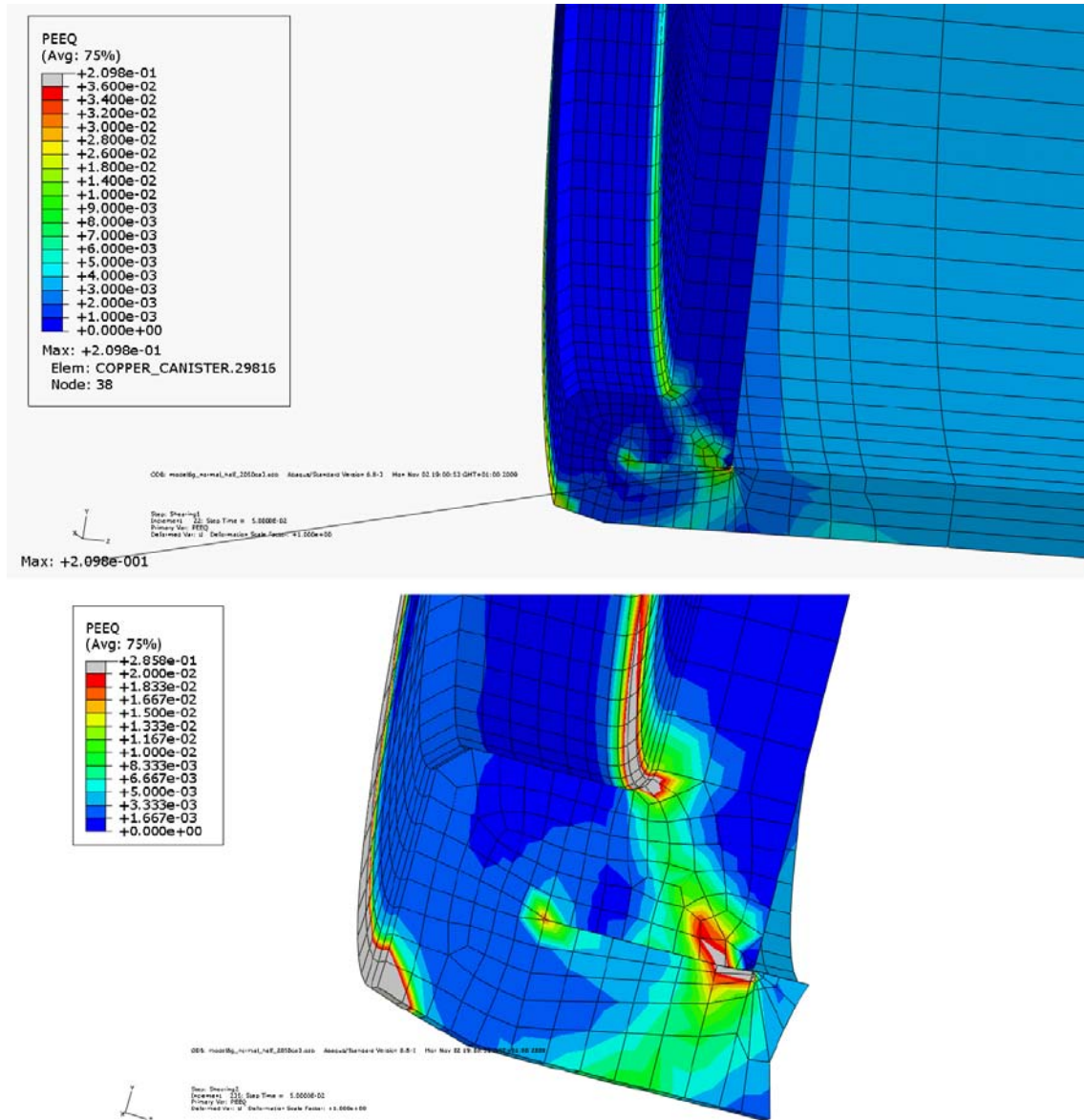


**Figure 9-2.** Plot of PEEQ at the copper bottom corner at mid normal compression. Hot spots at fillet, corner, weld and geometric discontinuity after 5 cm shearing (top) and after 10 cm shearing (bottom).

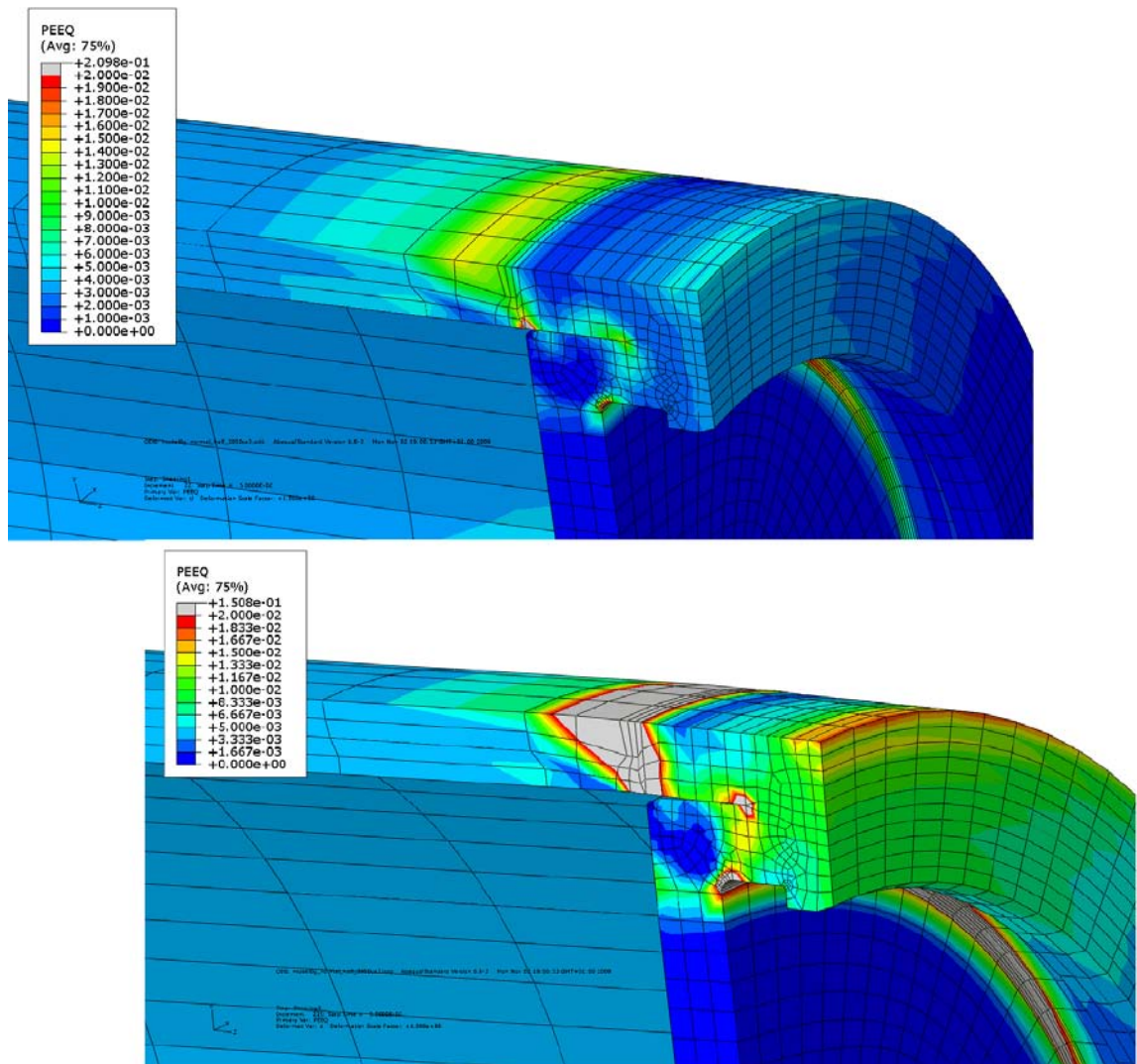
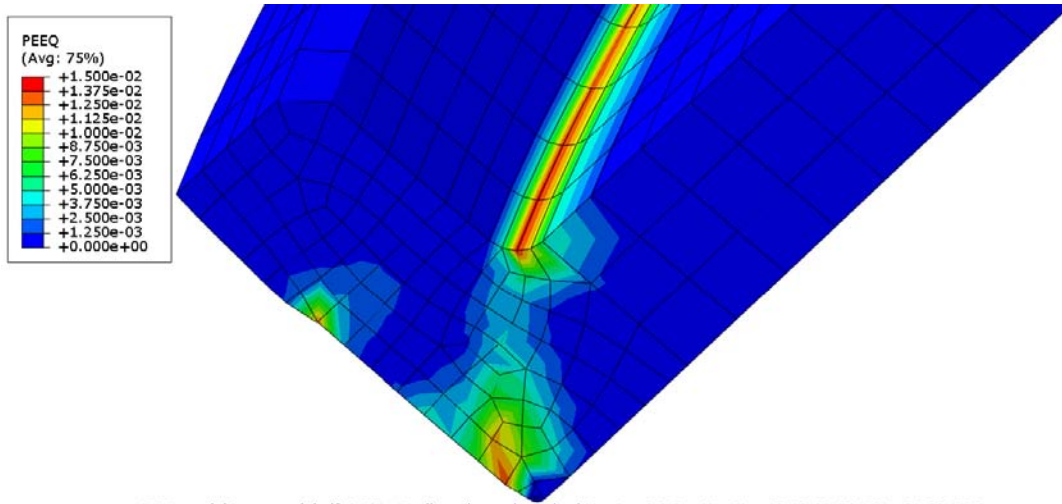


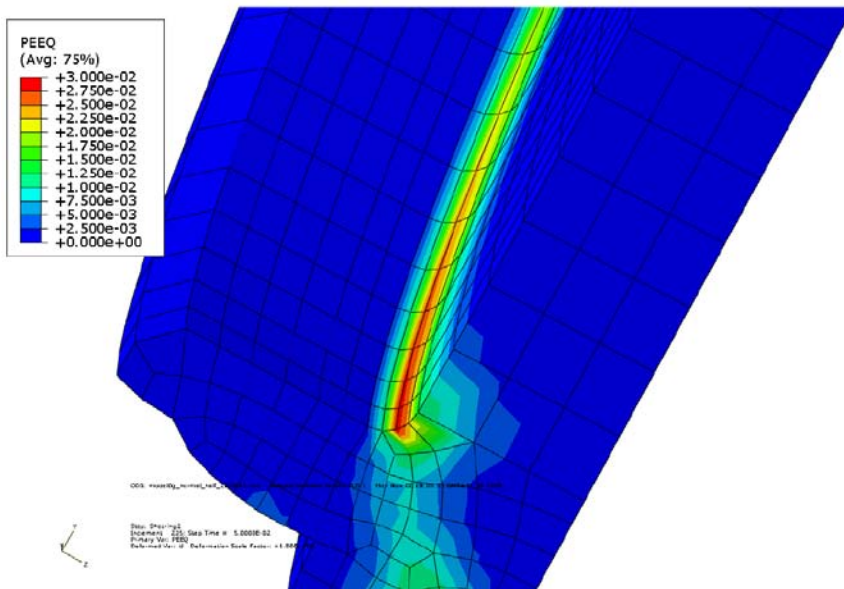
**Figure 9-3.** Plot of PEEQ at the copper top corner at mid normal compression. Hot spots at fillet, corner, weld and geometric discontinuity after 5 cm shearing (top) and after 10 cm shearing (bottom).



ODB: model6g\_normal\_half\_2050ca3.odb Abaqus/Standard Version 6.8-3 Mon Nov 02 19:00:53 GMT+01:00 2009



Step: Shearing1  
Increment: 22; Step Time = 5.0000E-02  
Primary Var: PEEQ  
Deformed Var: U Deformation Scale Factor: +1.000e+00



ODB: model6g\_normal\_half\_2050ca3.odb Abaqus/Standard Version 6.8-3 Mon Nov 02 19:00:53 GMT+01:00 2009



Step: Shearing1  
Increment: 25; Step Time = 5.0000E-02  
Primary Var: PEEQ  
Deformed Var: U Deformation Scale Factor: +1.000e+00

**Figure 9-4.** Plot of PEEQ at the copper bottom fillet at mid normal compression. Hot spots are at fillet after 5 cm shearing (top) and after 10 cm shearing (bottom).

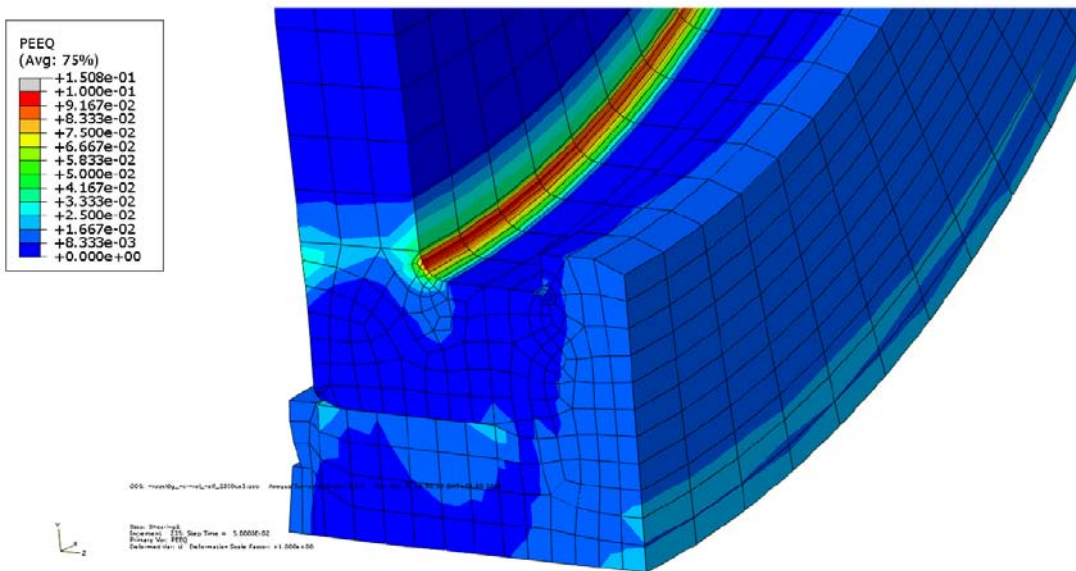
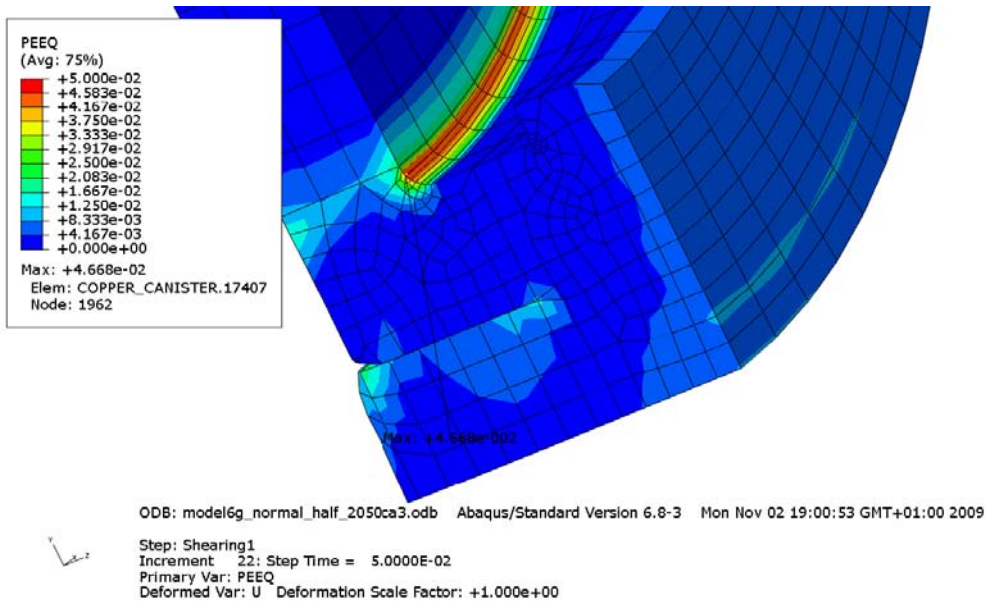


*Figure 9-5. Plot of PEEQ at the copper top fillet at mid normal compression. Hot spots are at fillet after 5 cm shearing (top) and after 10 cm shearing (bottom).*



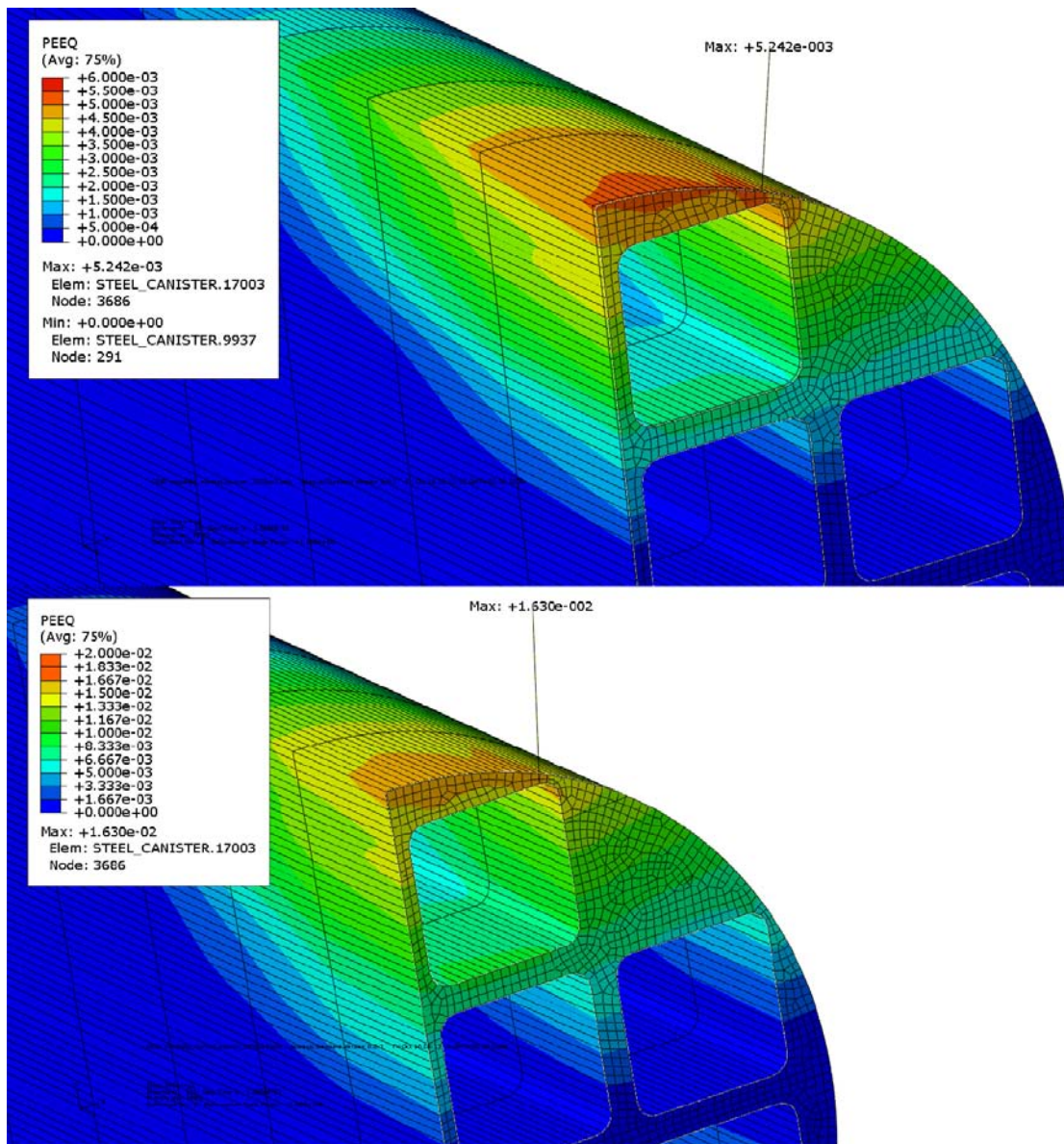


*Figure 9-6. Plot of PEEQ at the iron insert channel showing region with large magnitude at quarter point normal compression. Hot spots are at fillet after 5 cm shearing (top) and after 10 cm shearing (bottom).*

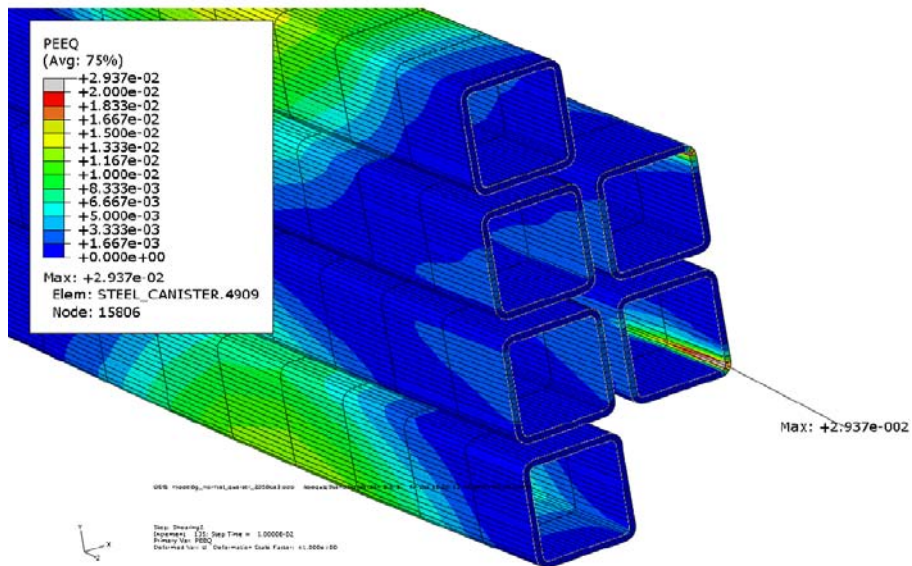
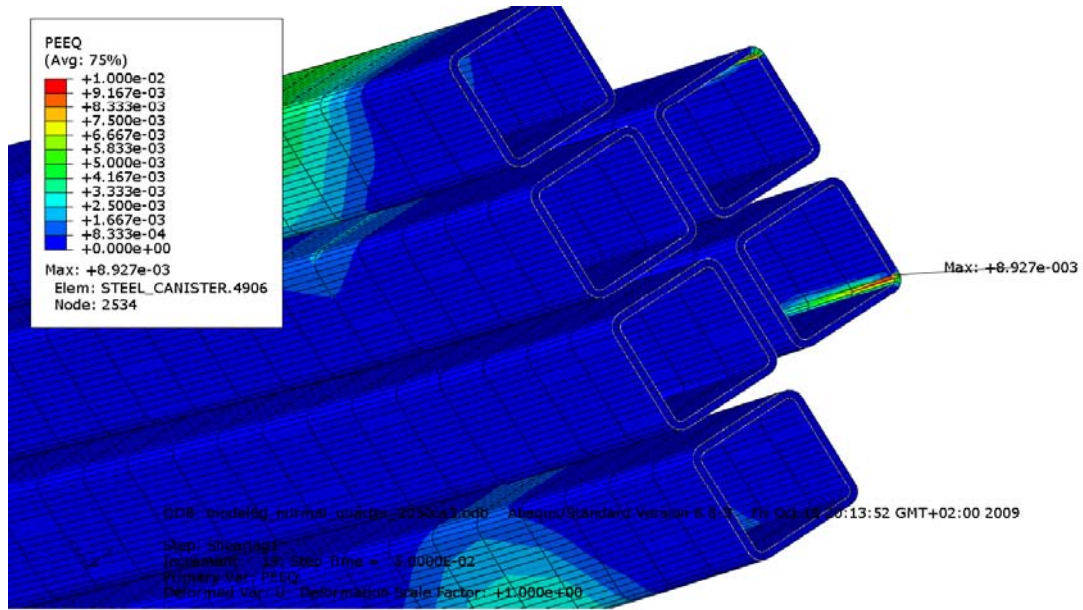


**Figure 9-7.** Plot of PEEQ at the insert steel channels showing region with large magnitude at quarter point normal compression. Hot spots are at fillet after 5 cm shearing (top) and after 10 cm shearing (bottom).

### 9.3 Results glacial load

In Table 9-9 the peak values for Mises' stress and equivalent plastic strain (PEEQ) or equivalent creep strain (CEEQ) are summarized. The highest value for CEEQ in the copper shell, 16%, occurs where the shell lid is welded to the flange. The insert has no plastic strains.

The numbers in Table 9-9 should be used with care and used in combination with the corresponding plots, see Figures 9-8–9-22.

C1: The high value for CEEQ in the copper shell is very local and is not expected to cause severe damage especially since creep will reduce the maximum strain.

C2: PEEQ in the insert is zero, see Figures 9-8–9-9.

Comparing the three models used for glacial load analyses shows small differences except for creep strain in areas where a plasticity model is used instead of the creep model which then could be used as a judgement for simplifying the model as the approach used for model6g\_glacier\_creep3\_2050ca3.

**Table 9-9. Summary of results for the glacial load analysis.**

Model model6g_xx	Step 1 – applied load after 1,000 seconds	Copper shell				Insert				Comments in text
		CEEQ [%]		Mises [MPa]		PEEQ [%]		Mises [MPa]		
	Step	1	2	1	2	1	2	1	2	
glacier_creep_2050ca3		15	18	275	245	0	0	284	358	C1 and C2
glacier_creep2_2050ca3		16	19	277	245	0	0	284	358	
glacier_creep3_2050ca3		7	13	278	208	0	0	283	358	

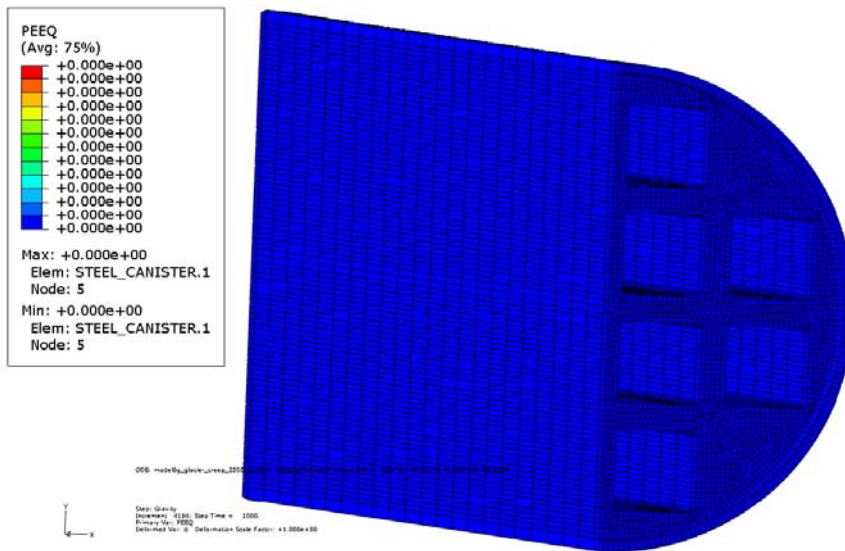


**Figure 9-8.** Plastic strain for insert after applying the load (1,000 seconds).

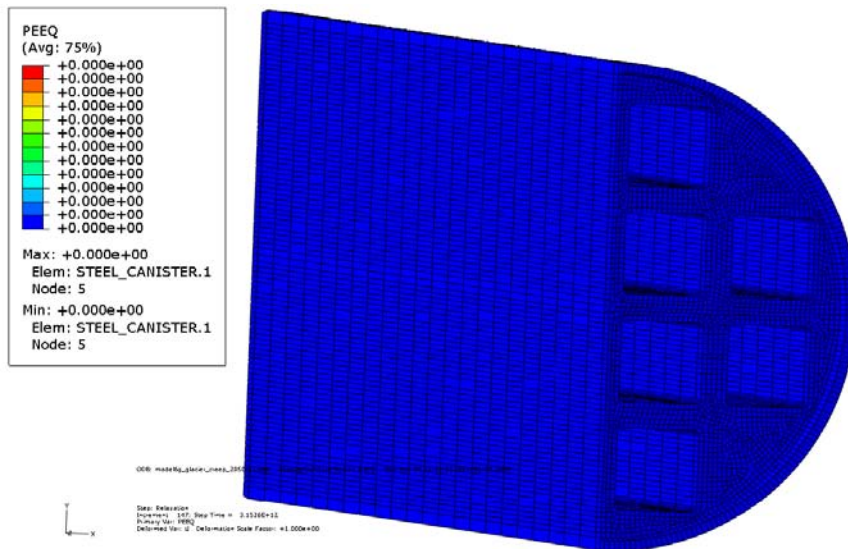


**Figure 9-9.** Plastic strain for the insert after relaxation (100,000 years).

Also the maximum Mises stress is at a corner of the square channels and will locally reach the yield surface but generally the magnitude is far from the yield surface, see Figures 9-10–9-11.

For the copper shell the maximum creep strain, 16%, occurs at a very small region where the copper lid is welded to the flange, see Figures 9-12–9-15.

Also the maximum Mises' stress for the copper shell occurs where the shell lid is welded to the flange, see Figures 9-16–9-17.

Mises' stress relaxes linearly with time in a lin-log diagram see Figure 9-18, where the time-history plot of Mises stress and equivalent creep strain is plotted for that element having largest equivalent creep strain.

The contour plots are based on extrapolated integration point values at the nodes and then averaged (e.g. Figure 9-15) and the history plot (Figure 9-18) shows integration point value. If the gradients in each element are small, then these averaged and extrapolated representations should be close to the calculated values.

The deformation plot of the shell shows that there will be some bending at the corners, see Figures 9-19–9-20.

The copper shell will deform when the glacial load is applied but mainly the initial gaps will be closed. The insert will have displacements less than 1 millimeter, see Figure 9-21. The displacements due to creep in the shell does not seem to affect the initial geometry used for a following earthquake induced rock shear analysis.

The stresses in the insert are shown in Figure 9-22 – mostly in compression and much below the yield stress.

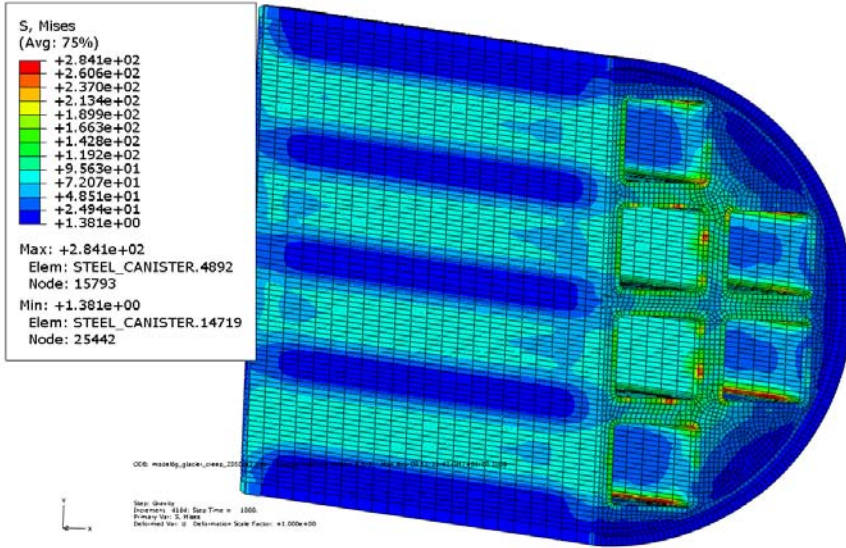


Figure 9-10. Mises stress for insert after applied load (1,000 seconds).

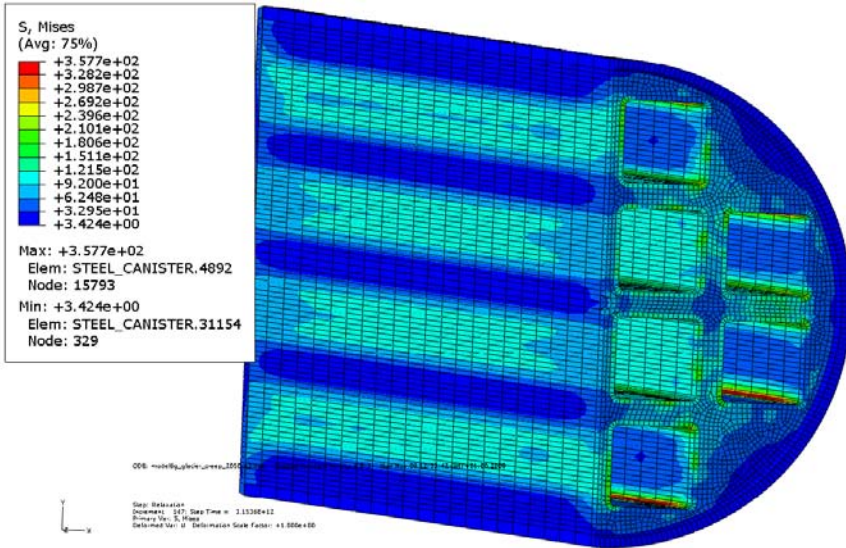


Figure 9-11. Mises stress for insert after relaxation (100,000 years).



Figure 9-12. Equivalent creep strain (CEEQ) after applying the glacial load (1,000 seconds).

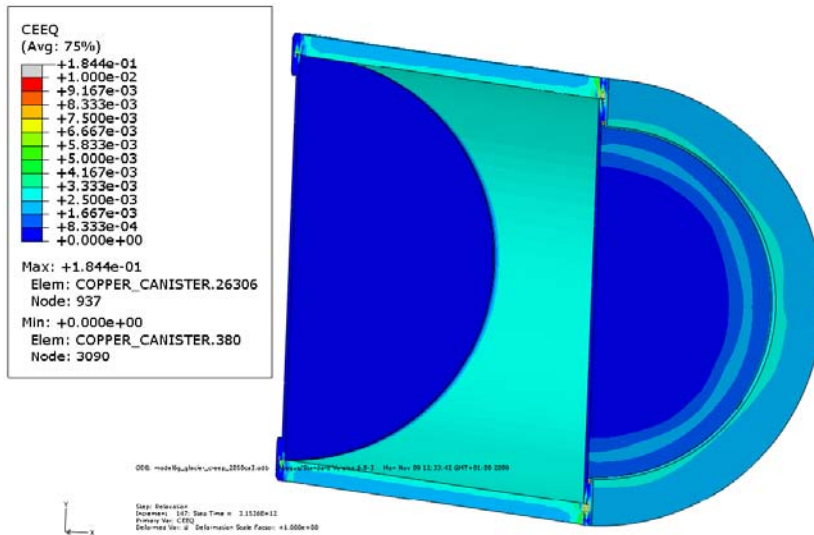
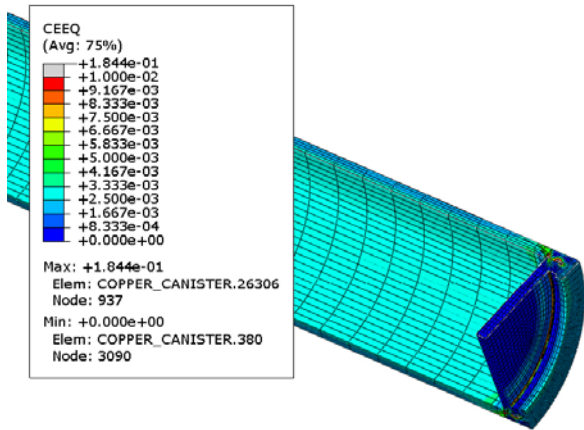


Figure 9-13. Equivalent creep strain (CEEQ) after relaxation (100,000 years).



CDE: msk8qj\_glsck\_pnes\_250x2.000 Abaqus/Standard Version 6.8-3 Mon Nov 09 12:32:43 GMT+01:00 2009



Step: Relaxation  
Increment: 107 Step Time = 3.15388e+11  
Display Var: CEEQ  
Deformation Scale Factor: +1.000e+00

Figure 9-14. Equivalent creep strain in copper shell after relaxation (100,000 years).

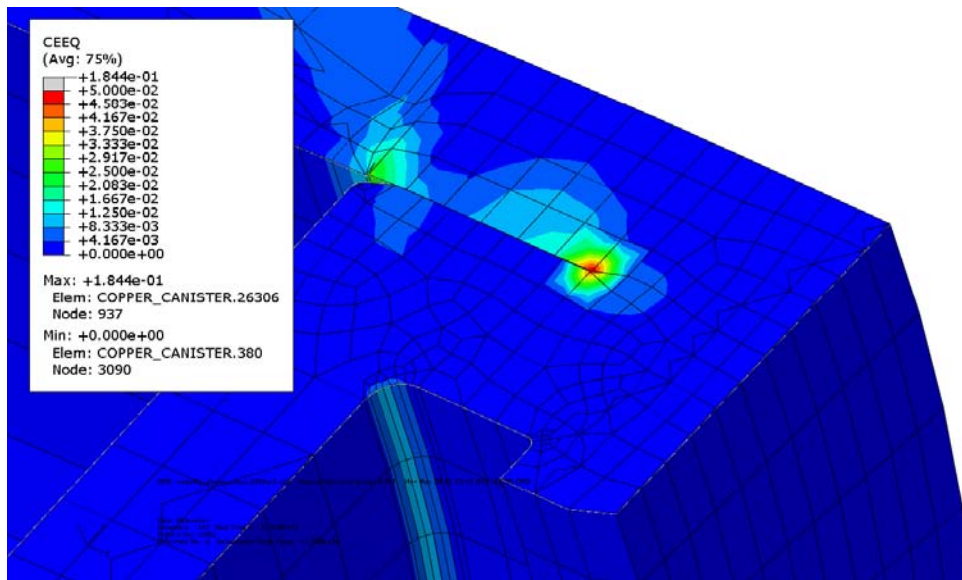


Figure 9-15. Detailed plot of equivalent creep strain (CEEQ) for the copper shell.

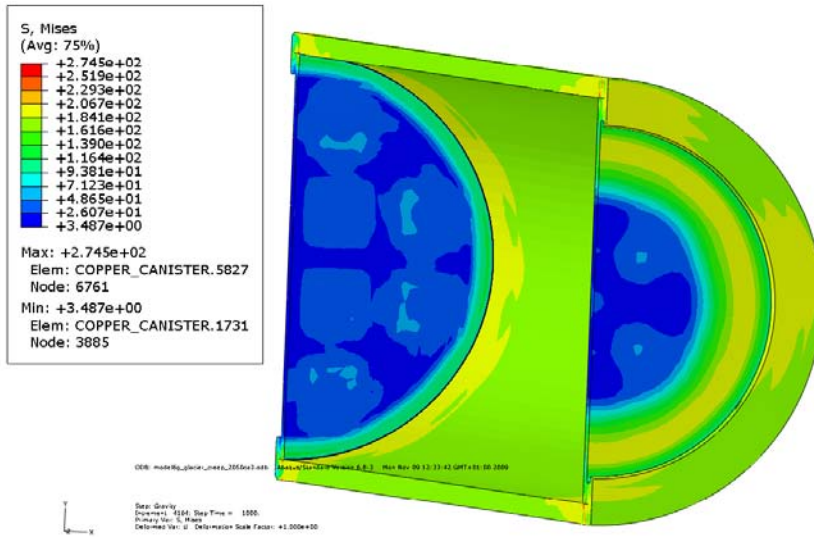


Figure 9-16. Mises stress after applied glacial load (1,000 seconds).

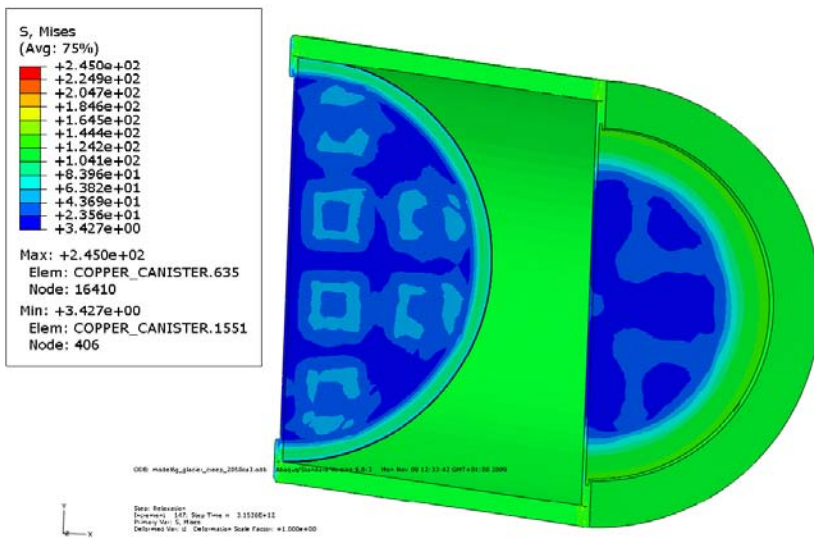


Figure 9-17. Mises stress after relaxation (100,000 years).



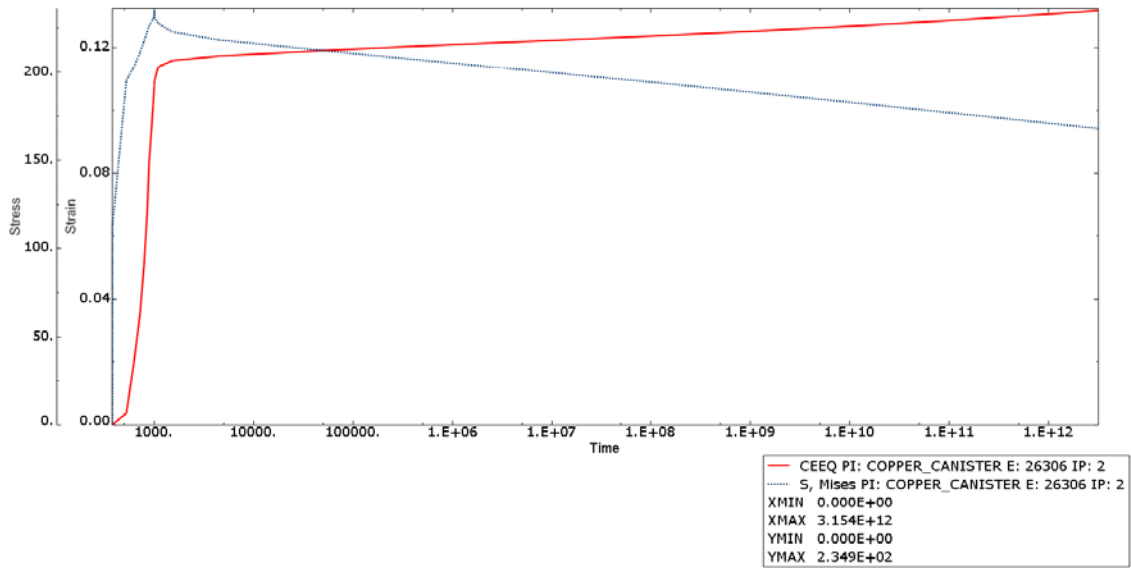


Figure 9-18. Mises stress and equivalent creep strain versus time for element 26306.

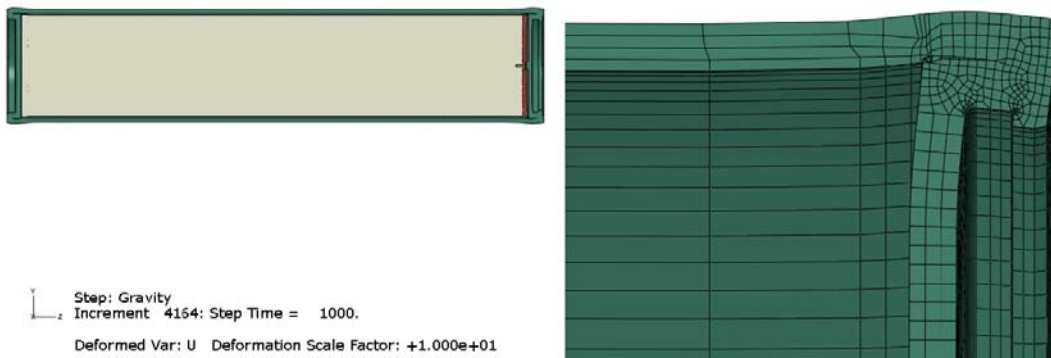


Figure 9-19. Deformed plot (displacements magnified by a factor of 10) after applied glacial load (1,000 seconds).

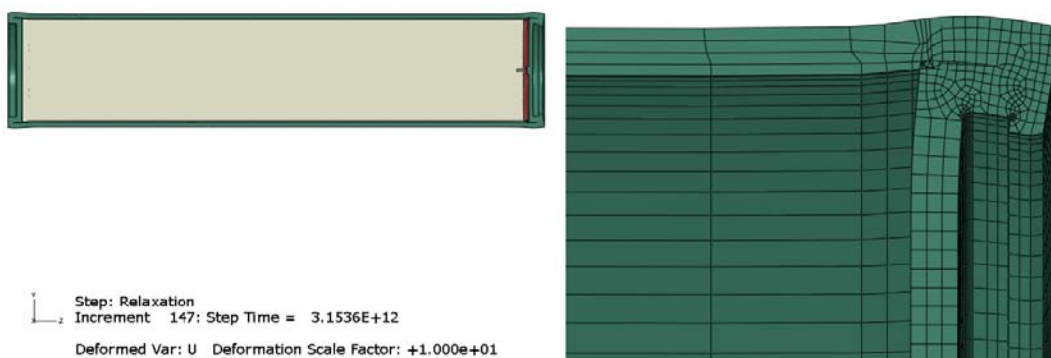
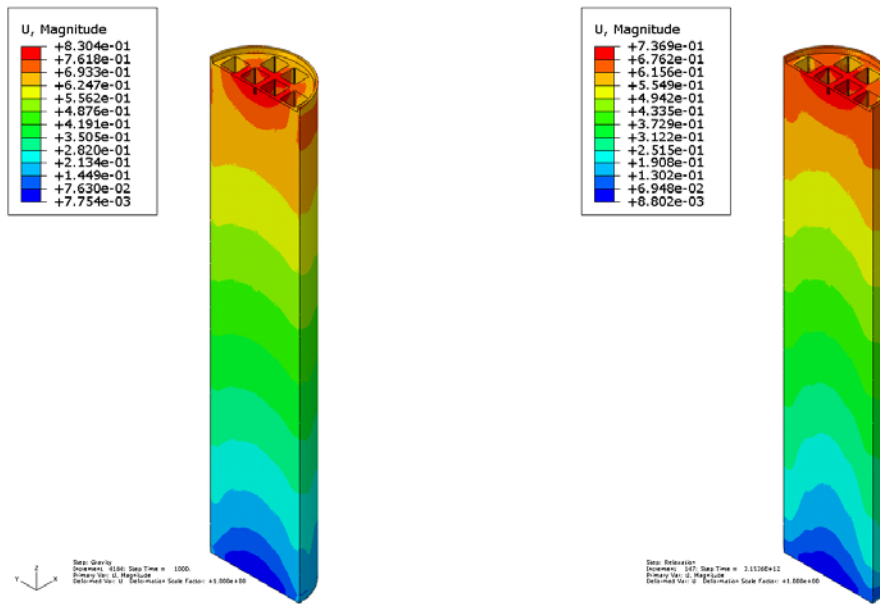
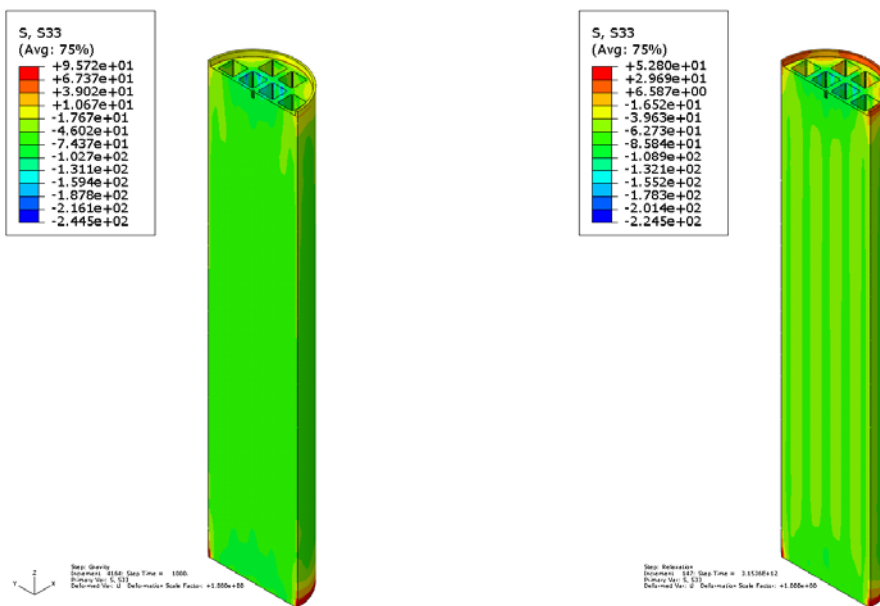


Figure 9-20. Deformed (displacements magnified by a factor of 10) plot after relaxation (100,000 years).



**Figure 9-21.** Magnitude of resultant displacement after applied load (left) and after relaxation (right).



**Figure 9-22.** Stress component in axial direction after applied glacial load (left) and after relaxation (right).

## 10 Uncertainties

The obtained results are based on several assumptions regarding loads and material properties. Also the discretization in the computer model will affect the results. Some of these influencing factors are addressed below:

- Strain rate effects for bentonite, copper and iron will affect the results. Copper shell will have the strain rate effect included when the creep model is used but most analyzes have been performed by using plasticity theory. The comparison, see Table 9-7, indicate that the creep model will reduce the maximum strain and stress level.
- The creep material model contains some uncertainties regarding the parameters defining the model. These are estimated to as most affect the creep strain rate by a factor of 5, see /Andersson-Östling and Sandström 2009/. The performed analysis did show low sensitivity for this uncertainty.
- All experiments used for material calibration have a spread which will imply a range for the properties defining each material model.
- Swelling pressure for the bentonite will affect the material stiffness. The experimental results have a spread in the results and the used data should be conservative in the sense that the obtained stress and strain magnitudes are overestimated.
- Element mesh is rather fine but nevertheless it is too coarse in some regions, especially at the welds and regions with geometric discontinuities. A more refined mesh will probably increase the maximum stress and strain levels. Fortunately, the use of non-linear material properties (such as plasticity and creep) will decrease the sensitivity on the used mesh. The used mesh has been judged to be accurate enough considering also the required computer resources to obtain the results. Since several models have been executed with different mesh densities it has been possible to compare and the conclusion is that the mesh in a global sense is accurate.
- The creep analysis in copper has been performed at 27°C but the material model data for the insert has experimental results for 0°C. The selection of these temperatures is made conservatively. The selection overestimates the creeping in copper and the stresses in the insert. The actual temperature is apparently between 0 and 27°C. Typically, Young's modulus differ less than one percent between these temperatures and a reasonable assumption is that the properties are accurate enough but has not so far been checked.
- Rock shear combined with glacial loads is treated in a simplified way:
  - For the case of a glacial before an earthquake, pore pressure elements have been used to add the hydrostatic pressure. However, the pore pressure has been prescribed to 30 MPa in the buffer for the following earthquake induced rock shear which corresponds to a very slow shearing displacement which probably will have an effect on the stresses and the strains. A more inhomogeneous pore pressure distribution will most likely increase the stresses and strains in the canister.
  - For the case of a glacial after an earthquake, a total stress theory has been used. The material model has been verified for fast shearing but will probably overestimate the stress level after long time (the pore pressure will be homogenized). The re-distribution of the effective stress in the buffer when adding the glacial load will be handled by rate-dependent material model for the bentonite.

# 11 Evaluation and conclusions

## 11.1 Rock shear analysis

The results obtained from the rock shear analyses could be summarized as:

- The stiffness of the bentonite has a great effect on stress and strain levels both for the copper shell and the insert (increased stiffness implies increased stress levels).
- The maximum plastic strain in copper shell occurs in fillets (besides regions containing singularities). At the global level the plastic strains are much lower. However, for inclined shearing (22.5 degrees) in tension, the plastic strain is high at the flange (region 9, the top reminding geometry) but is considered to not cause any severe damage even for the stiffest bentonite since this occurs in a very localized region and furthermore the load is displacement controlled. The maximum plastic strains in the insert occur at the corners of a specific channel. However, the magnitude is small compared to ultimate strains and is considered not to cause any severe damage.
- Maximum principal stress in the insert mainly comes from bending of the shell – the level depends mainly on material properties for the insert (and dimensions) and buffer.
- Creep does not seem to be a major concern since the copper deformation is controlled by the surrounding material which implies small creep strain rates as soon as the final deformation has been established. Also the bentonite will have some creep which will lower the stress level in the copper and thus contribute to less creep in the copper.
- Maximum creep strain (CEEQ) is close to maximum plastic strain (PEEQ) when comparing elastic-plastic and creep models.
- Material dependency on strain rate has been considered for all parts except for copper, which uses an elastic-plastic model with an estimated strain rate. However, models containing “creep” in the model name have been analyzed using the creep material model and for these cases the copper also contains strain rate dependency.
- The hydrostatic case might need additional calculations since the used material model for the bentonite is not the correct one. However, the obtained results indicate the glacial load case in combination with rock shear is not the most critical ones.
- Finally, a comparison between the BWR and PWR canister shows that as expected, the stress and strain magnitudes with equal load assumptions are considerably lower in the PWR canister than in the BWR canister (assuming the same material properties).

The conclusions based on improved FE-model, more accurate material models and geometry will in general lead to similar conclusions as obtained by previous studies. This could be summarized as:

- The improved mesh implies an increased maximum strain magnitude, which is expected. The highest values are very local – on the global level the values are close to those previously calculated.
- The reference material for the buffer has been changed to Ca-bentonite with density 2,050 kg/m<sup>3</sup>, which will imply increased strains in both the copper shell and the cast iron insert.
- Using rate-dependent material (creep) for the copper shell decreases the maximum strain in the copper shell and has a minor influence on the strain magnitude for the insert, which also was the conclusion based on previous calculations. The reason for this is that the rate-dependency will make the material stiffer during the shearing which will decrease the strain even though creep in general will increase the strain after long time.
- In previous calculations the inclined shearing (22.5 degrees) was most harmful for the copper shell but now the rock shear perpendicular to the canister axis at the midpoint seems to cause the largest plastic strains. This is most evidently due to the better modeling of the fillets but also the more accurate modeling of the buffer, which distributes the loading better and then decreases the previously reported extreme values.

## 11.2 Rock shear combined with glacial loads

Two cases are simulated:

- A glacial load of 30 MPa followed by an earthquake induced rock shear displacement of 5 and 10 cm.
  - Plastic strains decrease in the iron insert and the steel channels compared with the corresponding reference case.
  - Mises stress increases in the iron insert and steel channels compared with the reference case.
  - Axial stress decreases in the iron insert compared with the reference case.
  - Plastic strains increase in the copper shell (maximum 17% compared to 16%) at 10 cm shearing. However, this is at a very local spot where the geometry is discontinuous. In the mid shell the maximum value is 1.4% compared to 2.0% for the reference case.
- An earthquake induced rock shear displacement of 5 or 10 cm followed by a glacial load of 30 MPa.
  - Plastic strains increase in the iron insert and the steel channels compared with the corresponding reference case. However, the magnitudes are rather low.
  - Mises stress increase in the iron insert and the steel channels but the axial stress in the iron insert decrease compared with the reference case.
  - Plastic strains increase in copper shell (maximum 23% compared to 16%) at 10 cm shearing. However, this is at a very local spot where the geometry is discontinuous. In the mid shell the maximum value is 2.7% compared to 2.0% for the reference case.

## 11.3 Glacial load

The results obtained from glacial load analysis could be summarized as:

- The maximum plastic strains in the insert occur at the corners of a specific channel. However, the magnitude is rather low.
- The maximum creep strain in copper shell occurs where the lid is welded to the flange. At the global level the strains are much lower.
- The copper shell will deform when the glacial load is applied but mainly the initial gaps will be closed. The insert will have displacements less than 1 millimeter. The displacements due to creep in the shell does not seem to affect the initial geometry used for a following earthquake induced rock shear analysis.
- The stresses in the insert are mostly in compression and much below the yield stress.

## 12 References

SKB's (Svensk Kärnbränslehantering AB) publications can be found at [www.skb.se/publications](http://www.skb.se/publications).  
References to SKB's unpublished documents are listed separately at the end of the reference list.  
Unpublished documents will be submitted upon request to [document@skb.se](mailto:document@skb.se).

**Andersson-Östling H C M, Sandström R, 2009.** Survey of creep properties of copper intended for nuclear waste disposal. SKB TR-09-32, Svensk Kärnbränslehantering AB.

**Börgesson L, 1986.** Model shear tests of canisters with smectite clay envelopes in deposition holes. SKB TR 86-26, Svensk Kärnbränslehantering AB.

**Börgesson L, Hernelind J, 2006.** Earthquake induced rock shear through a deposition hole. Influence of shear plane inclination and location as well as buffer properties on the damage caused to the canister. SKB TR-06-43, Svensk Kärnbränslehantering AB.

**Börgesson L, Johannesson L-E, Sandén T, Hernelind J, 1995.** Modelling of the physical behavior of water saturated clay barriers. Laboratory tests, material models and finite element application. SKB TR 95-20, Svensk Kärnbränslehantering AB.

**Börgesson L, Johannesson L-E, Hernelind J, 2004.** Earthquake induced rock shear through a deposition hole. Effect on the canister and the buffer. SKB TR-04-02, Svensk Kärnbränslehantering AB.

**Börgesson L, Dueck A, Johannesson L-E, 2010.** Material model for shear of the buffer. Evaluation of laboratory test results. SKB TR-10-31, Svensk Kärnbränslehantering AB.

**Dillström P, Alverlind P, Andersson M, 2010.** Framtagning av acceptanskriterier samt skadetålighetsanalyser av segjärnsinsatsen. SKB R-10-11, Svensk Kärnbränslehantering AB.

**Hernelind J, 2006.** Earthquake induced rock shear through a deposition hole when creep is considered – first model. Effect on the canister and the buffer. SKB R-06-87, Svensk Kärnbränslehantering AB.

**Jin L-Z, Sandström R, 2008.** Creep of copper canisters in power-law breakdown. Computational Materials Science, 43, pp 403–416.

**Sandström R, Andersson H C M, 2008.** Creep in phosphorus alloyed copper during power-law breakdown. Journal of Nuclear Materials, 372, pp 76–88.

**Sandström R, Hallgren J, Burman G, 2009.** Stress strain flow curves for Cu-OFP. SKB R-09-14, Svensk Kärnbränslehantering AB.

**SKB, 2009.** Design premises for a KBS-3V repository based on results from the safety assessment SR-Can and some subsequent analyses. SKB TR-09-22, Svensk Kärnbränslehantering AB.

**SSAB, 2008.** Domex – New Steelfacts. [Online]. Available at:  
<https://steelfactssvc.ssab.com/steelfact/strain.aspx?product=DOMEX355MC> [August 1, 2010]

**SS-EN 10025-2:2004.** Hot rolled products of structural steels – Part 2: Technical delivery conditions for non-alloy structural steels. Stockholm: Swedish Standards Institute.

### Unpublished documents

SKBdoc id, version	Title	Issuer, year
1203875 ver 1.0	Ritningsförteckning för kapselkomponenter	SKB, 2009
1201865 ver 1.0	Dragprovning av gjutjärn	KTH, 2009

**Short term rock shear perpendicular to canister axis at quarter point 2050ca3**

Plots showing deformed geometry, plastic strain (PEEQ), Mises stress (MISES) for shearing magnitudes 5 and 10 cm.

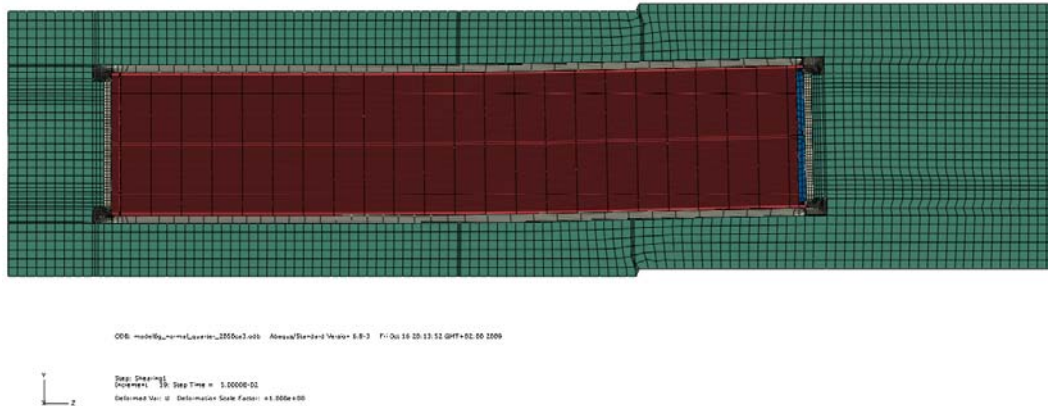


*Figure A1-1. Deformed plot – 5 cm shearing magnitude.*

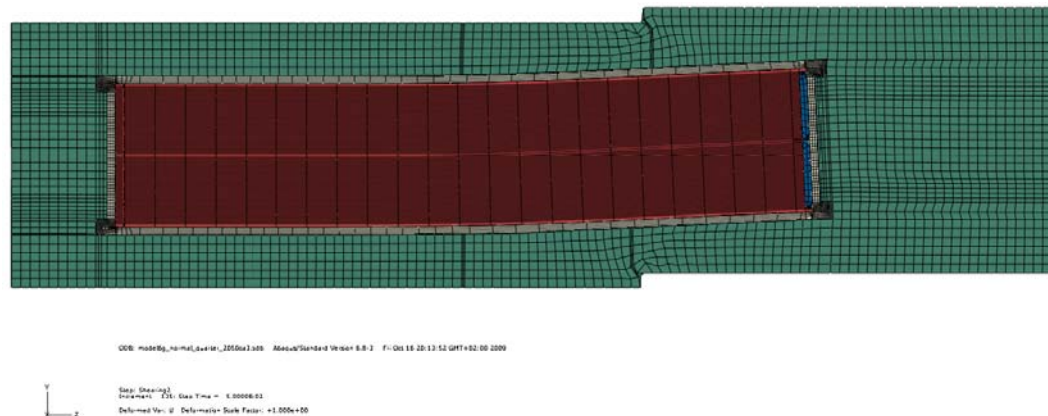


*Figure A1-2. Deformed plot – 10 cm shearing magnitude.*

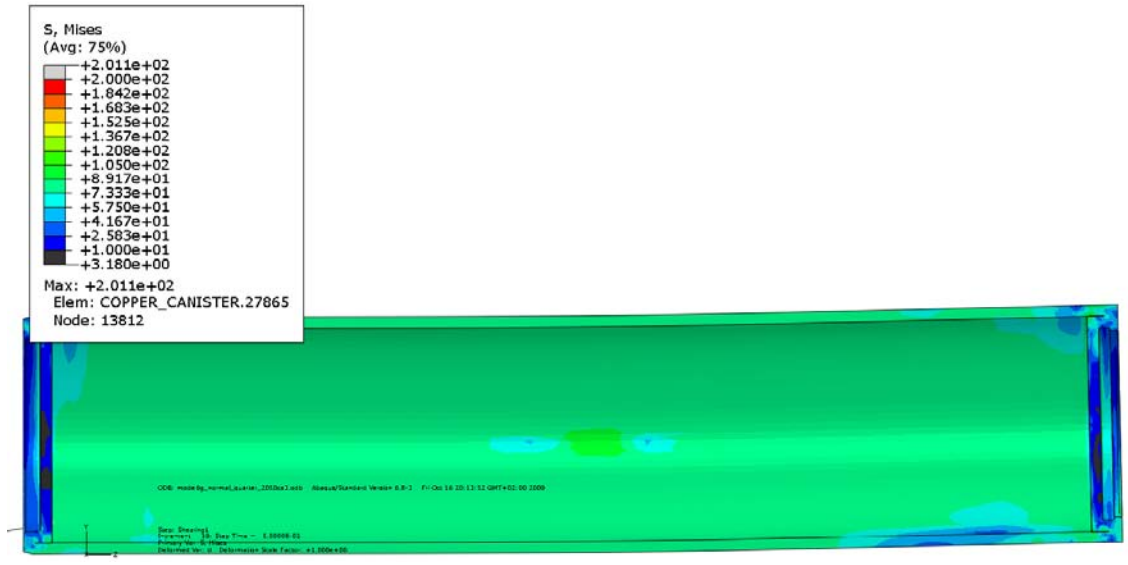


Figure A1-3. Mises stress for copper shell – 5 cm shearing magnitude.

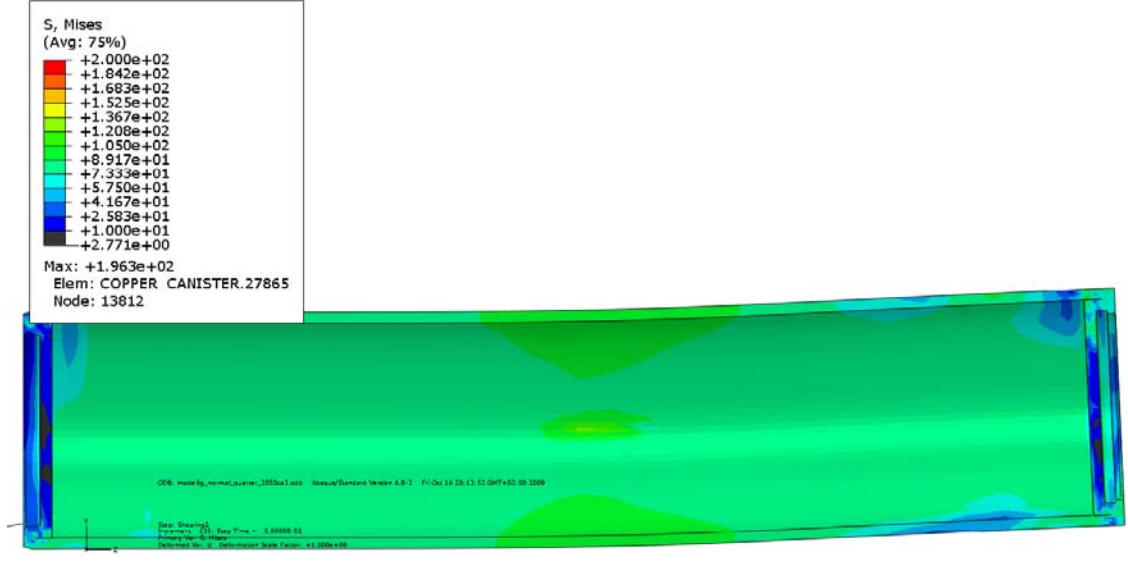


Figure A1-4. Mises stress for copper shell – 10 cm shearing magnitude.



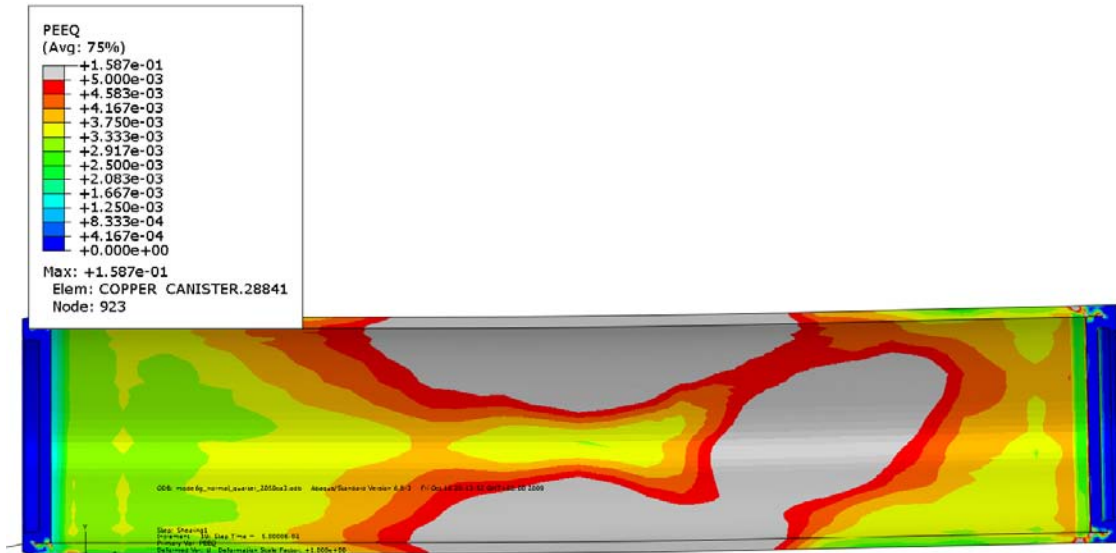


Figure A1-5. Plastic strain (PEEQ) for copper shell – 5 cm shearing magnitude.

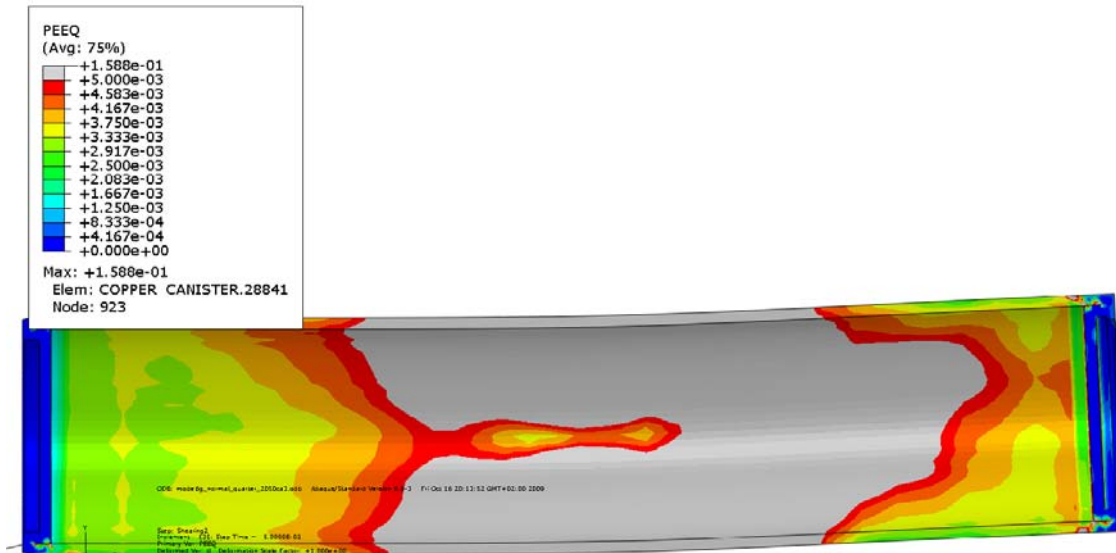


Figure A1-6. Plastic strain (PEEQ) for copper shell – 10 cm shearing magnitude.

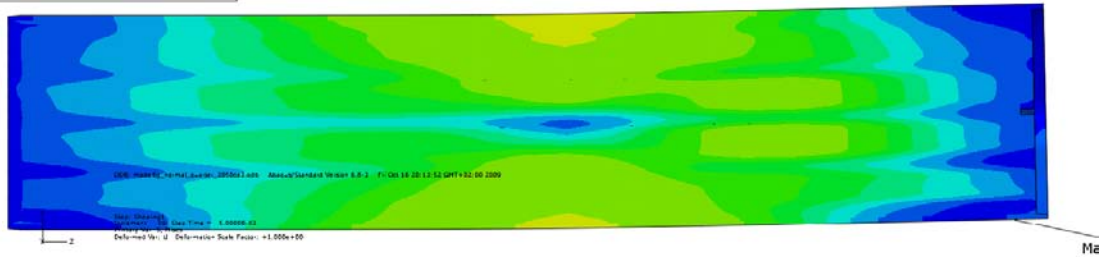
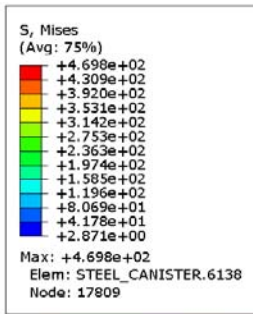


Figure A1-7. Mises stress for insert – 5 cm shearing magnitude.

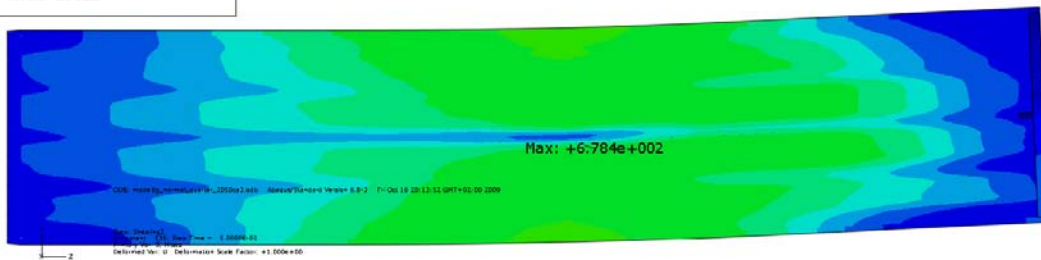
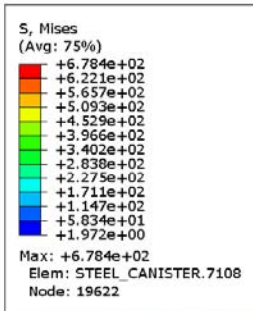


Figure A1-8. Mises stress for insert – 10 cm shearing magnitude.

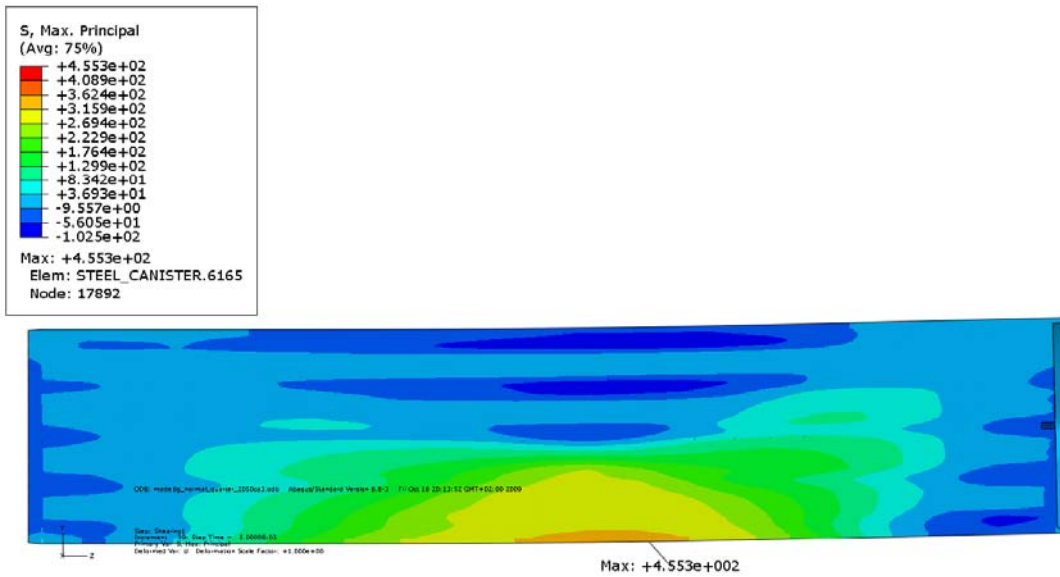


Figure A1-9. Max principal stress for insert – 5 cm shearing magnitude.

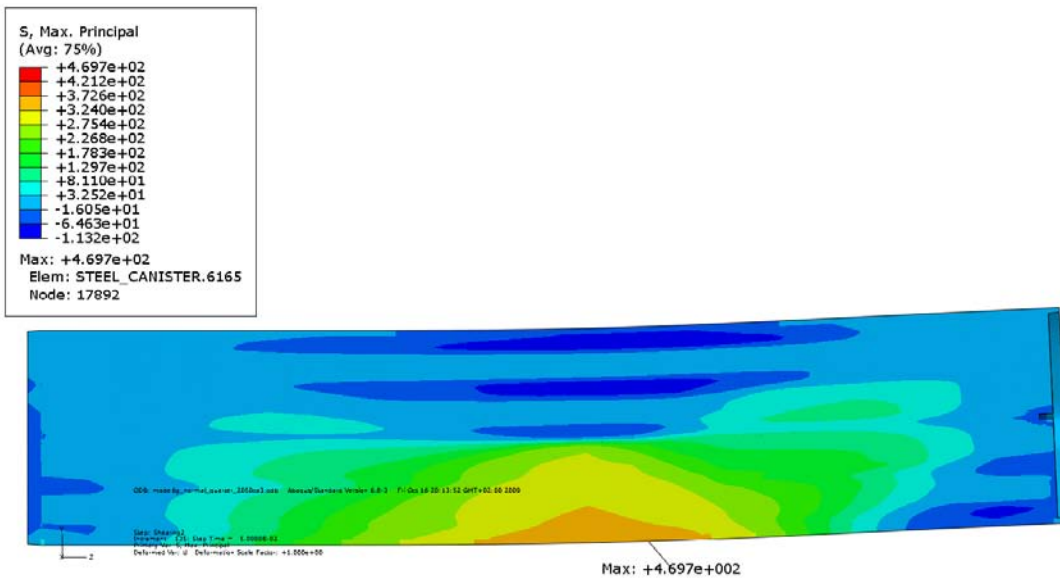


Figure A1-10. Max principal stress for insert – 10 cm shearing magnitude.

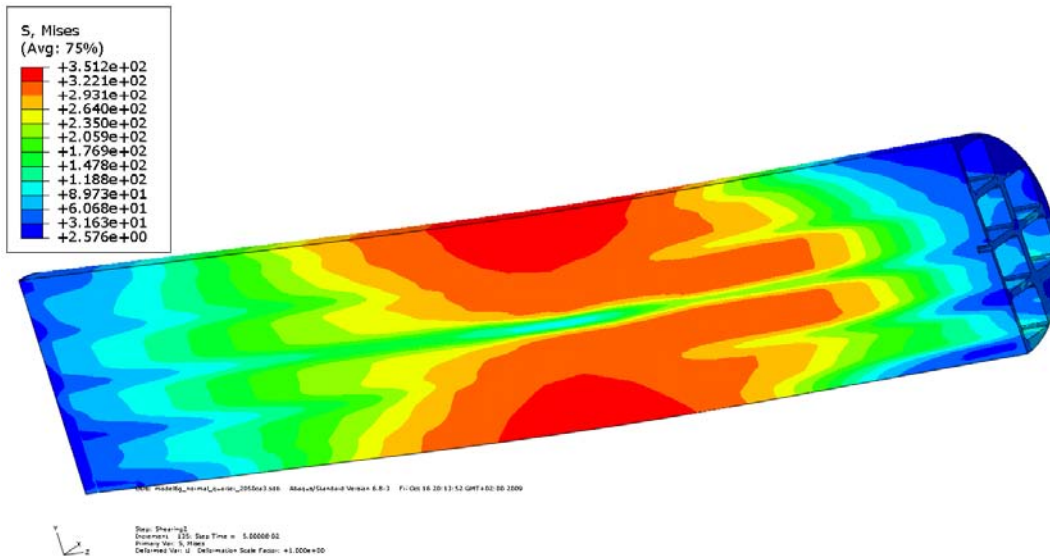


Figure A1-11. Mises stress in cast iron insert – 10 cm shearing magnitude.

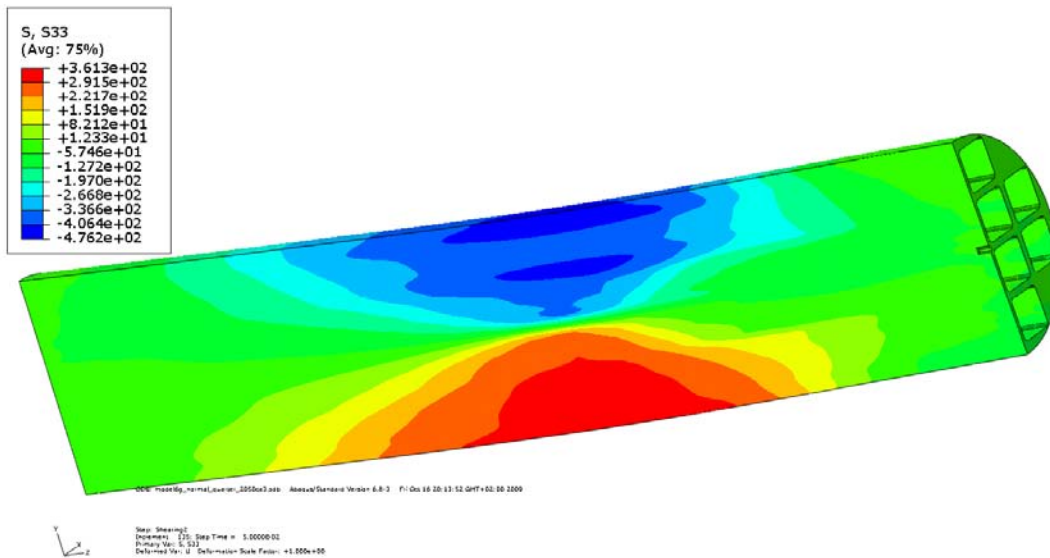


Figure A1-12. Axial stress (S33) in cast iron insert – 10 cm shearing magnitude.

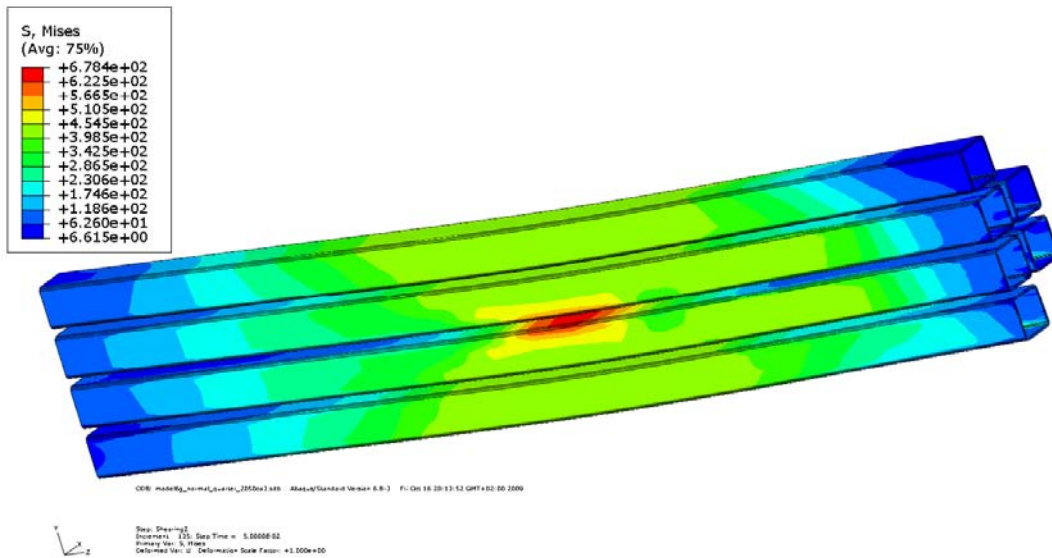


Figure A1-13. Mises stress in steel channels – 10 cm shearing magnitude.

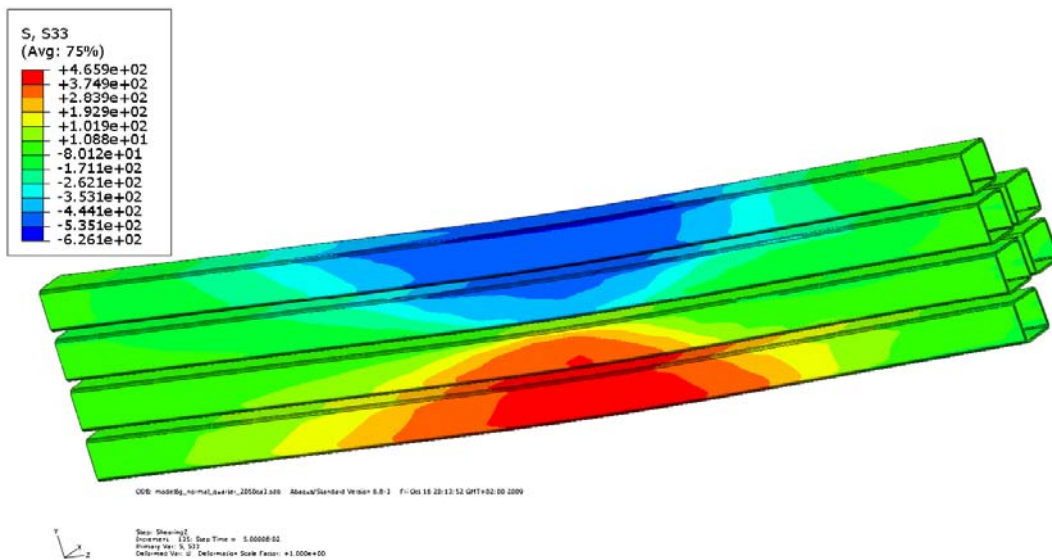


Figure A1-14. Axial stress (S33) in steel channels – 10 cm shearing magnitude.

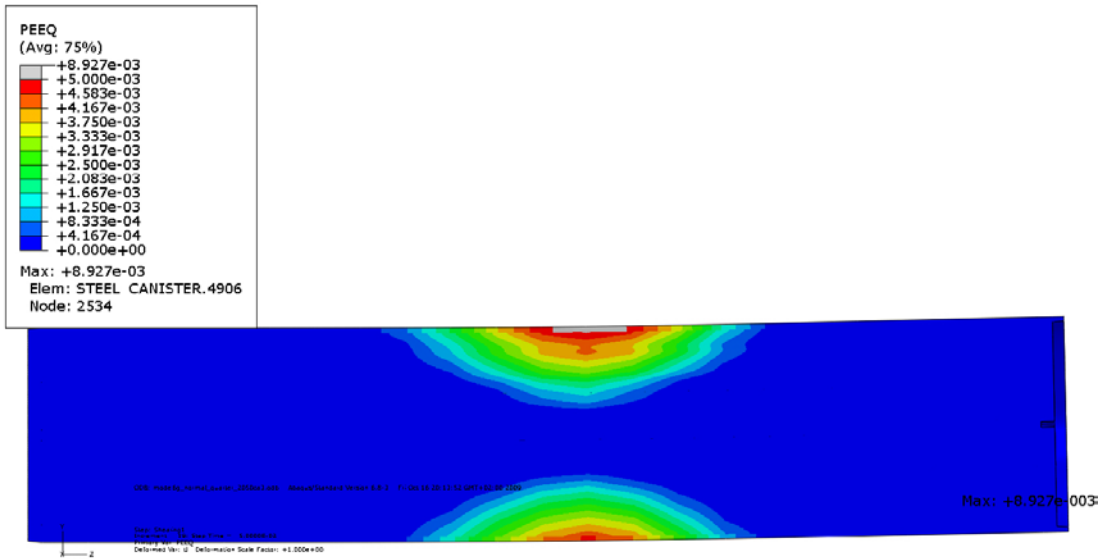


Figure A1-15. Plastic strain (PEEQ) for insert – 5 cm shearing magnitude.

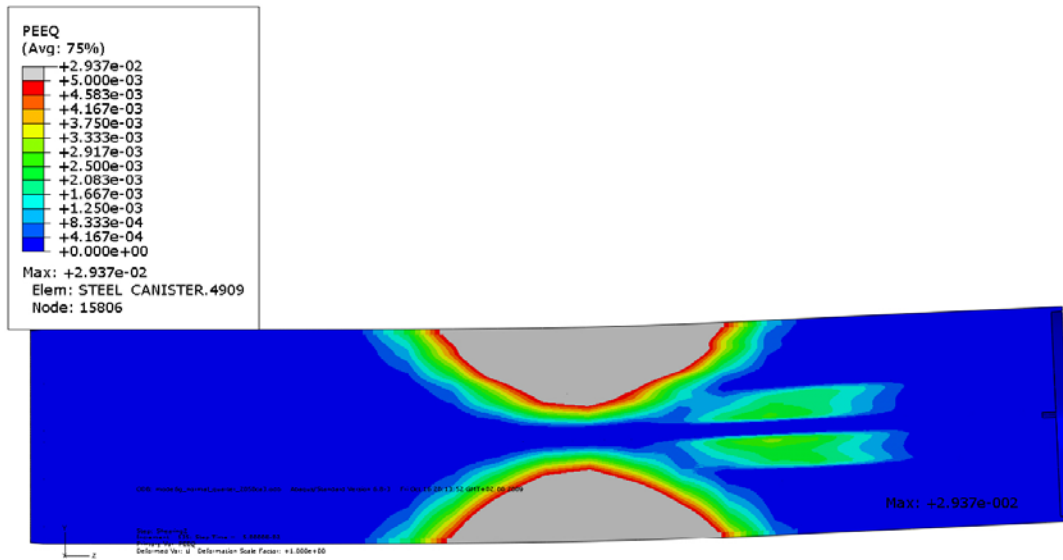


Figure A1-16. Plastic strain (PEEQ) for insert – 10 cm shearing magnitude.

**Short term rock shear perpendicular to canister axis at mid point 2050ca3**

Plots showing deformed geometry, plastic strain (PEEQ), Mises stress (MISES) for shearing magnitudes 5 and 10 cm.



*Figure A2-1. Deformed plot – 5 cm shearing magnitude.*

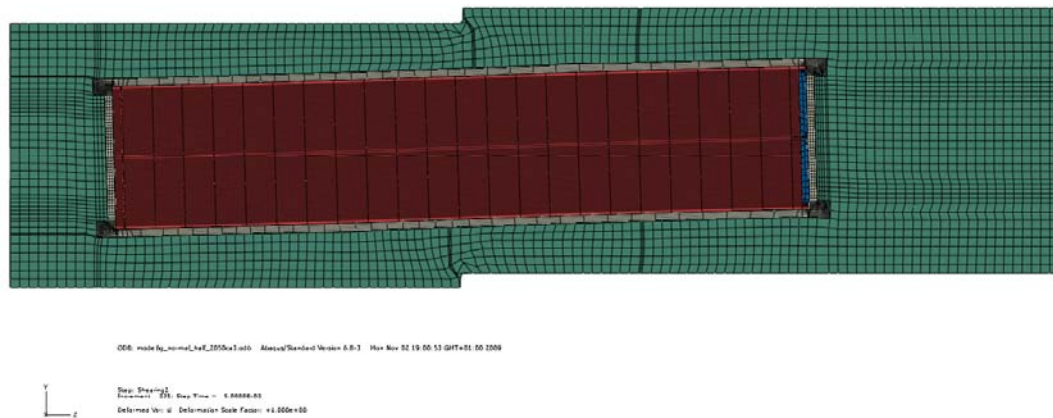


*Figure A2-2. Deformed plot – 10 cm shearing magnitude.*

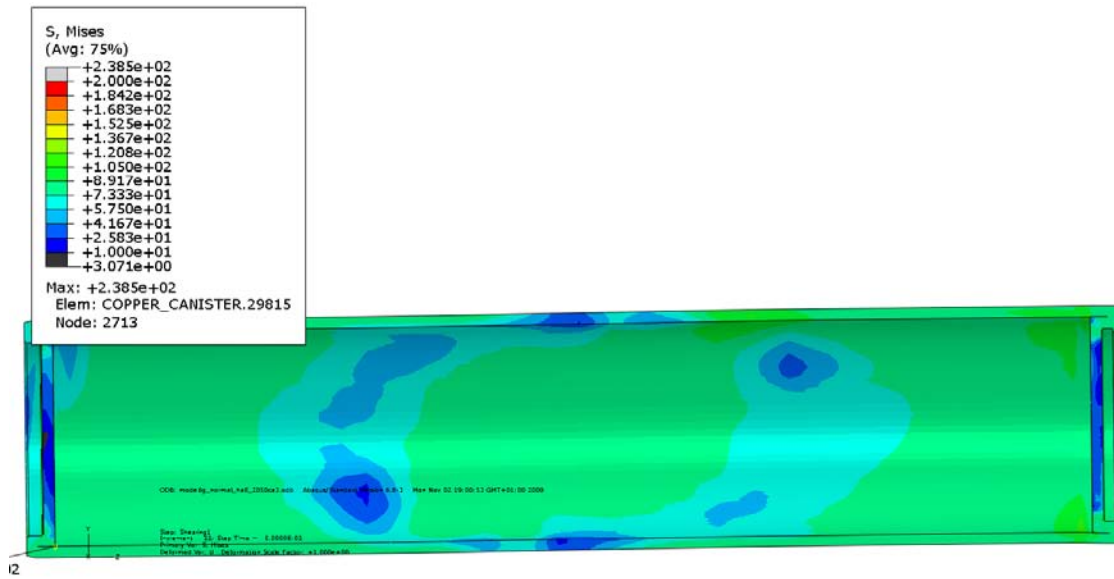


Figure A2-3. Mises stress for copper shell – 5 cm shearing magnitude.

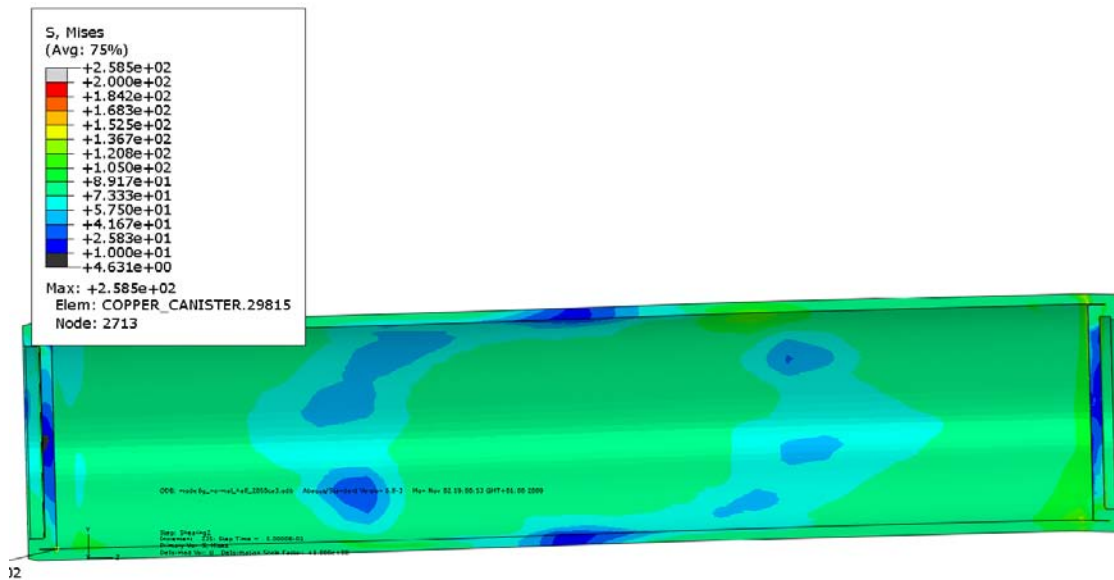


Figure A2-4. Mises stress for copper shell – 10 cm shearing magnitude.



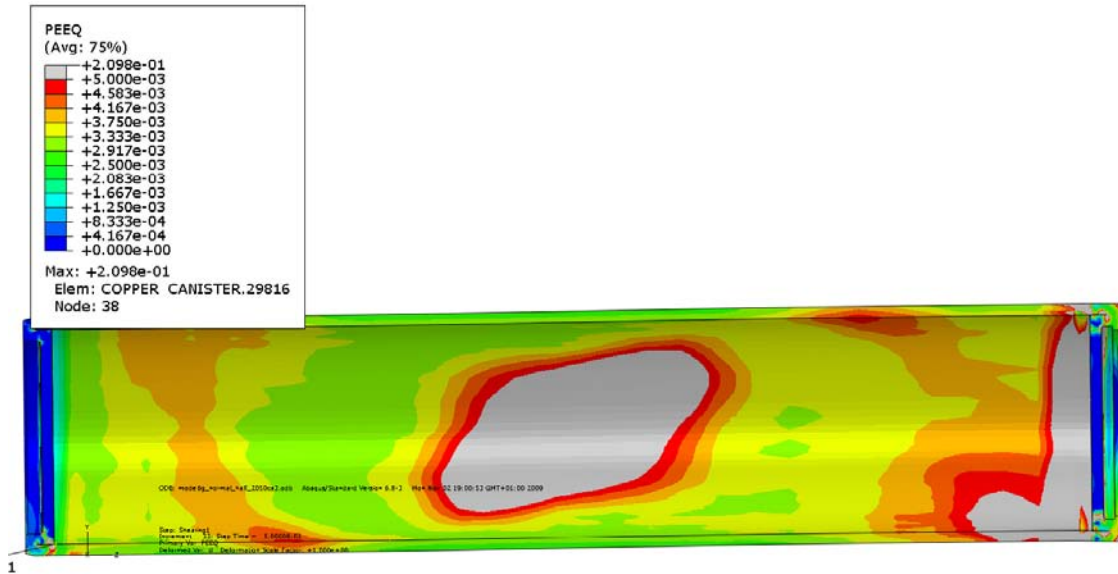


Figure A2-5. Plastic strain (PEEQ) for copper shell – 5 cm shearing magnitude.

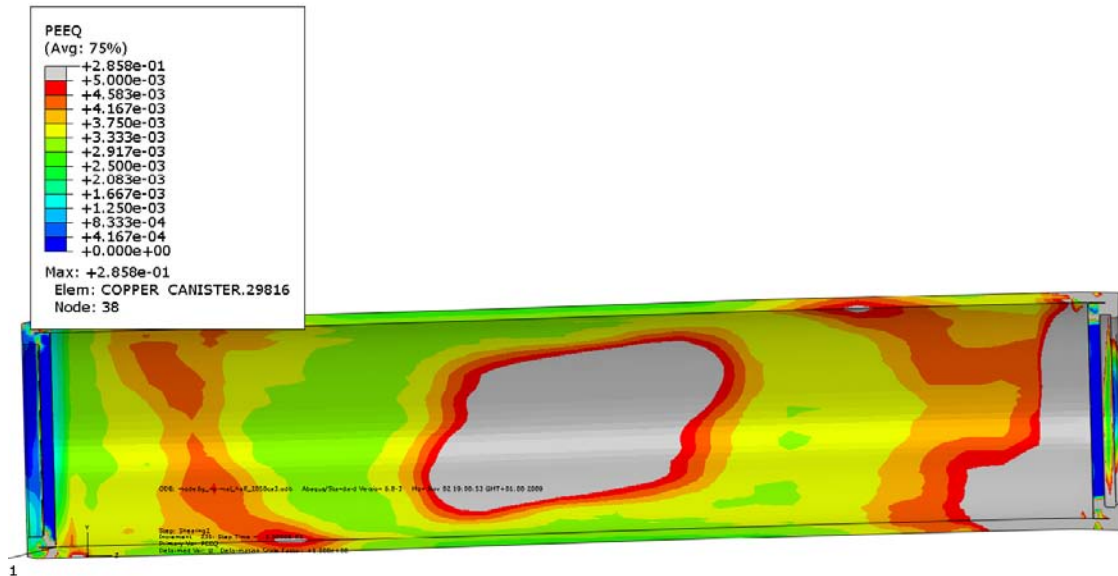


Figure A2-6. Plastic strain (PEEQ) for copper shell – 10 cm shearing magnitude.

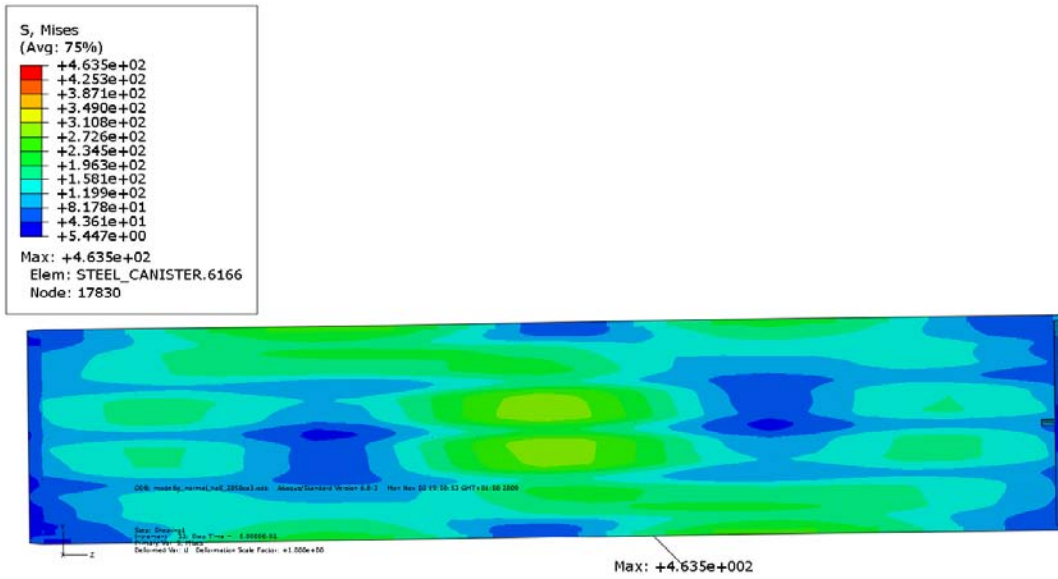


Figure A2-7. Mises stress for insert – 5 cm shearing magnitude.

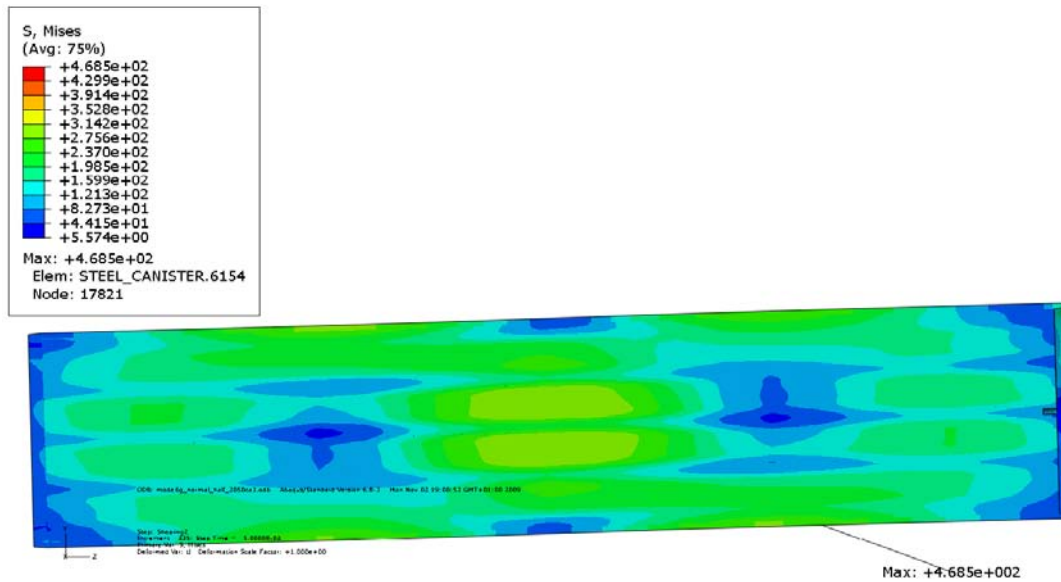


Figure A2-8. Mises stress for insert – 10 cm shearing magnitude.

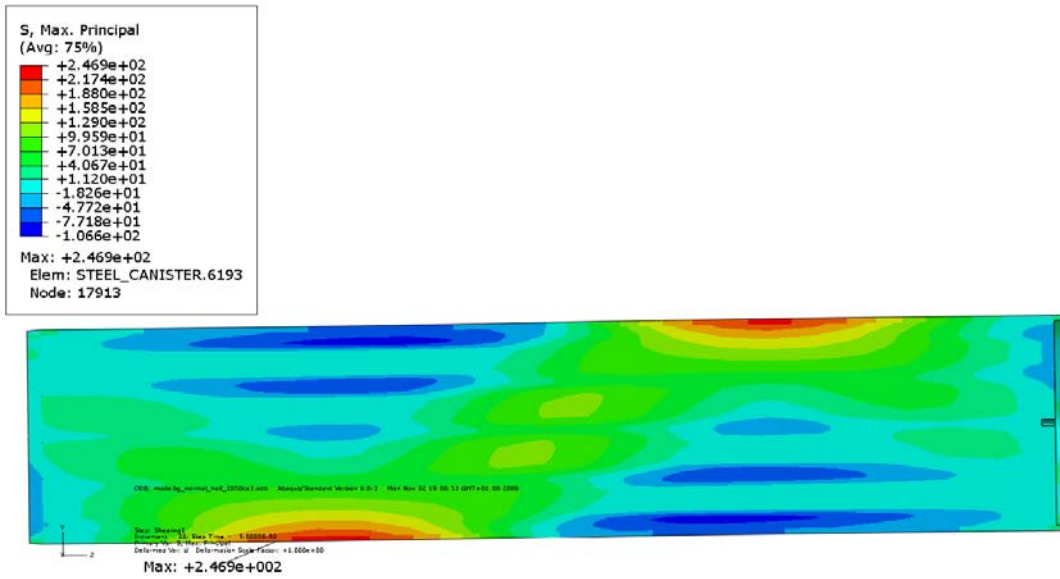


Figure A2-9. Max principal stress for insert – 5 cm shearing magnitude.

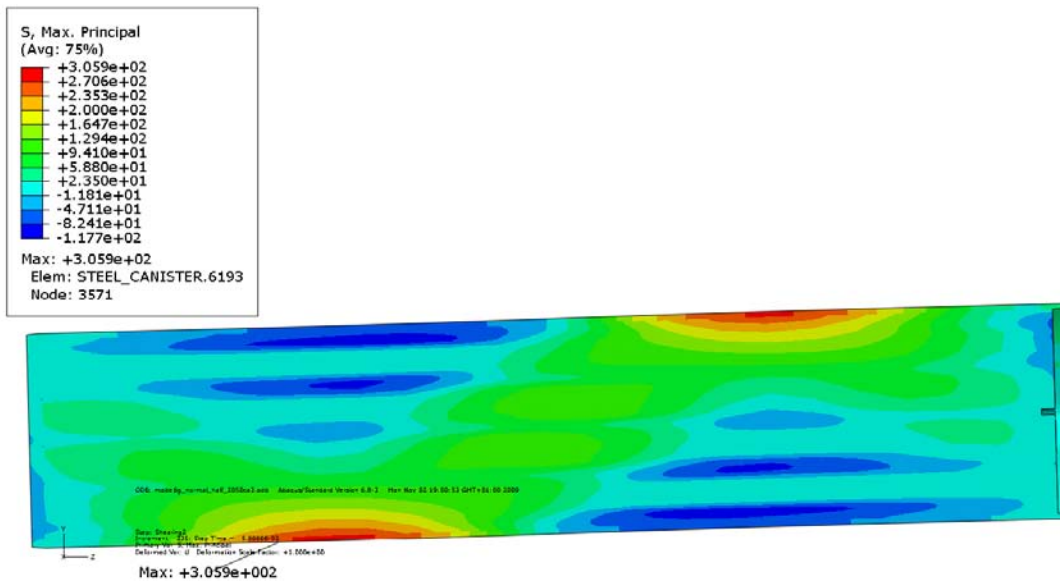


Figure A2-10. Max principal stress for insert – 10 cm shearing magnitude.

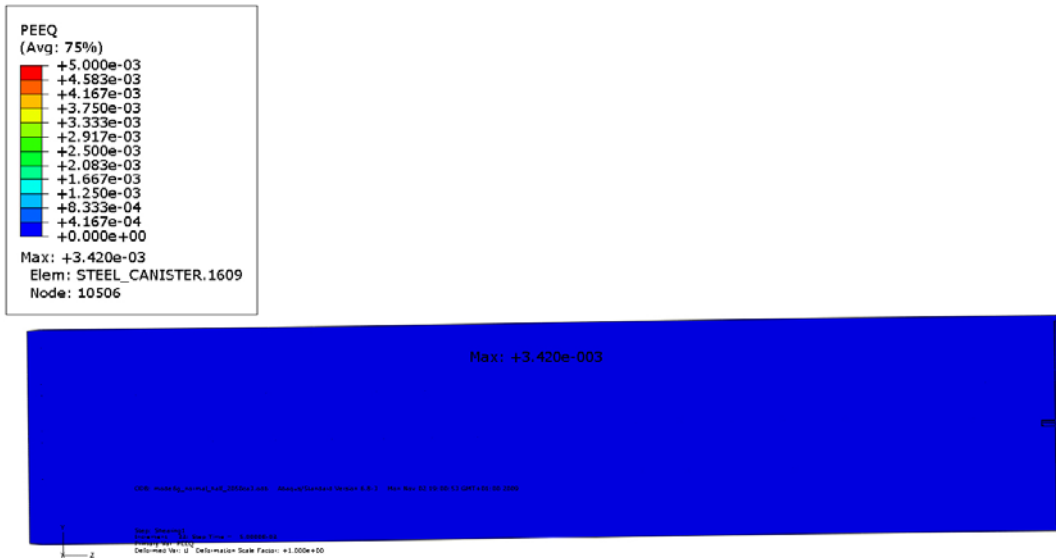


Figure A2-11. Plastic strain (PEEQ) for insert – 5 cm shearing magnitude.

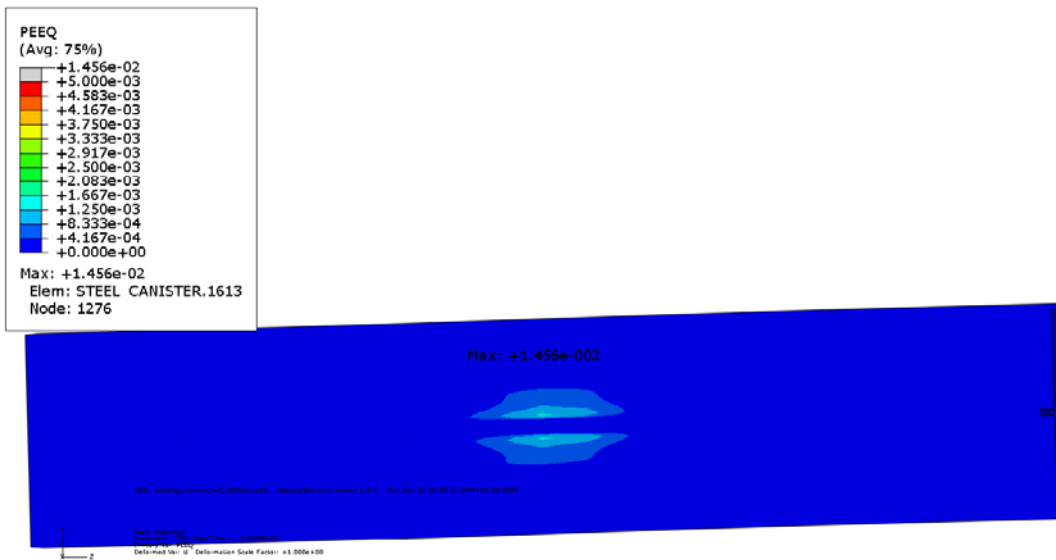
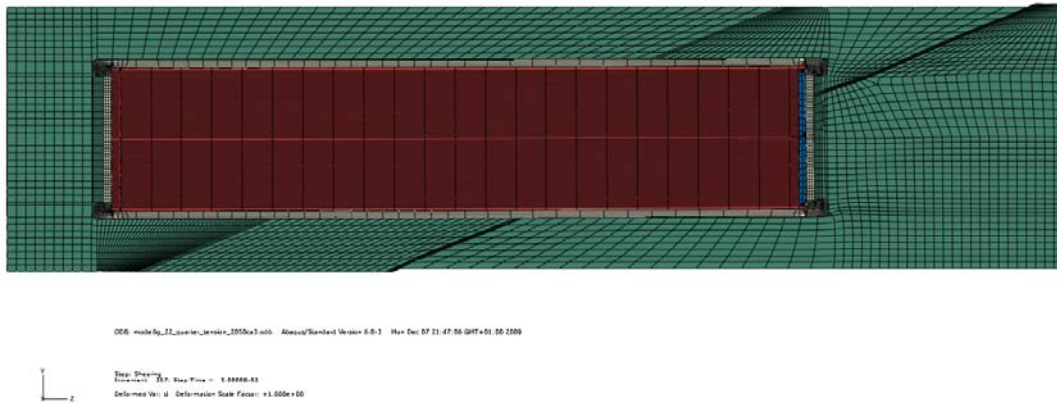


Figure A2-12. Plastic strain (PEEQ) for insert – 10 cm shearing magnitude.

**Short term rock shear inclined 22.5 degrees to canister axis at quarter point 2050ca3 (tension)**

Plots showing deformed geometry, plastic strain (PEEQ), Mises stress (MISES) for shearing magnitudes 5 and 10 cm.



*Figure A3-1. Deformed plot – 5 cm shearing magnitude.*

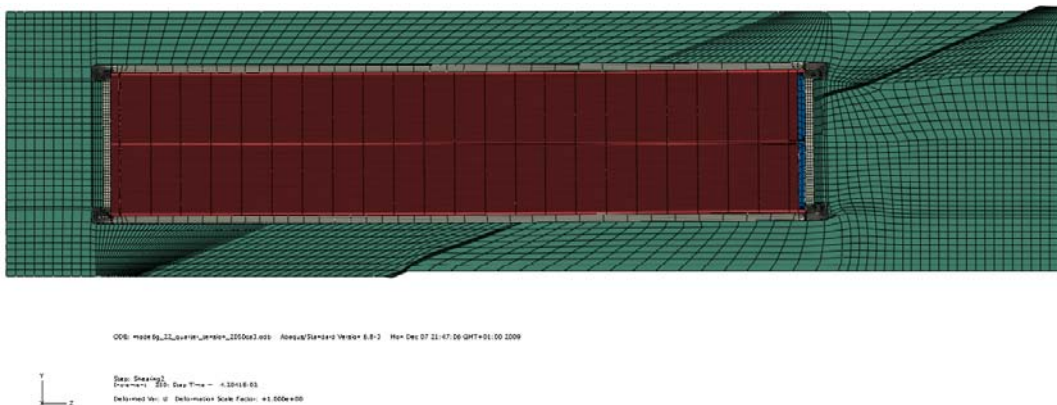


*Figure A3-2. Deformed plot – 10 cm shearing magnitude.*

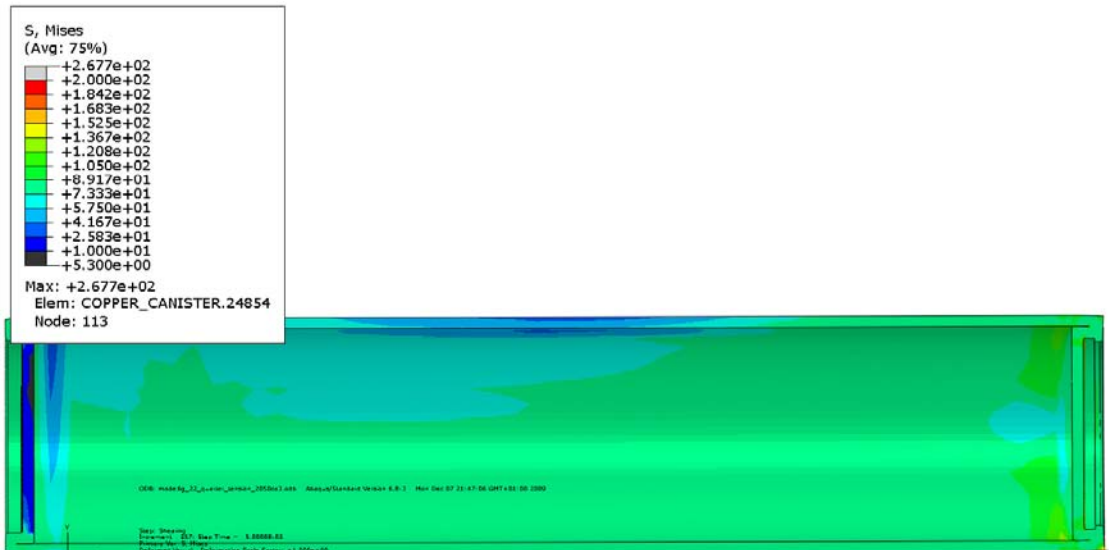


Figure A3-3. Mises stress for copper shell – 5 cm shearing magnitude.

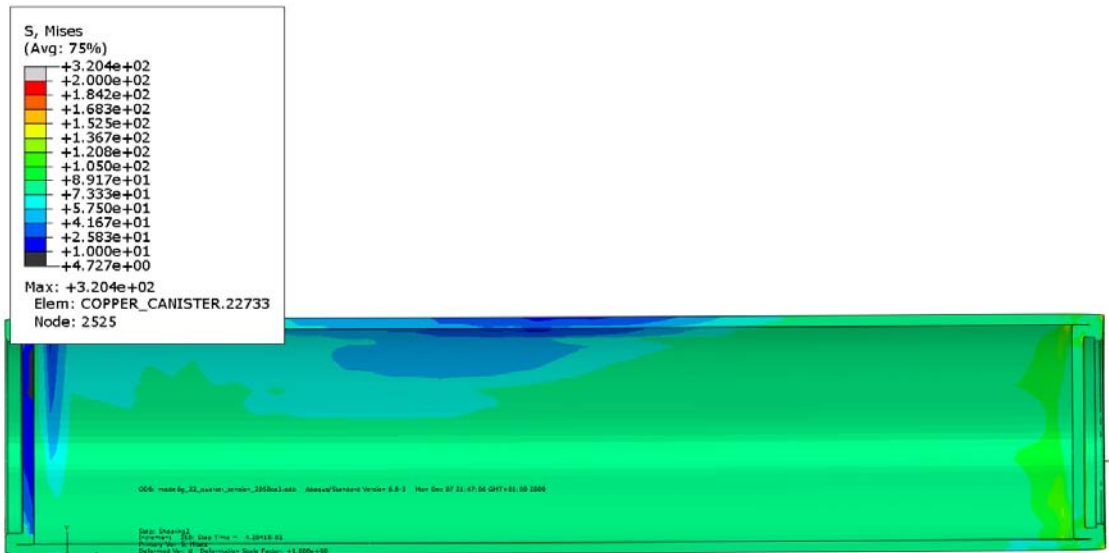


Figure A3-4. Mises stress for copper shell – 10 cm shearing magnitude.

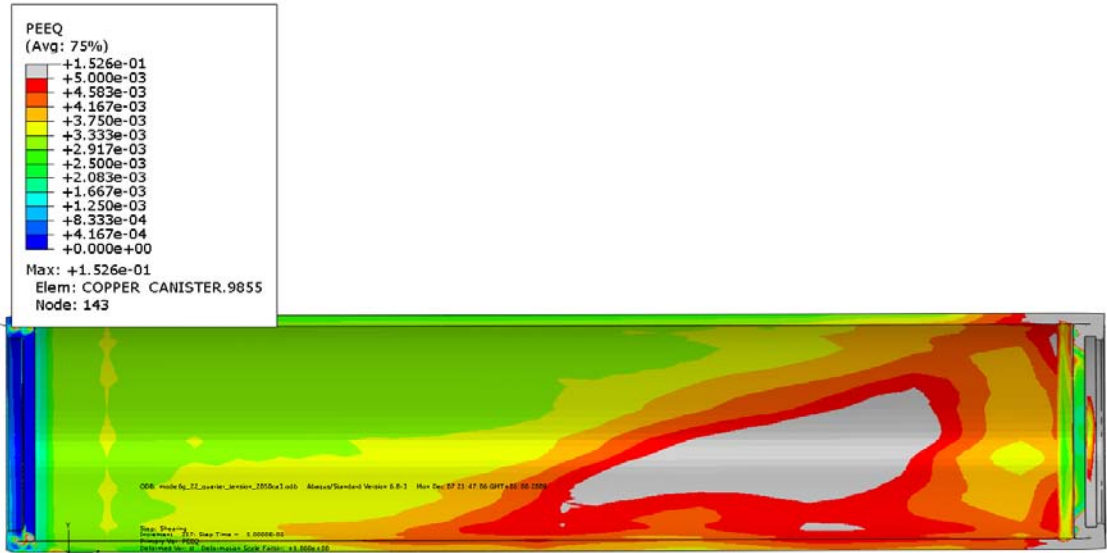


Figure A3-5. Plastic strain (PEEQ) for copper shell – 5 cm shearing magnitude.

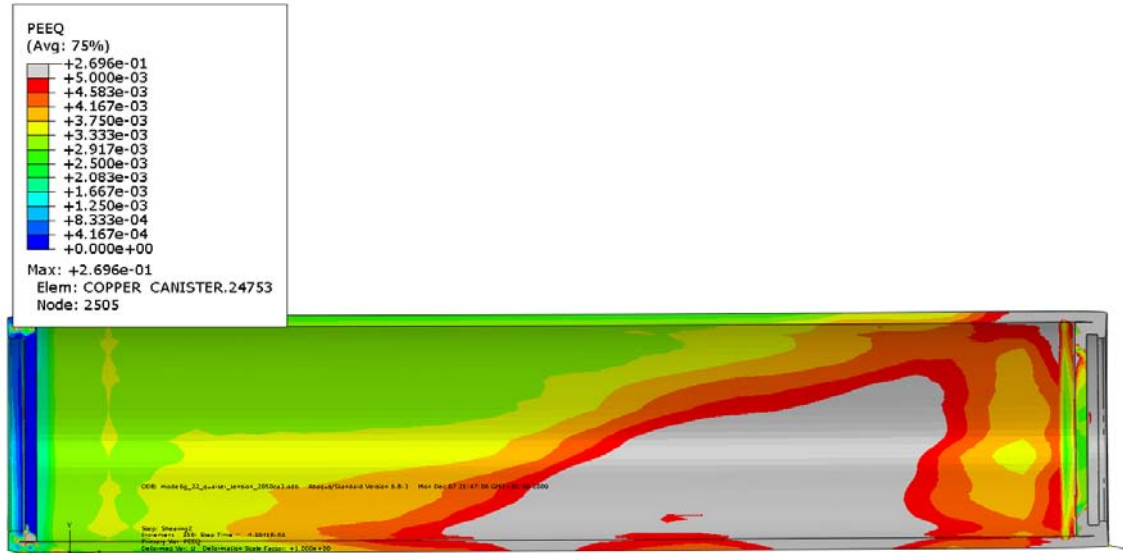


Figure A3-6. Plastic strain (PEEQ) for copper shell – 10 cm shearing magnitude.

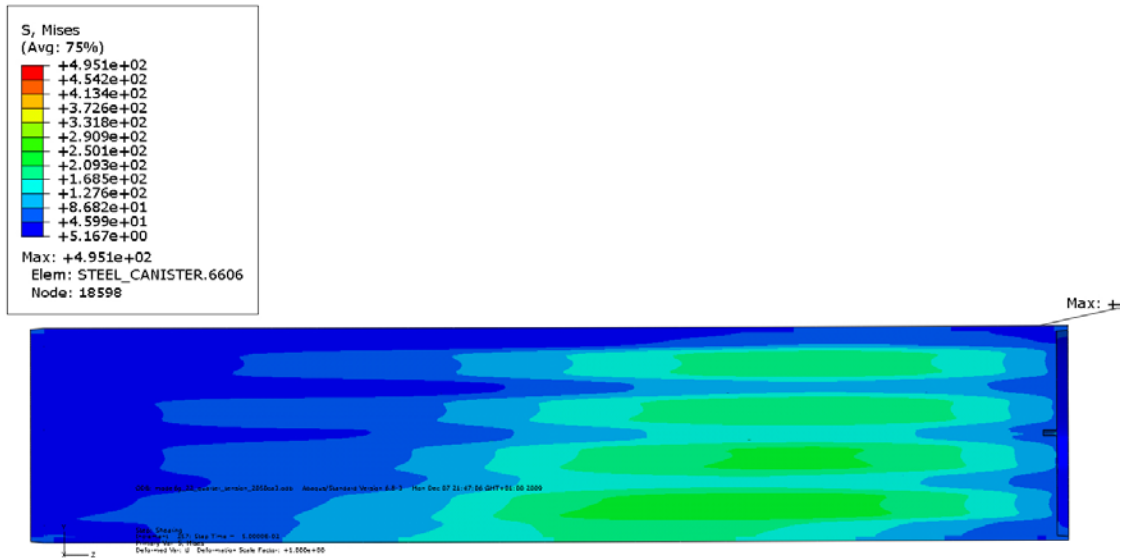


Figure A3-7. Mises stress for insert – 5 cm shearing magnitude.

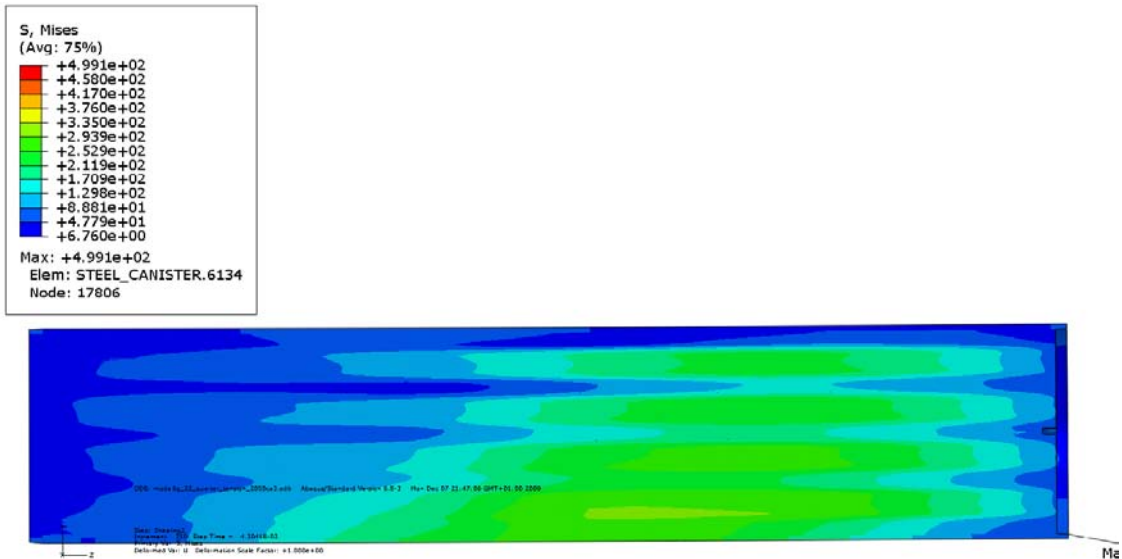


Figure A3-8. Mises stress for insert – 10 cm shearing magnitude.



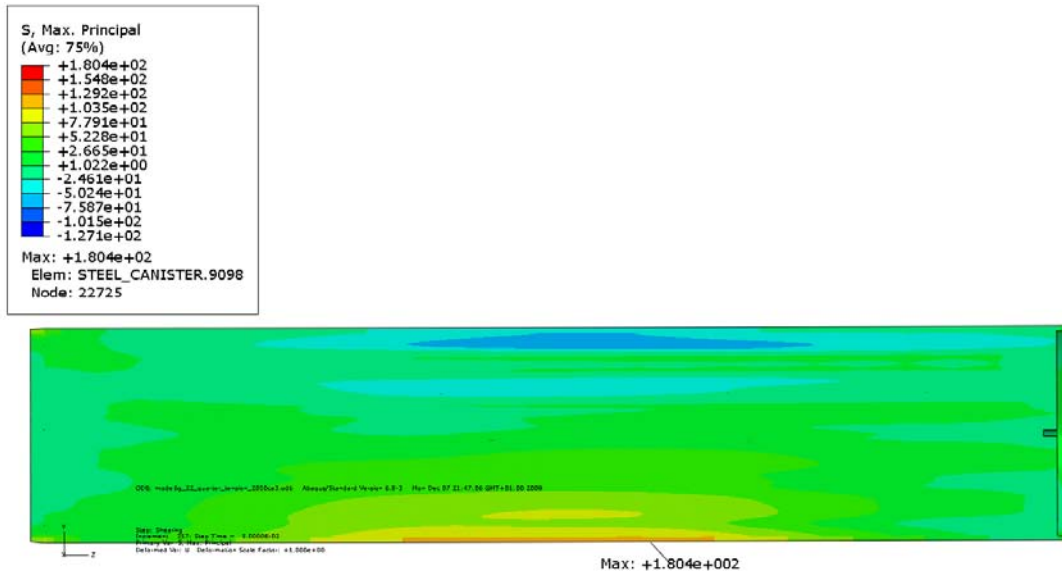


Figure A3-9. Max principal stress for insert – 5 cm shearing magnitude.

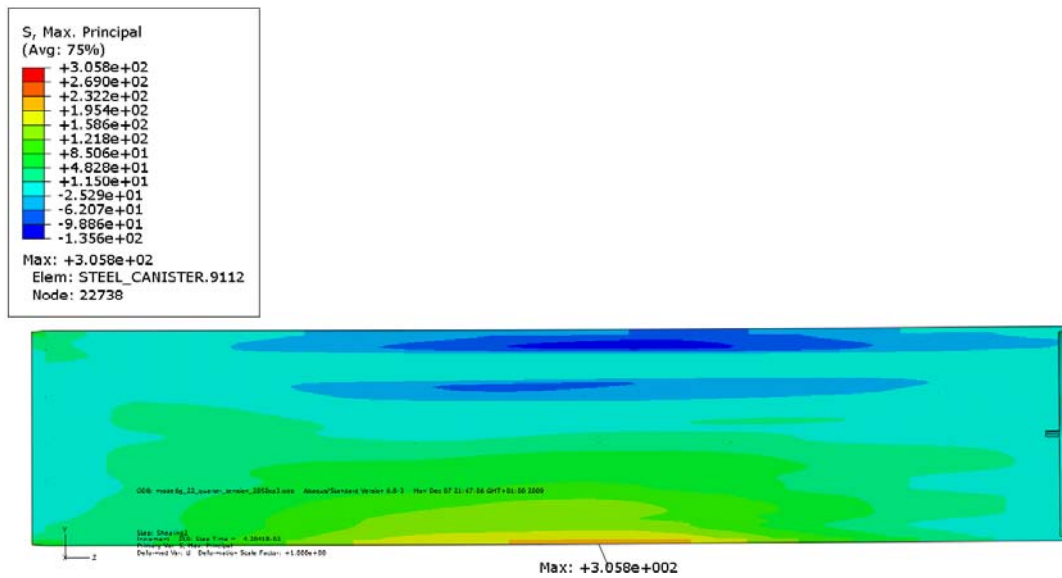


Figure A3-10. Max principal stress for insert – 10 cm shearing magnitude.

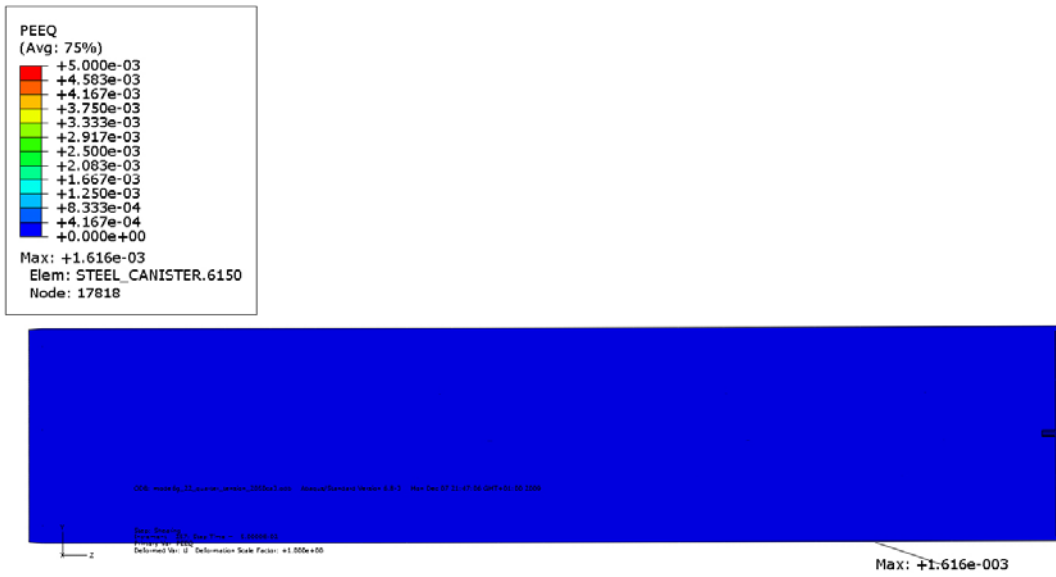


Figure A3-11. Plastic strain (PEEQ) for insert – 5 cm shearing magnitude.

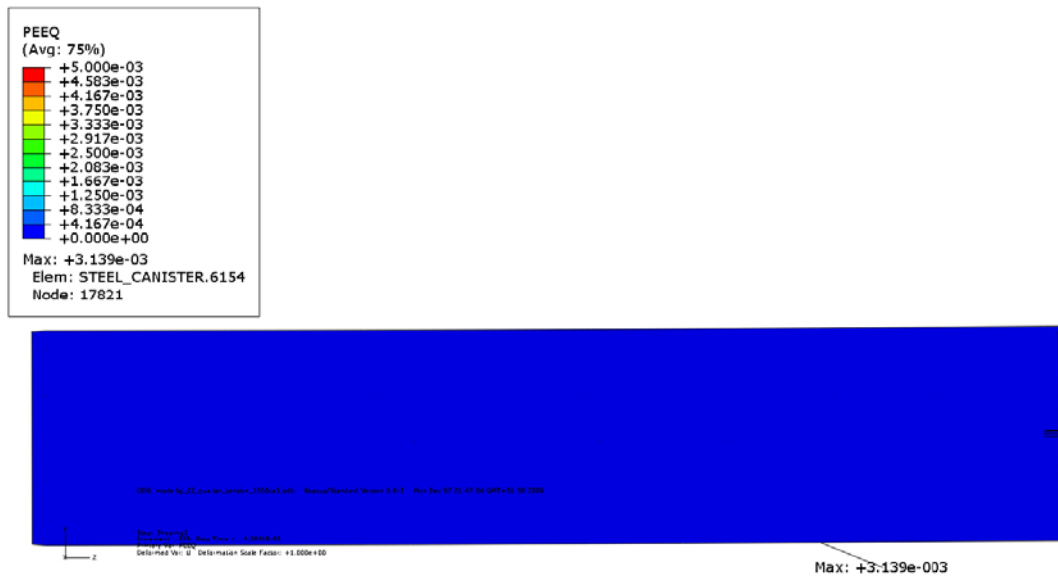
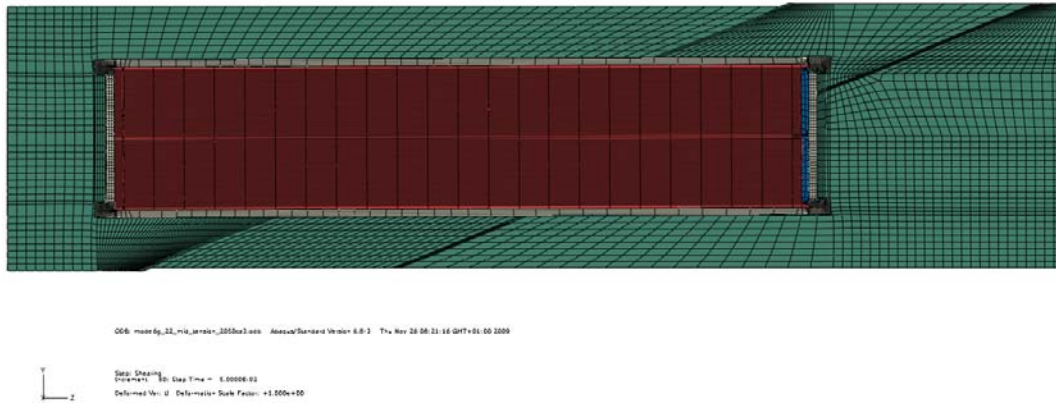


Figure A3-12. Plastic strain (PEEQ) for insert – 10 cm shearing magnitude.

**Short term rock shear inclined 22.5 degrees to canister axis at mid point 2050ca3 (tension)**

Plots showing deformed geometry, plastic strain (PEEQ), Mises stress (MISES) for shearing magnitudes 5 and 10 cm.



*Figure A4-1. Deformed plot – 5 cm shearing magnitude.*

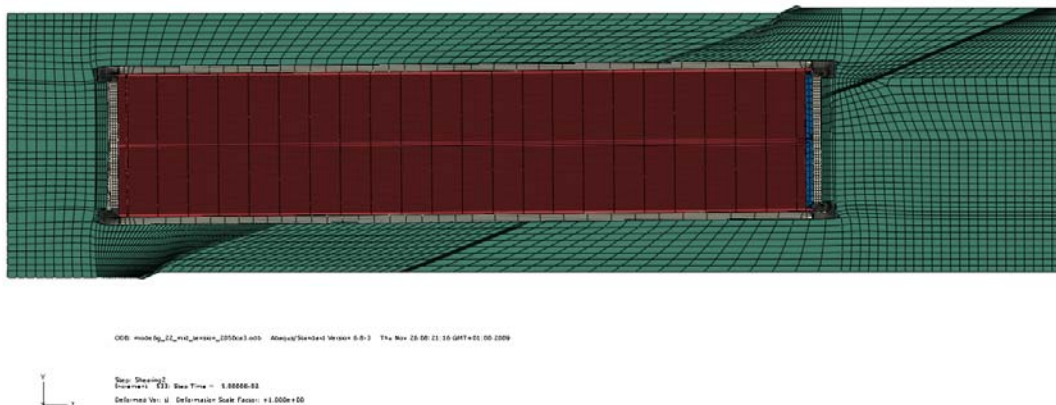


*Figure A4-2. Deformed plot – 10 cm shearing magnitude.*



Figure A4-3. Mises stress for copper shell – 5 cm shearing magnitude.

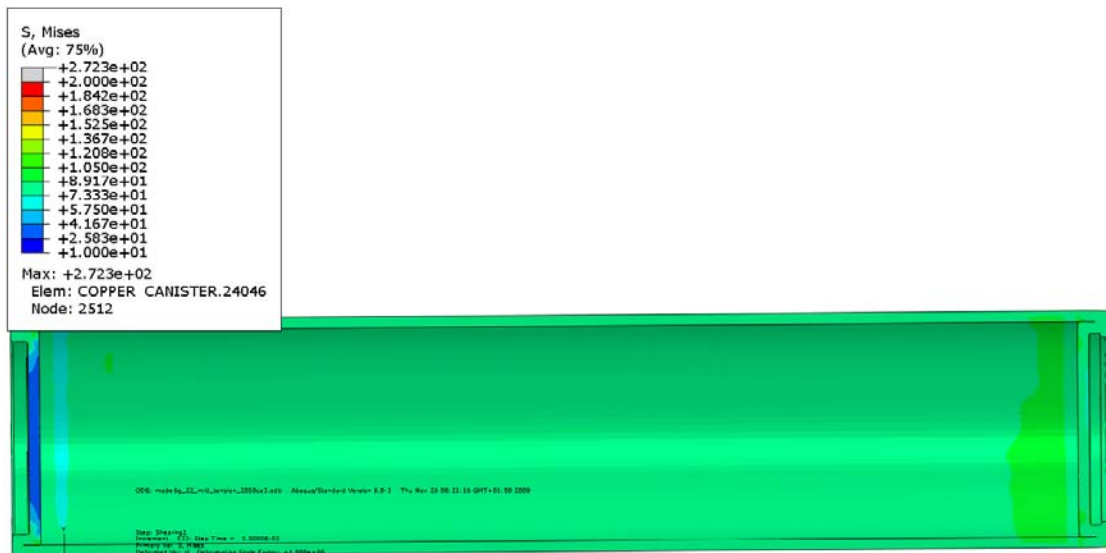


Figure A4-4. Mises stress for copper shell – 10 cm shearing magnitude.

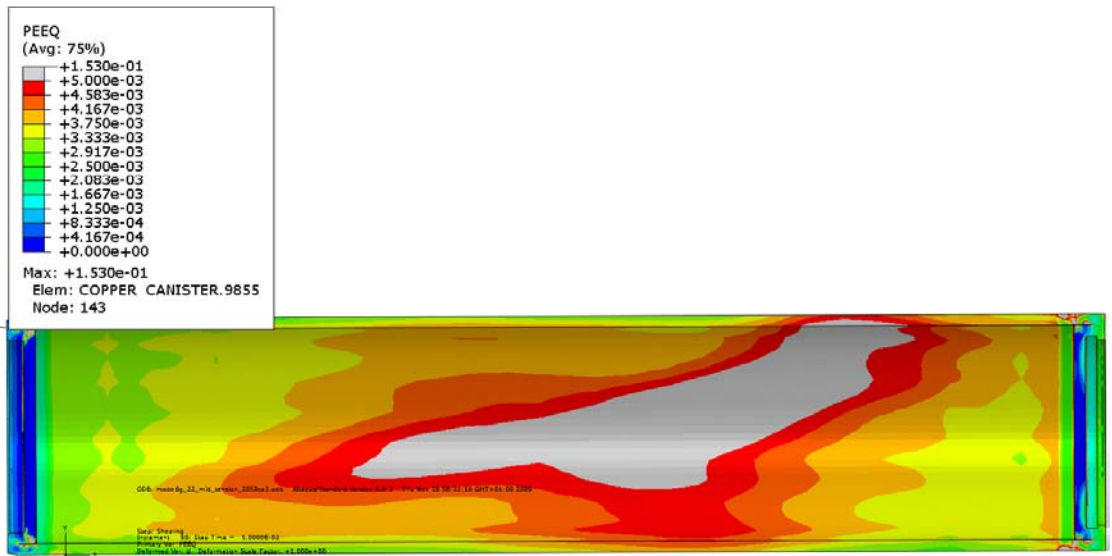


Figure A4-5. Plastic strain (PEEQ) for copper shell – 5 cm shearing magnitude.

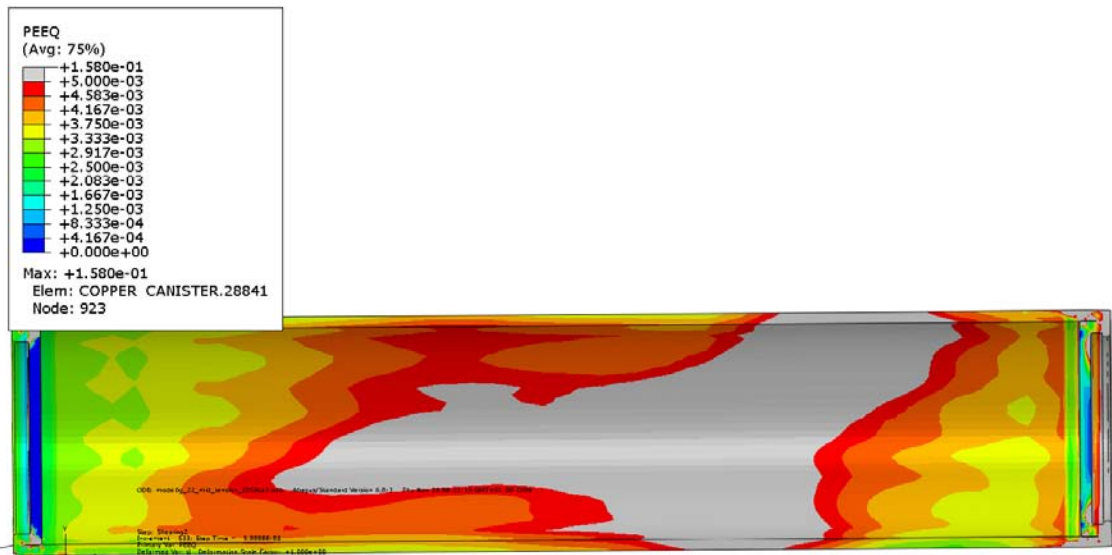


Figure A4-6. Plastic strain (PEEQ) for copper shell – 10 cm shearing magnitude.

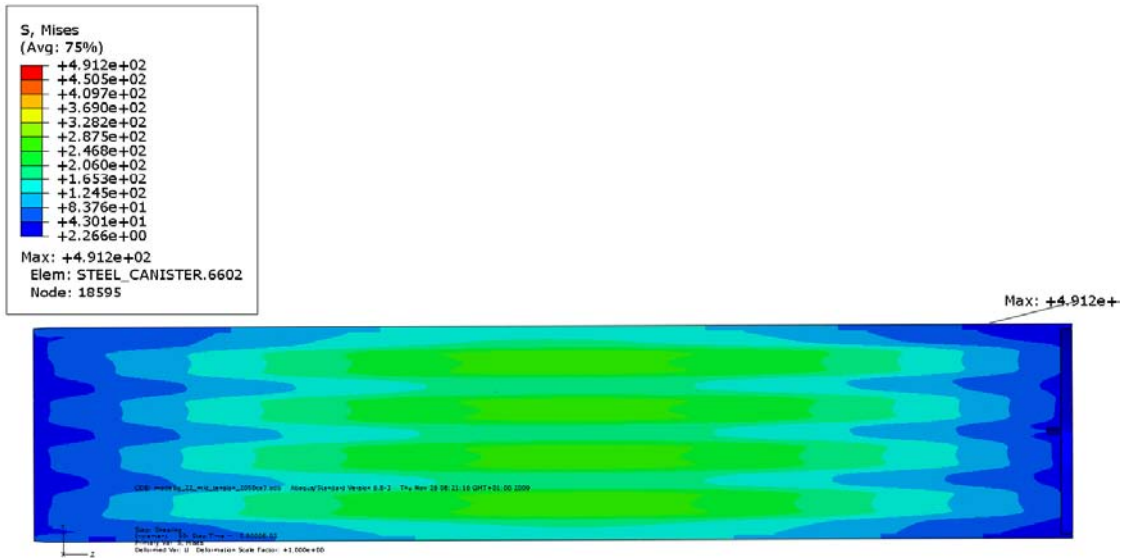


Figure A4-7. Mises stress for insert – 5 cm shearing magnitude.

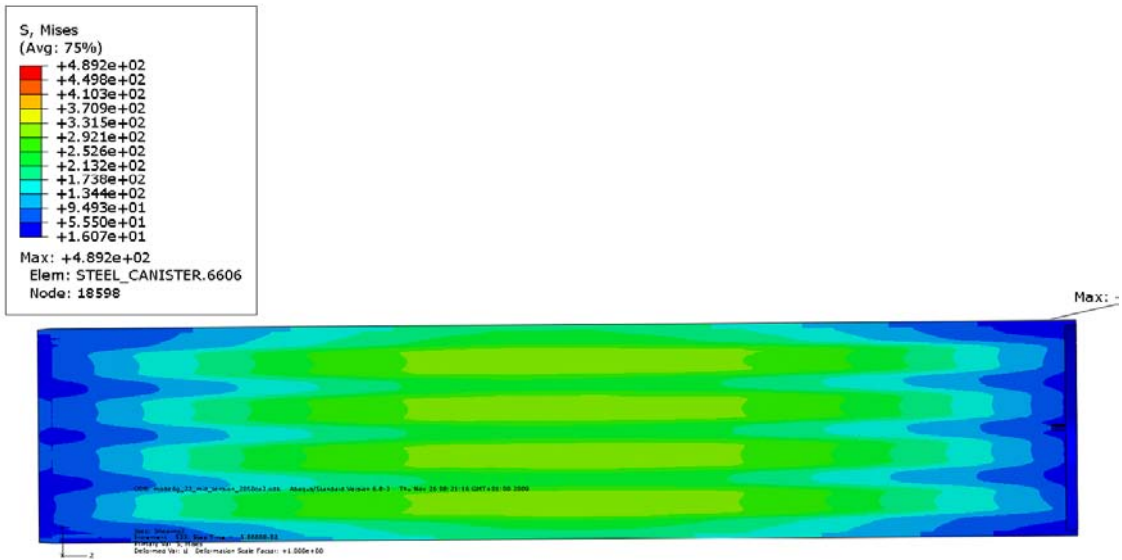
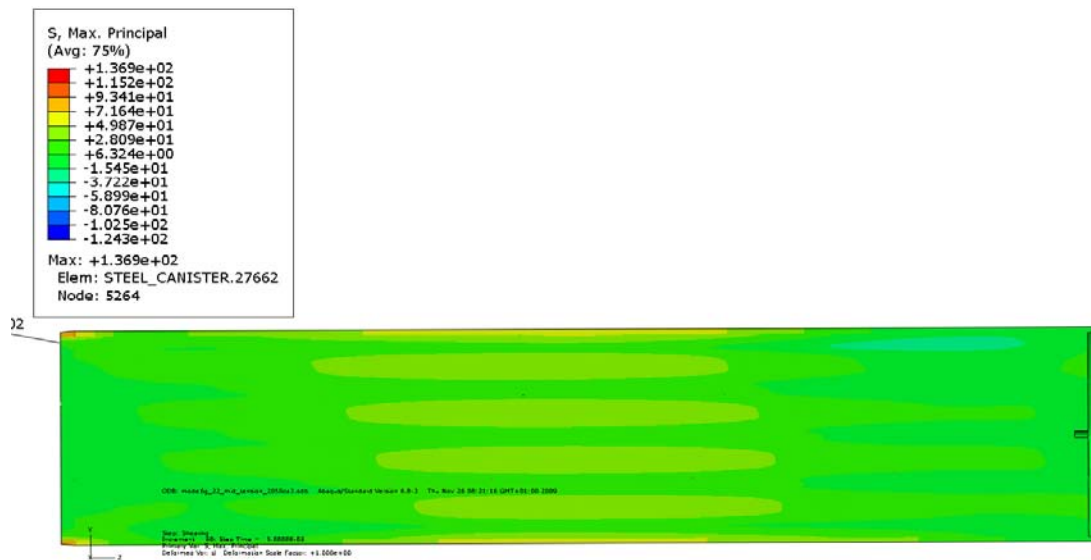
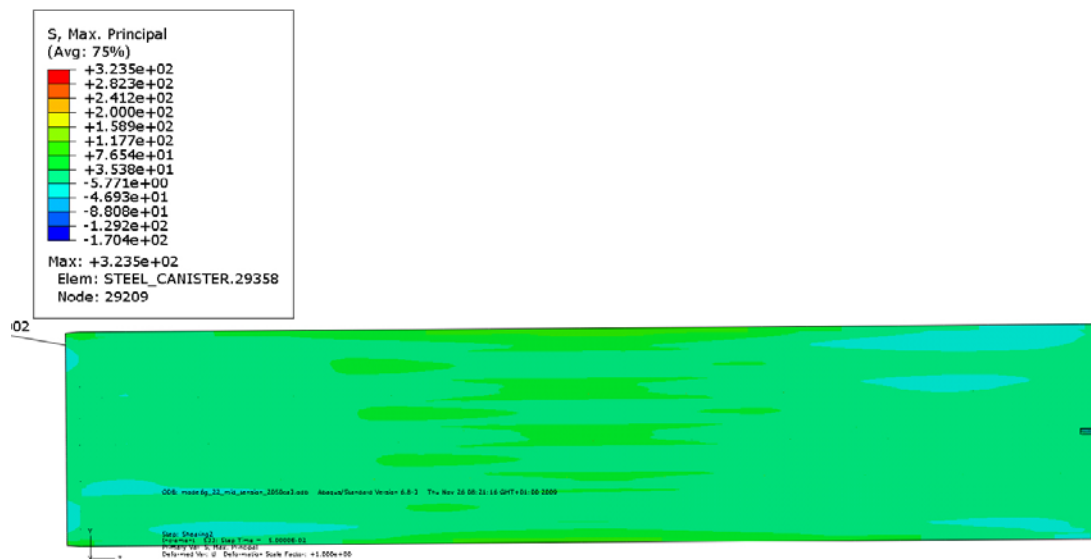


Figure A4-8. Mises stress for insert – 10 cm shearing magnitude.



*Figure A4-9. Max principal stress for insert – 5 cm shearing magnitude.*



*Figure A4-10. Max principal stress for insert – 10 cm shearing magnitude.*

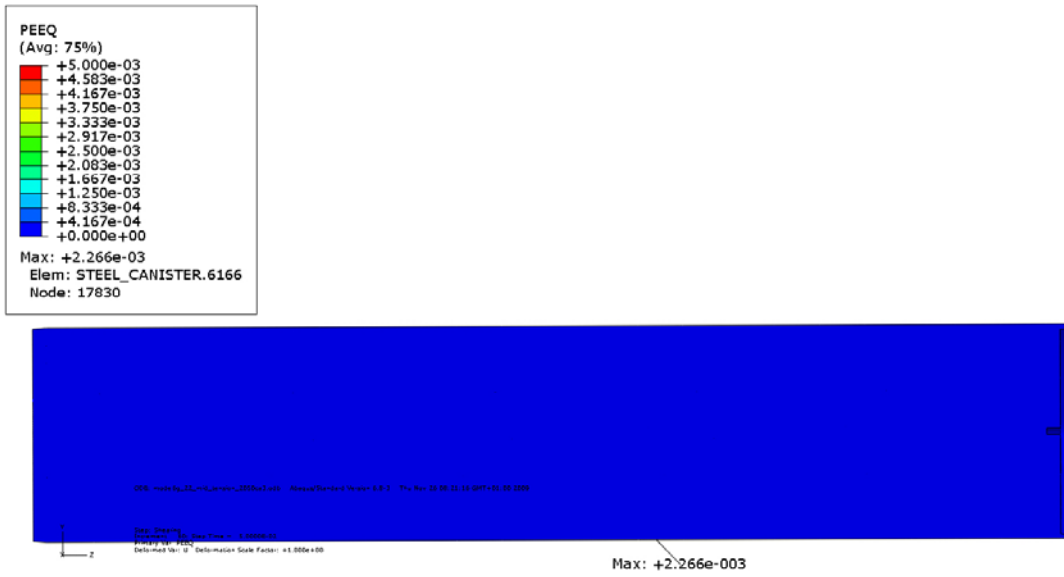


Figure A4-11. Plastic strain (PEEQ) for insert – 5 cm shearing magnitude.

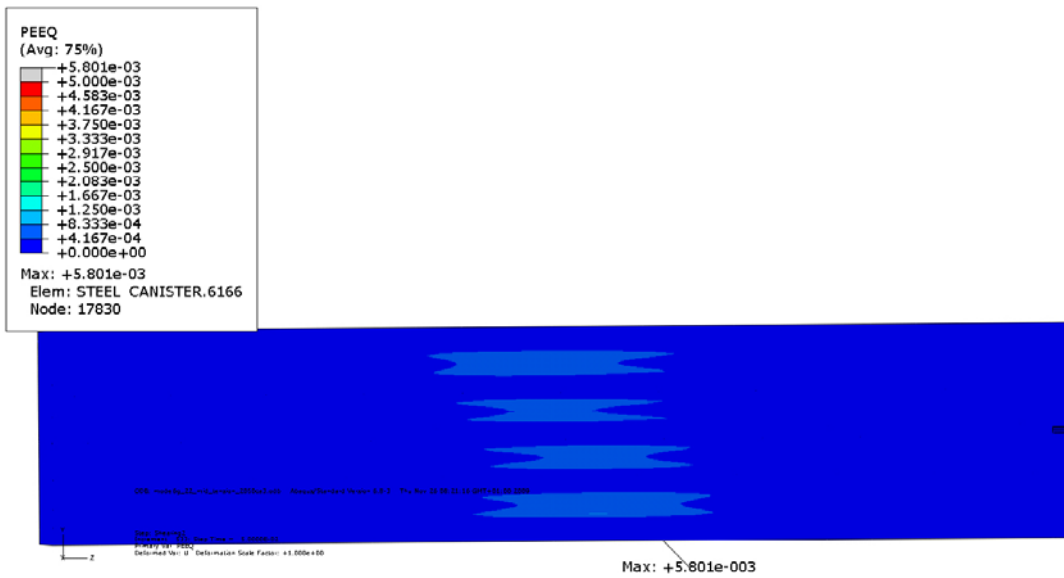
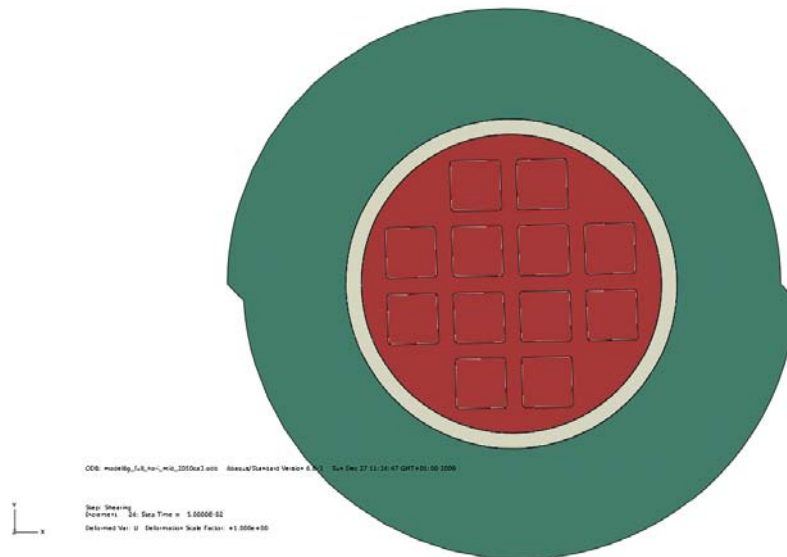


Figure A4-12. Plastic strain (PEEQ) for insert – 10 cm shearing magnitude.



**Short term rock shear in horizontal direction at a vertical plane (mid section) 2050ca3**

Plots showing deformed geometry, plastic strain (PEEQ), mises stress (MISES) for shearing magnitudes 5 and 10 cm.



*Figure A5-1. Deformed plot – 5 cm shearing magnitude.*

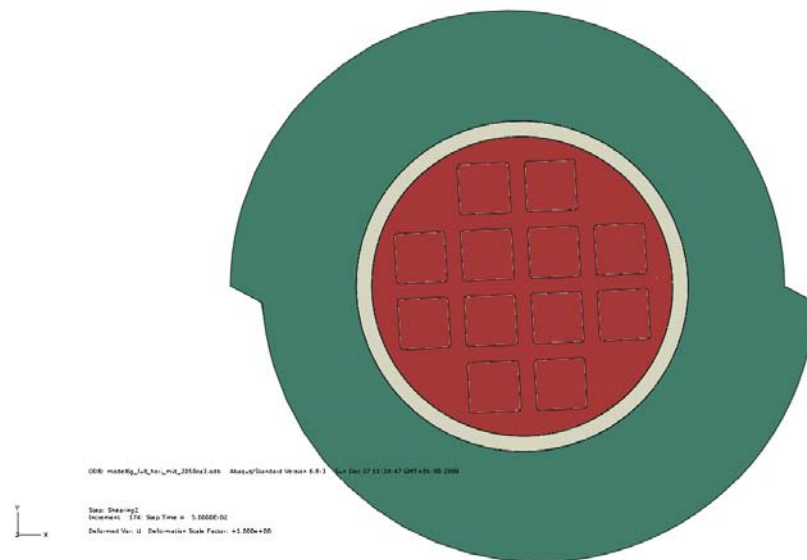


*Figure A5-2. Deformed plot – 10 cm shearing magnitude.*



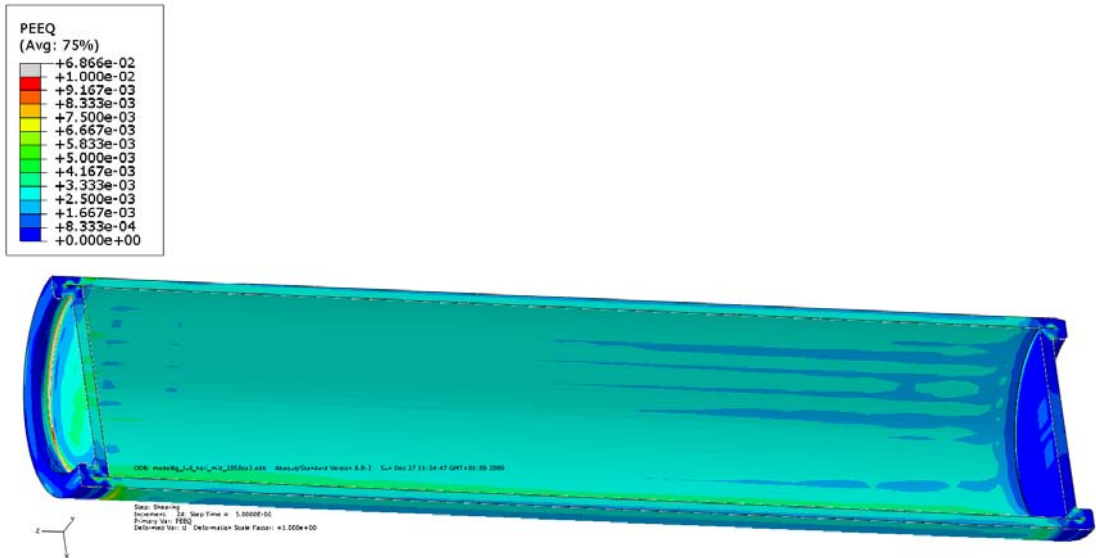


*Figure A5-5. Plastic strain (PEEQ) for copper shell – 5 cm shearing magnitude.*

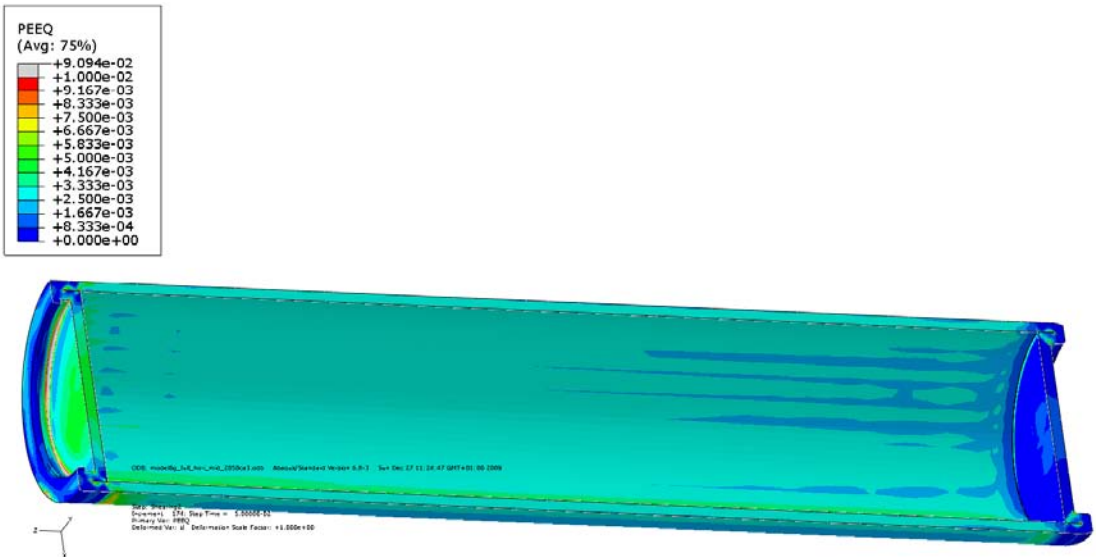


*Figure A5-6. Plastic strain (PEEQ) for copper shell – 10 cm shearing magnitude.*

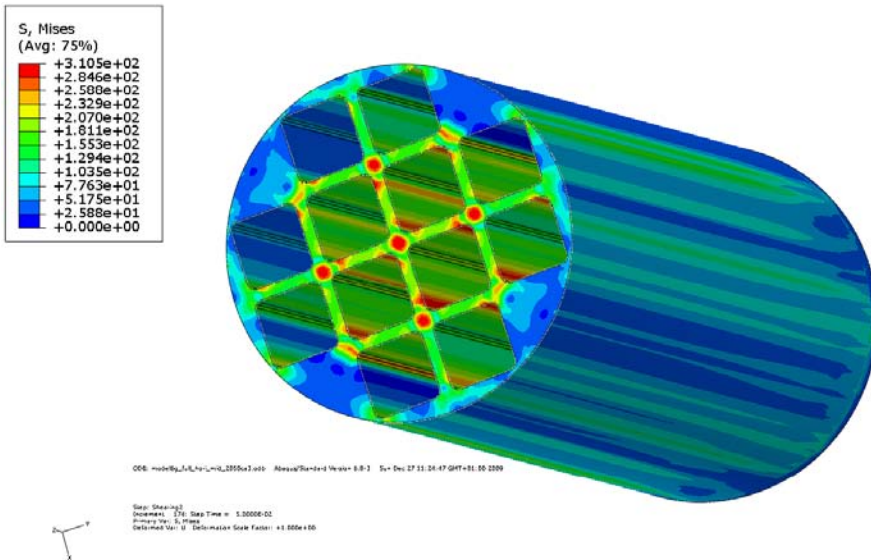


Figure A5-7. Mises stress for insert – 10 cm shearing magnitude.

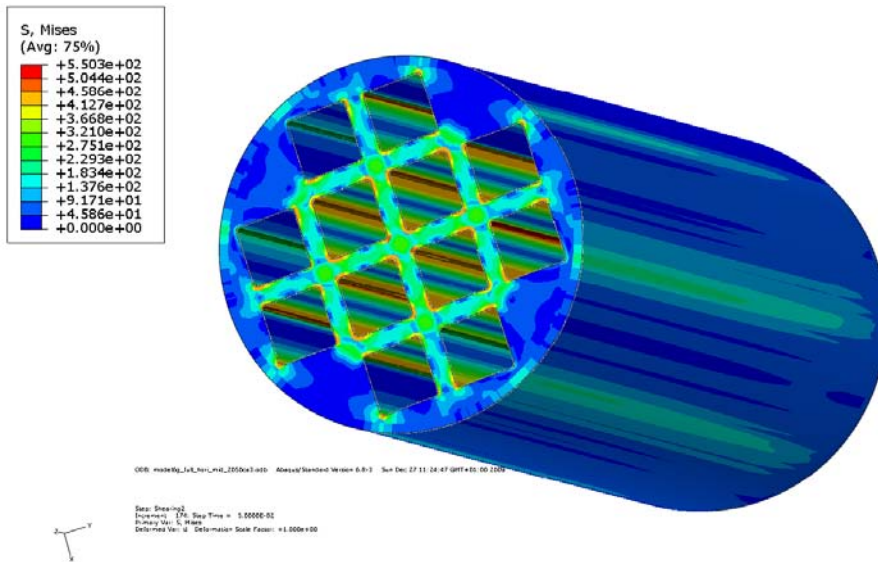
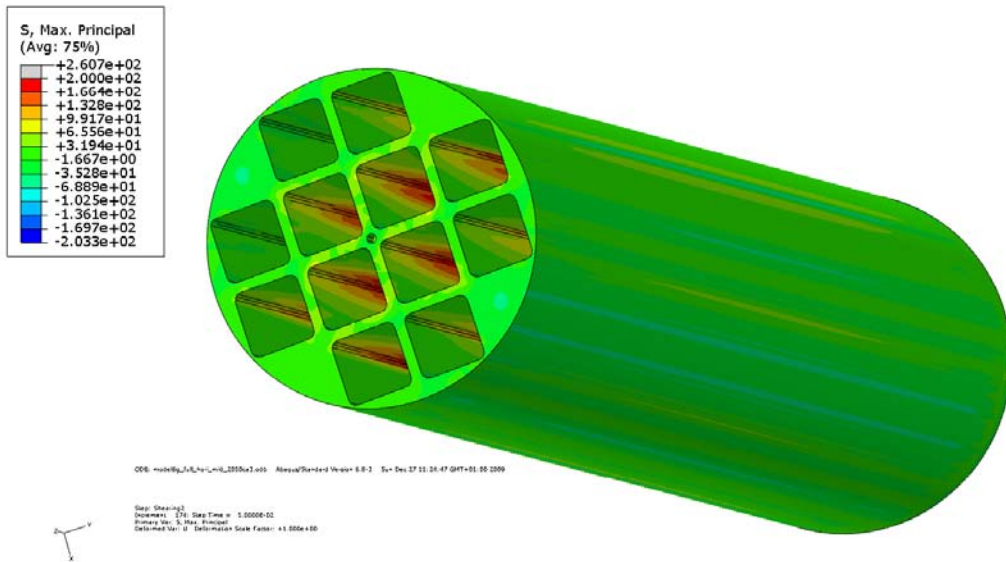
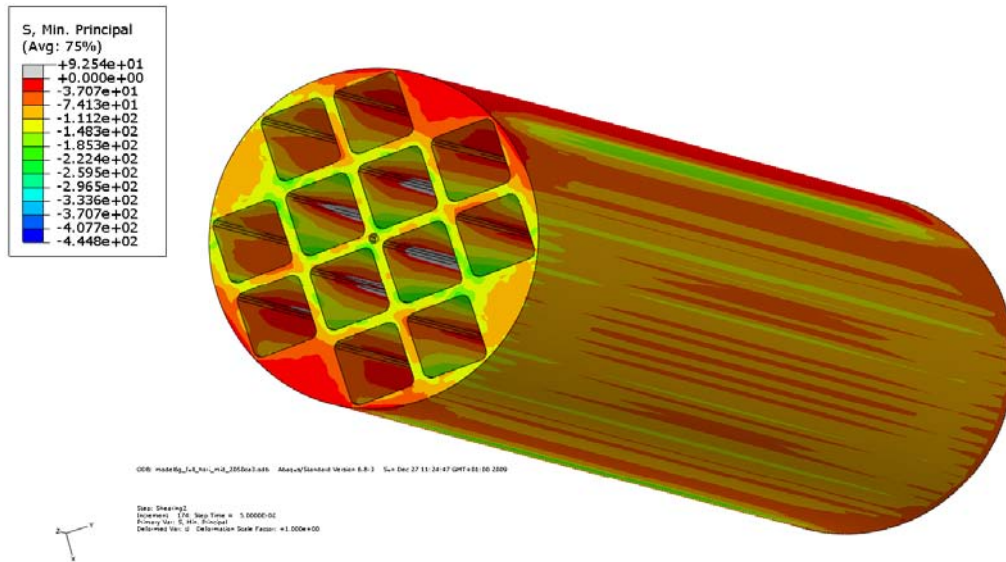


Figure A5-8. Mises stress for insert and tubes – 10 cm shearing magnitude.



*Figure A5-9. Max principal stress for insert – 10 cm shearing magnitude.*



*Figure A5-10. Min principal stress for insert – 10 cm shearing magnitude.*

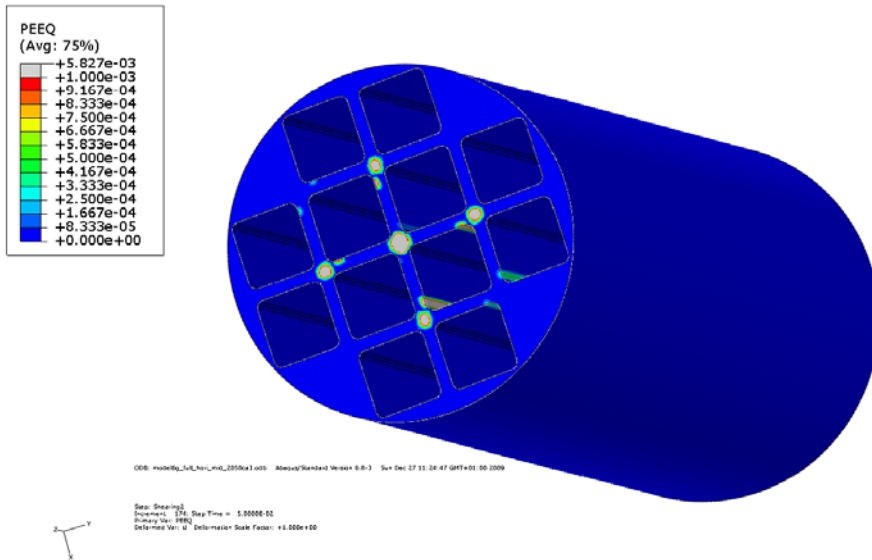


Figure A5-11. Plastic strain (PEEQ) for insert – 10 cm shearing magnitude.

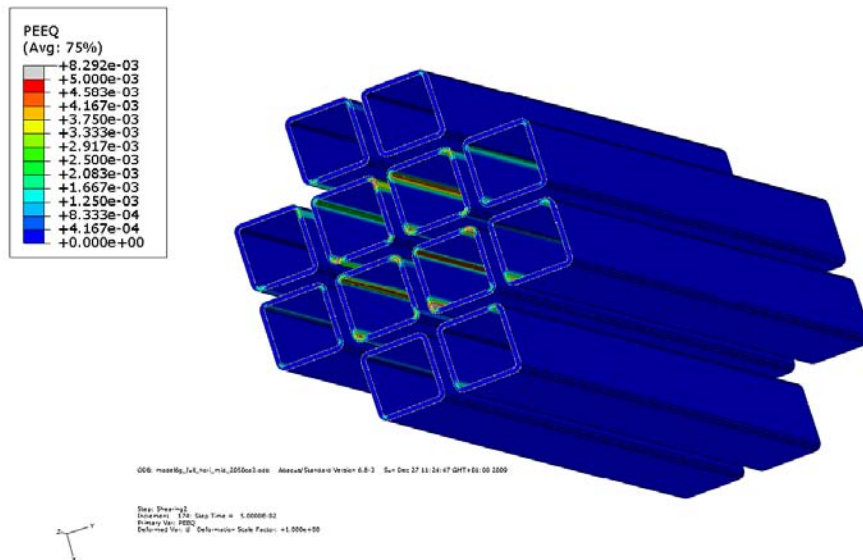


Figure A5-12. Plastic strain (PEEQ) for insert tubes – 10 cm shearing magnitude.



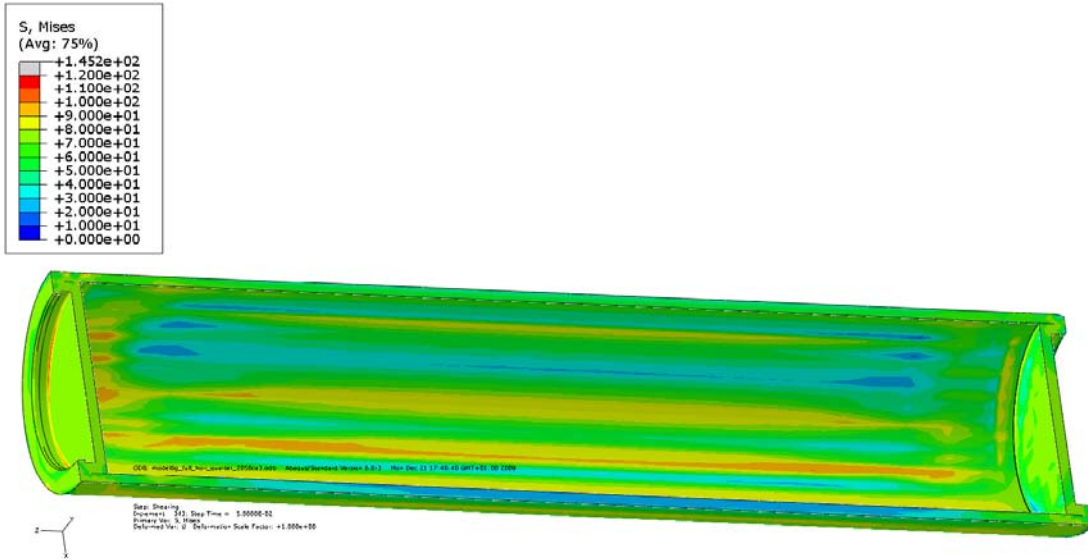


Figure A6-3. Mises stress for copper shell – 5 cm shearing magnitude.

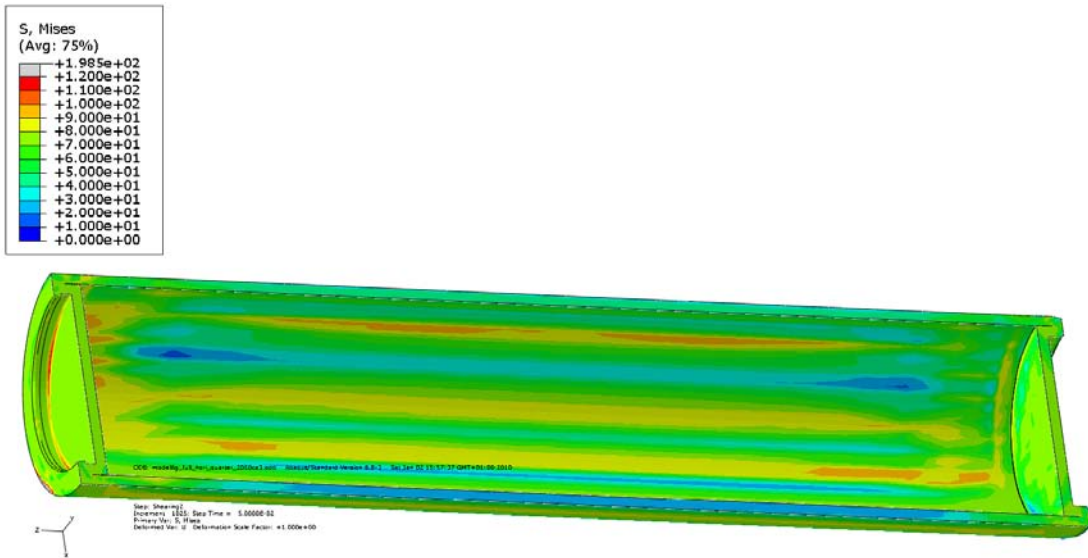


Figure A6-4. Mises stress for copper shell – 10 cm shearing magnitude.



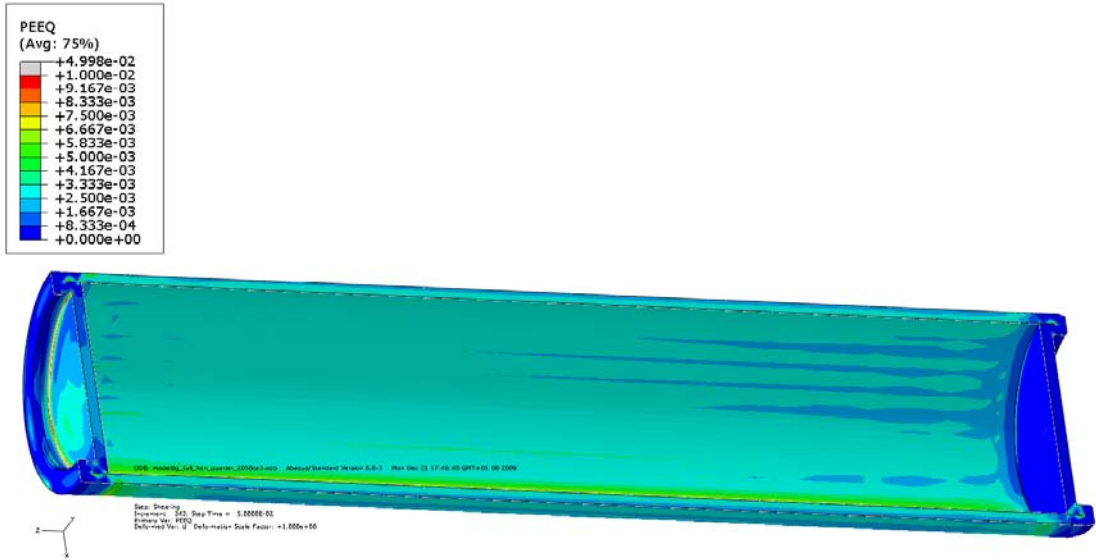


Figure A6-5. Plastic strain (PEEQ) for copper shell – 5 cm shearing magnitude.

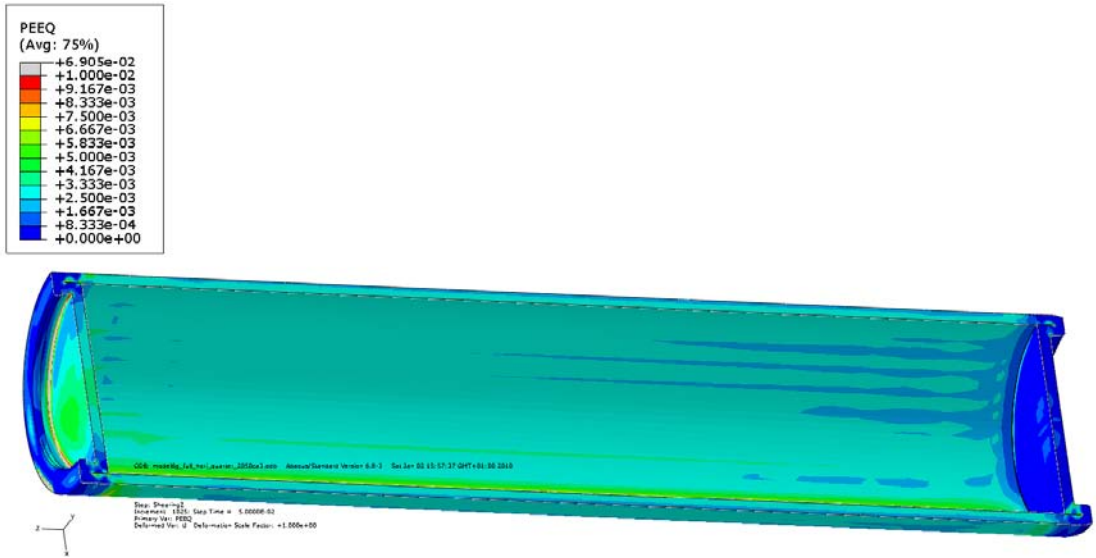


Figure A6-6. Plastic strain (PEEQ) for copper shell – 10 cm shearing magnitude.

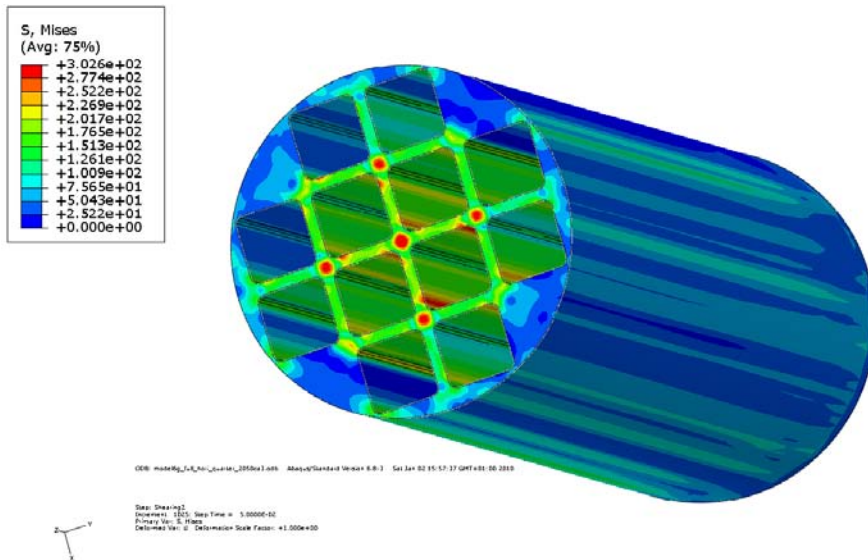


Figure A6-7. Mises stress for iron insert – 10 cm shearing magnitude.

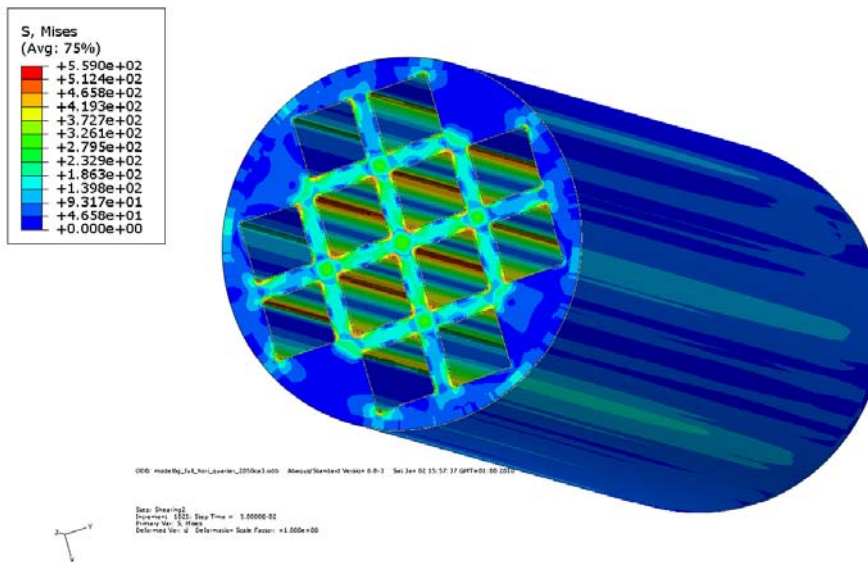


Figure A6-8. Mises stress for insert and tubes – 10 cm shearing magnitude.

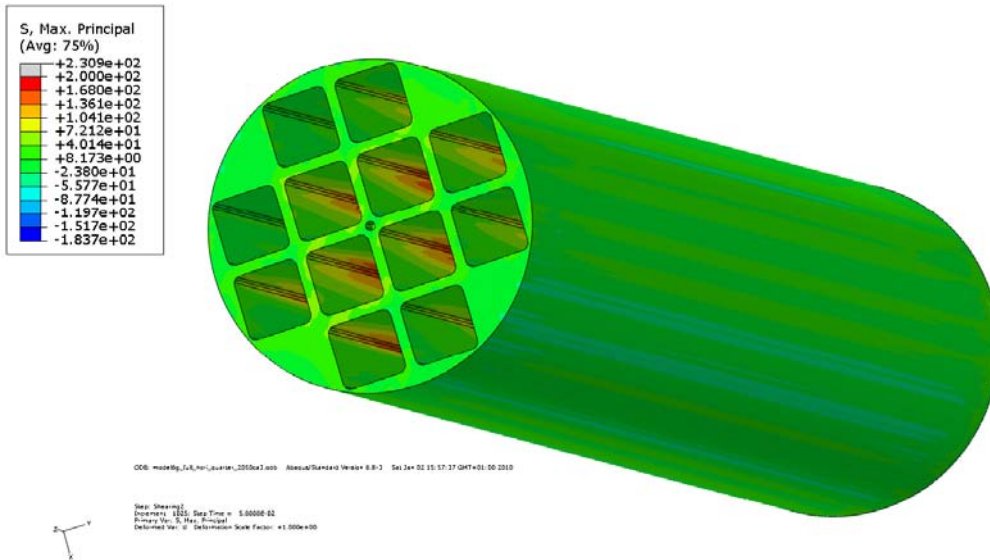


Figure A6-9. Max principal stress for insert – 10 cm shearing magnitude.

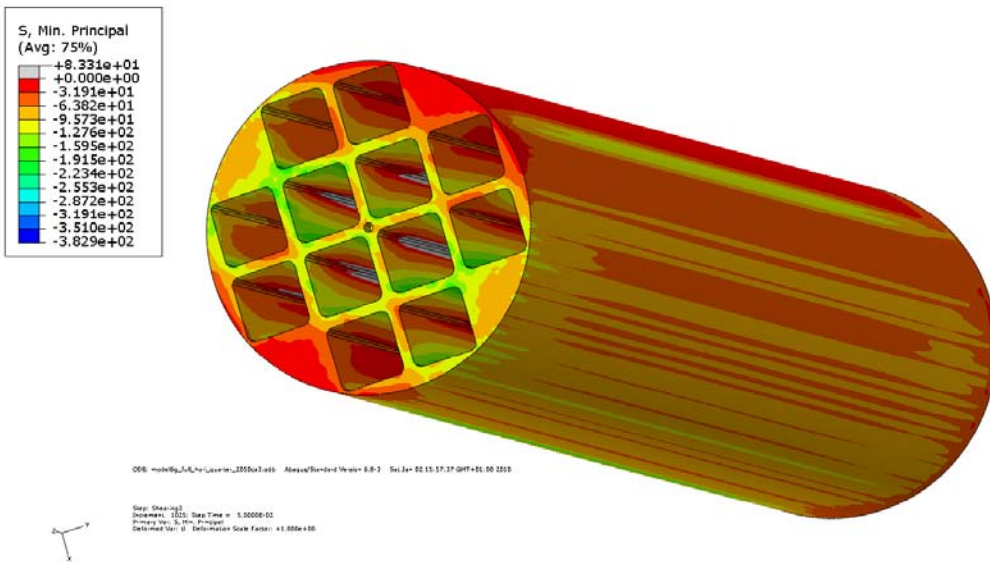


Figure A6-10. Min principal stress for insert – 10 cm shearing magnitude.

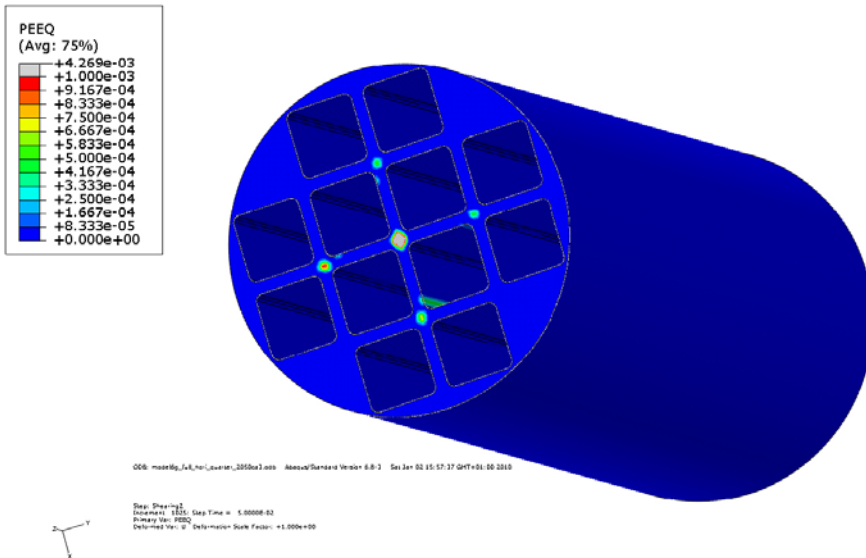


Figure A6-11. Plastic strain (PEEQ) for iron insert – 10 cm shearing magnitude.

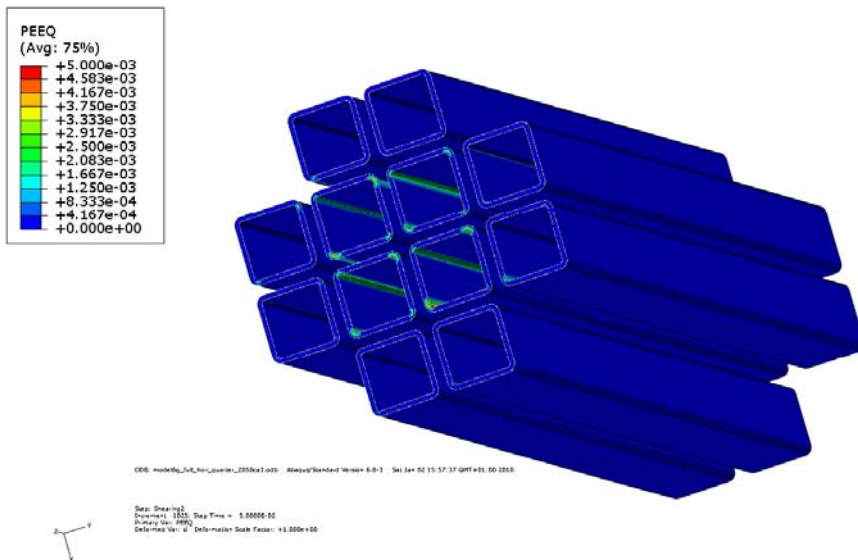
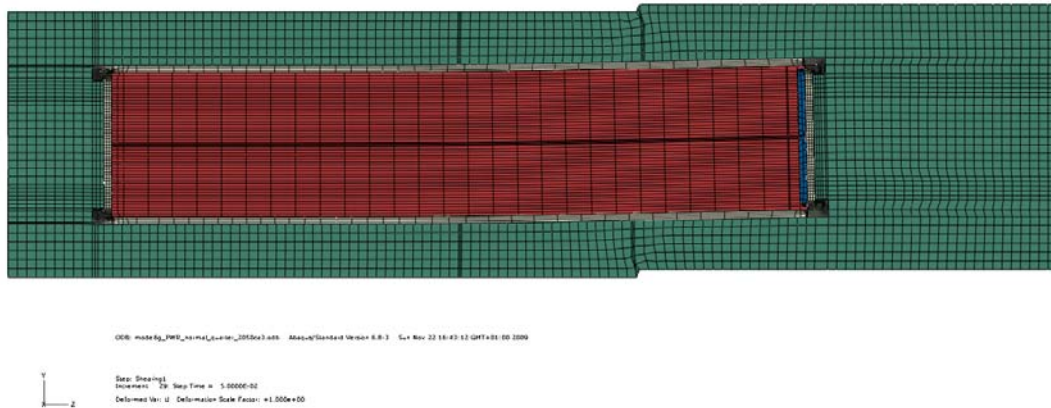


Figure A6-12. Plastic strain (PEEQ) for insert tubes – 10 cm shearing magnitude.

**Short term rock shear normal direction at quarter point 2050ca3 for PWR**

Plots showing deformed geometry, plastic strain (PEEQ), Mises stress (MISES) for shearing magnitudes 5 and 10 cm.



*Figure A7-1. Deformed plot – 5 cm shearing magnitude.*

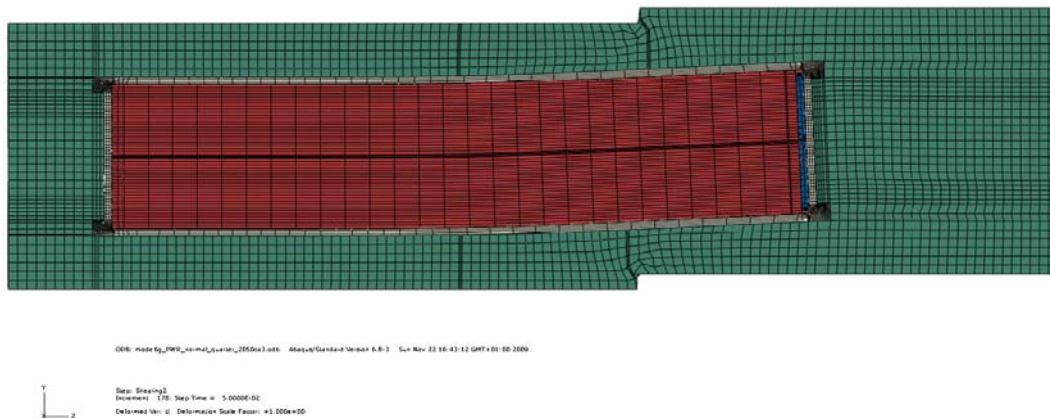


*Figure A7-2. Deformed plot – 10 cm shearing magnitude.*

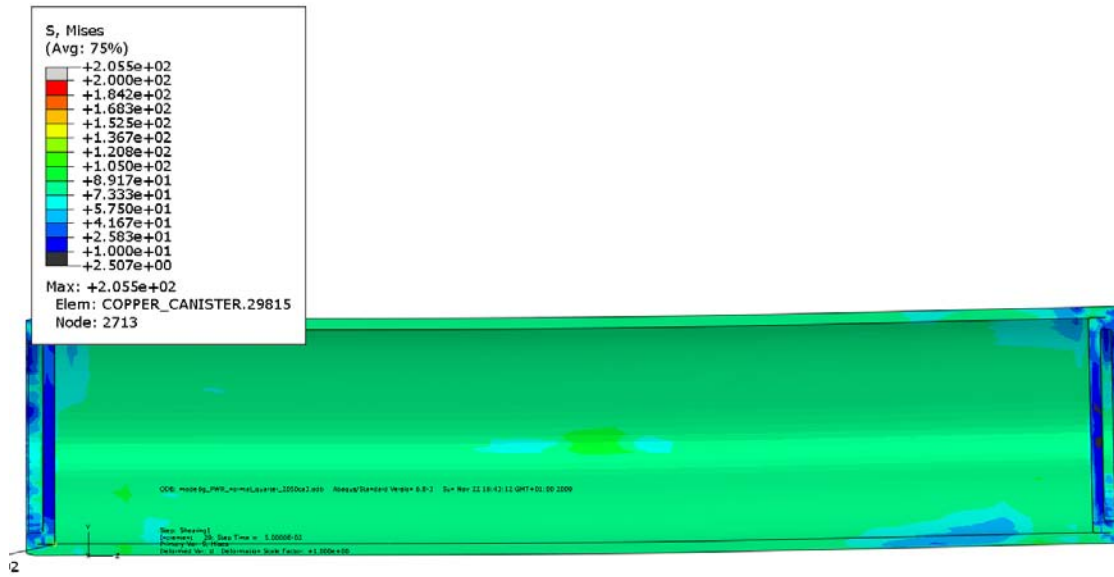


Figure A7-3. Mises stress for copper shell – 5 cm shearing magnitude.

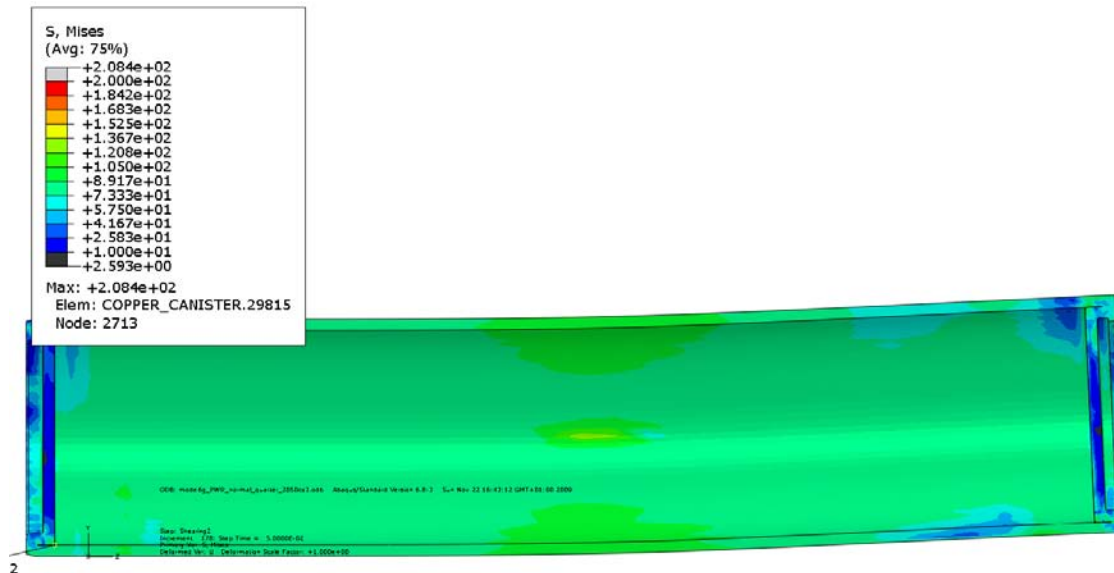


Figure A7-4. Mises stress for copper shell – 10 cm shearing magnitude.

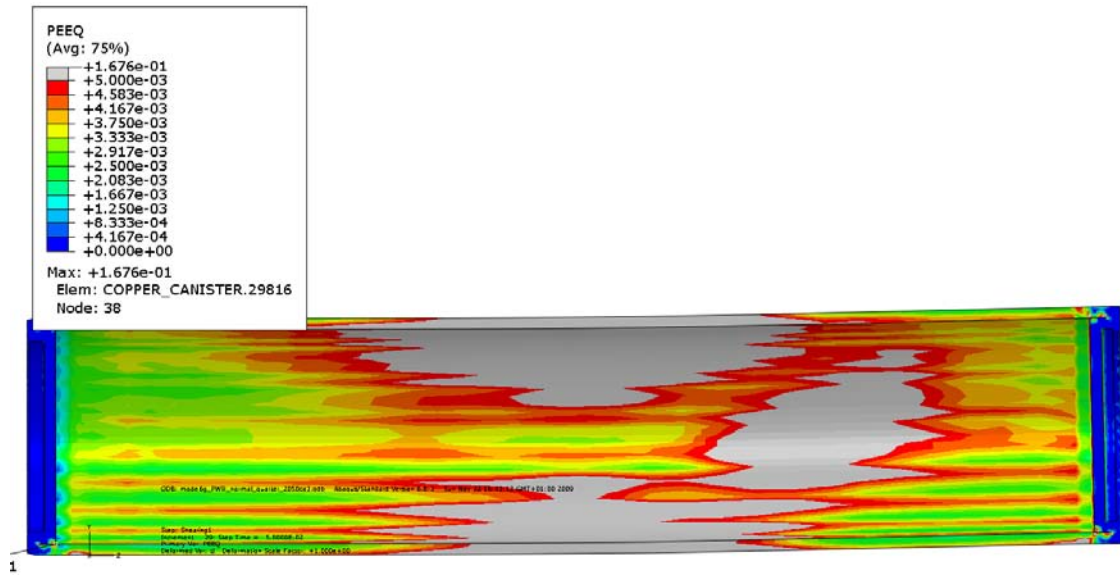


Figure A7-5. Plastic strain (PEEQ) for copper shell – 5 cm shearing magnitude.

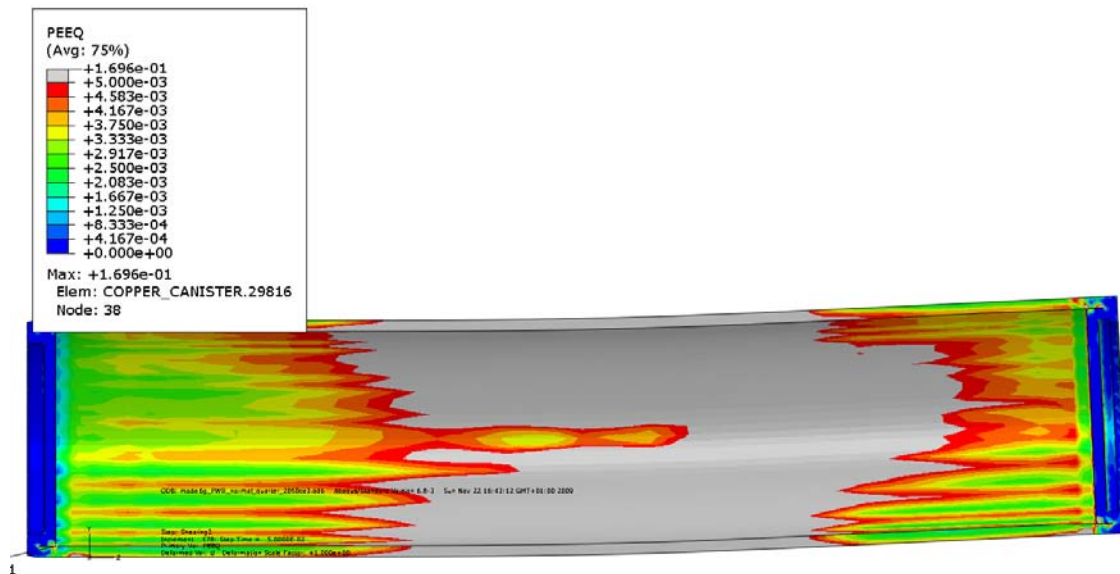


Figure A7-6. Plastic strain (PEEQ) for copper shell – 10 cm shearing magnitude.

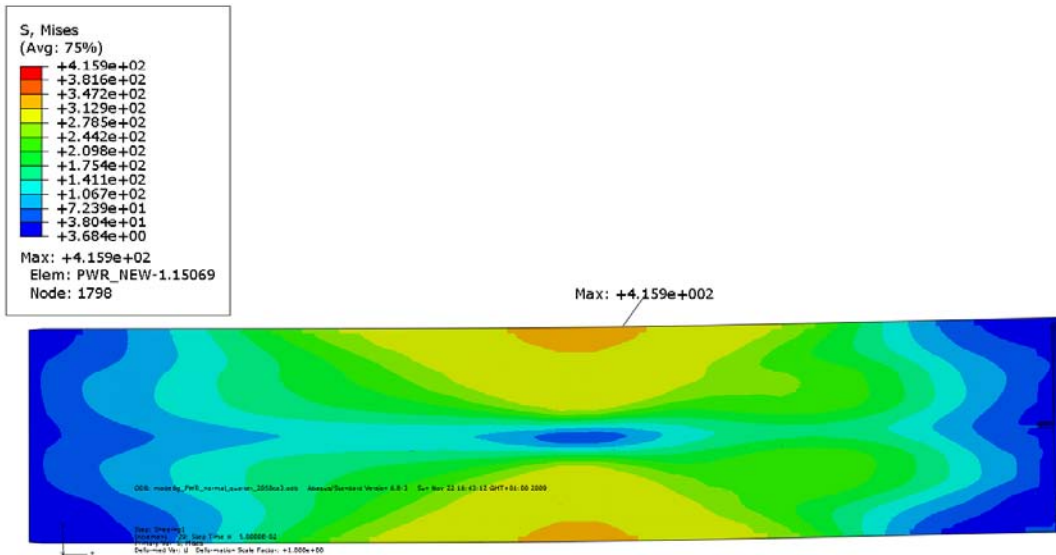


Figure A7-7. Mises stress for insert – 5 cm shearing magnitude.

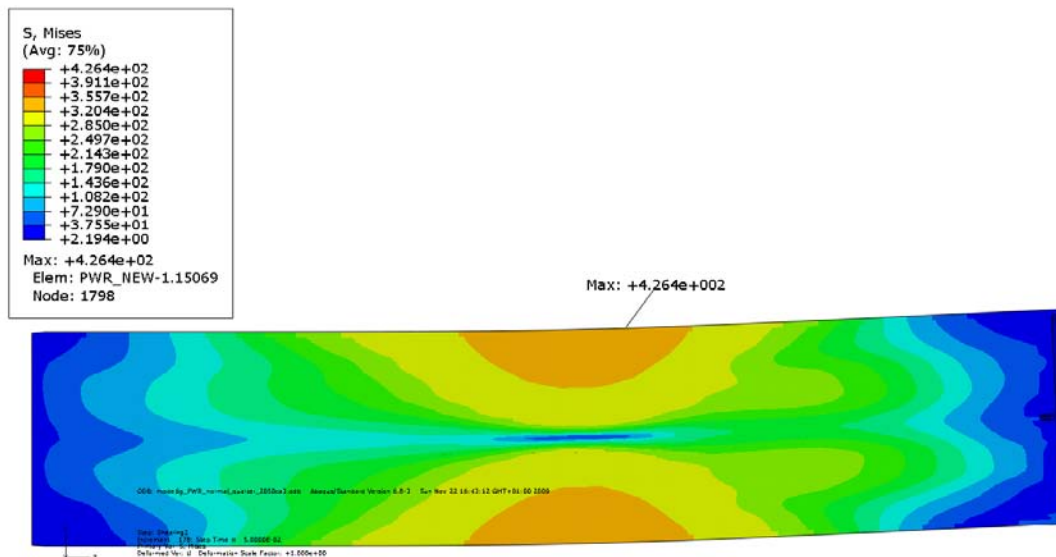


Figure A7-8. Mises stress for insert – 10 cm shearing magnitude.



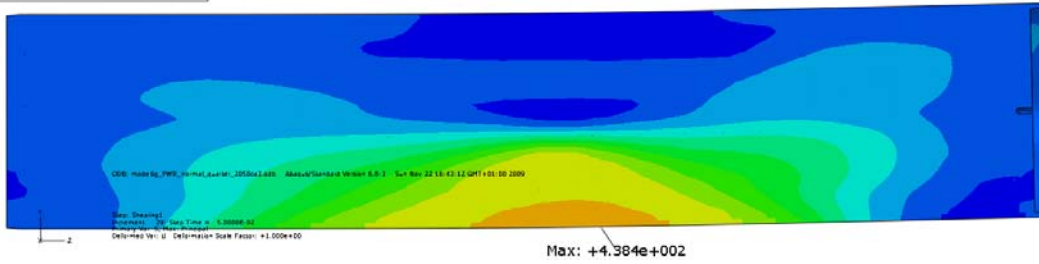
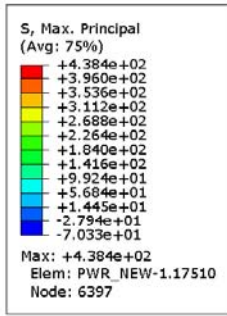


Figure A7-9. Max principal stress for insert – 5 cm shearing magnitude.

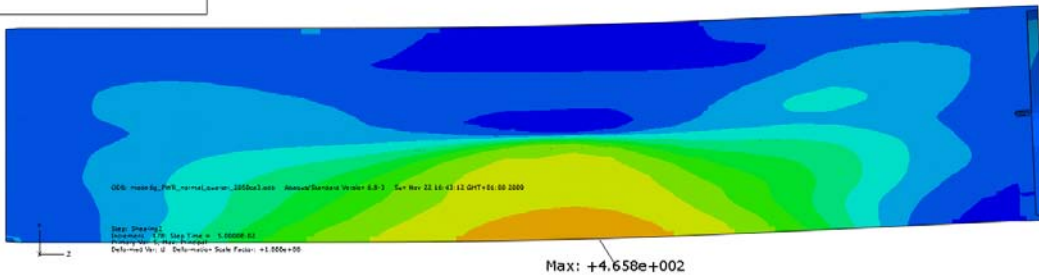
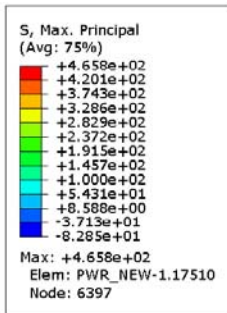


Figure A7-10. Max principal stress for insert – 10 cm shearing magnitude.

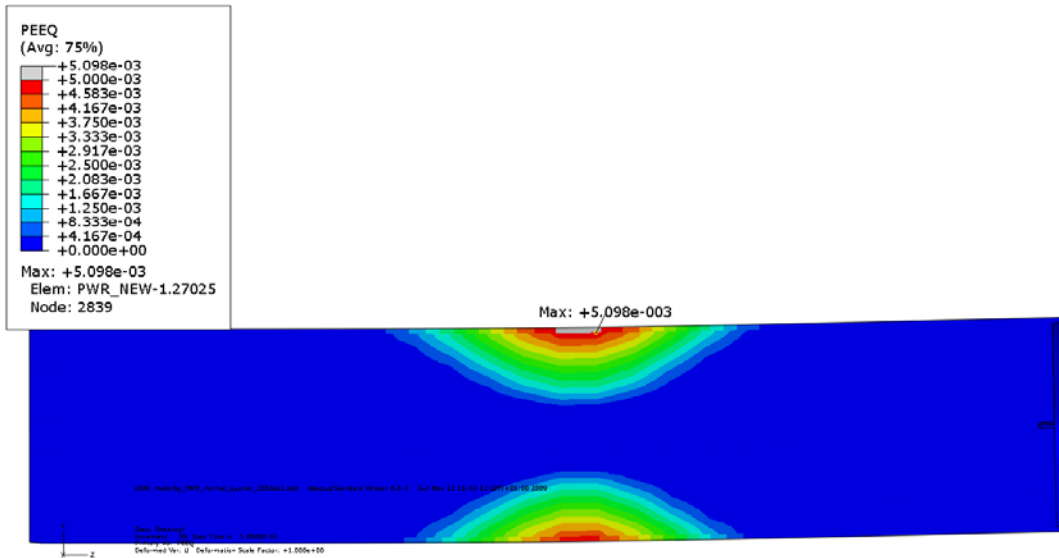


Figure A7-11. Plastic strain (PEEQ) for insert – 5 cm shearing magnitude.

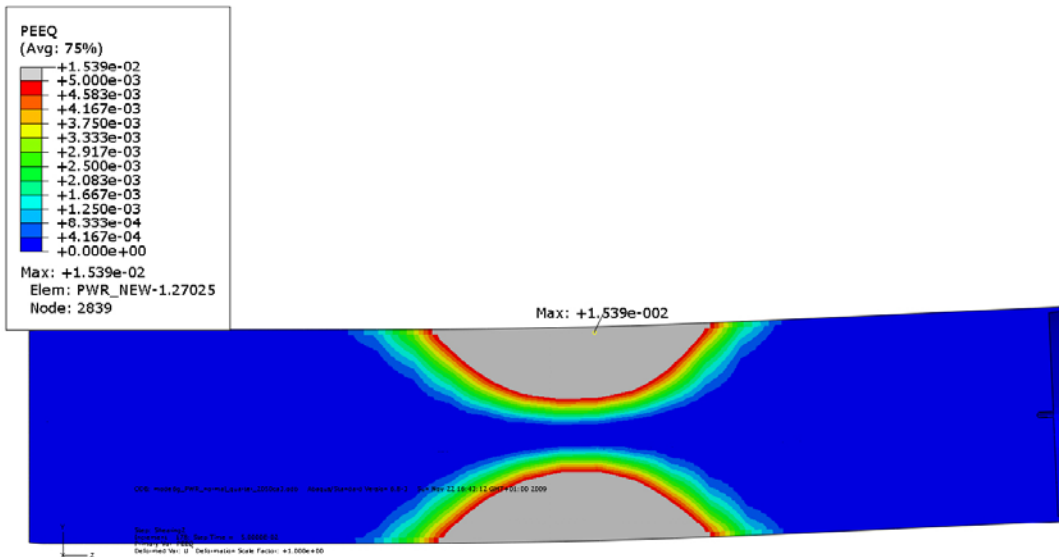
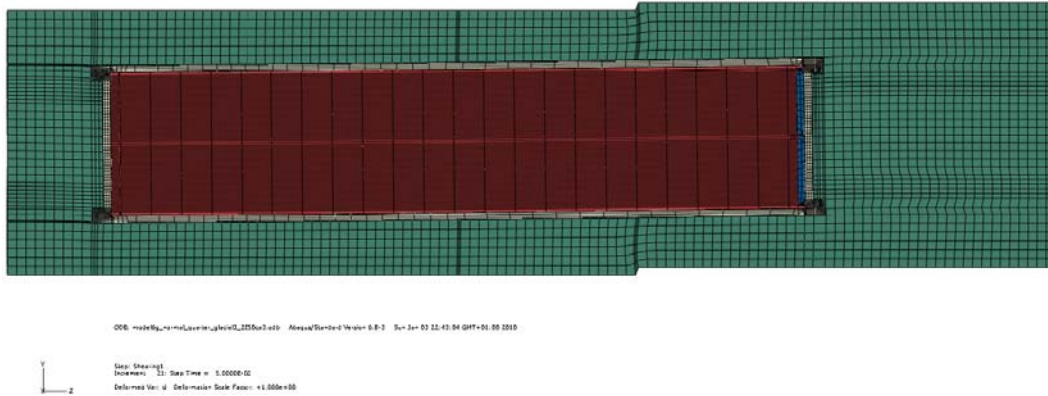


Figure A7-12. Plastic strain (PEEQ) for insert – 10 cm shearing magnitude.

**Short term rock shear normal direction at quarter point 2050ca3 at glacial pressure 30 MPa**

Plots showing deformed geometry, plastic strain (PEEQ), Mises stress (MISES) for shearing magnitudes 5 and 10 cm.



*Figure A8-1. Deformed plot – 5 cm shearing magnitude.*



*Figure A8-2. Deformed plot – 10 cm shearing magnitude.*

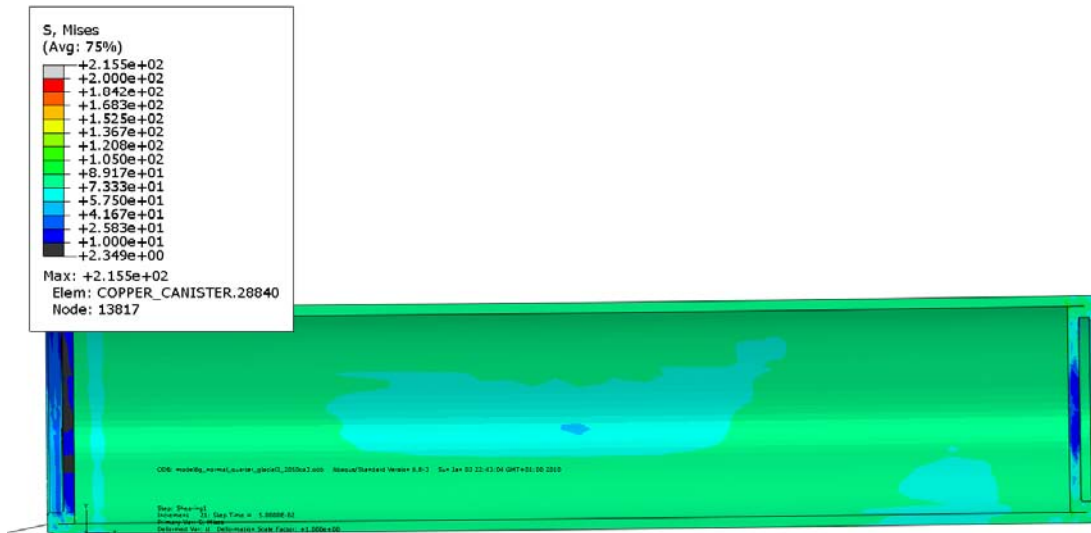


Figure A8-3. Mises stress for copper shell – 5 cm shearing magnitude.

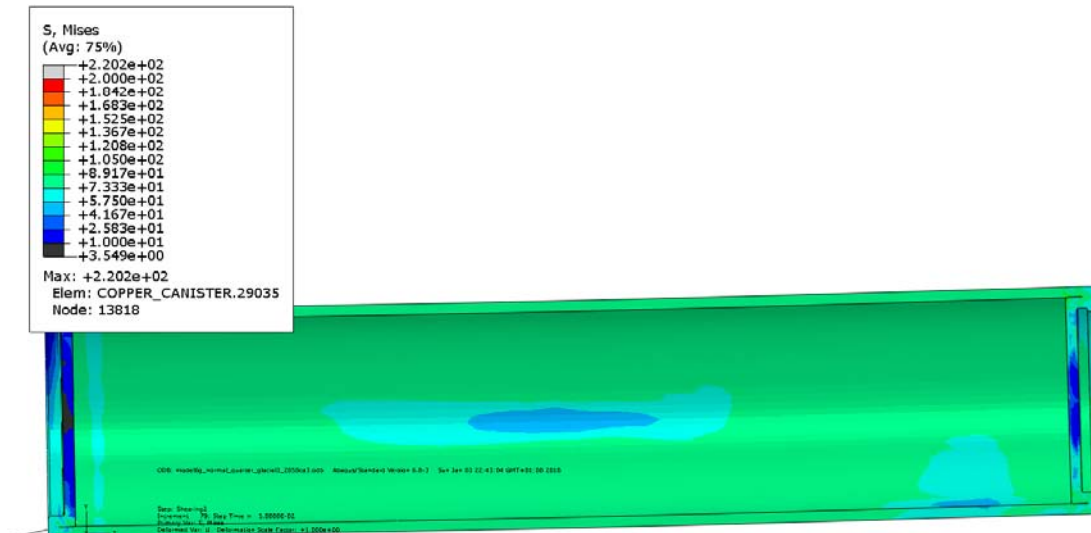


Figure A8-4. Mises stress for copper shell – 10 cm shearing magnitude.

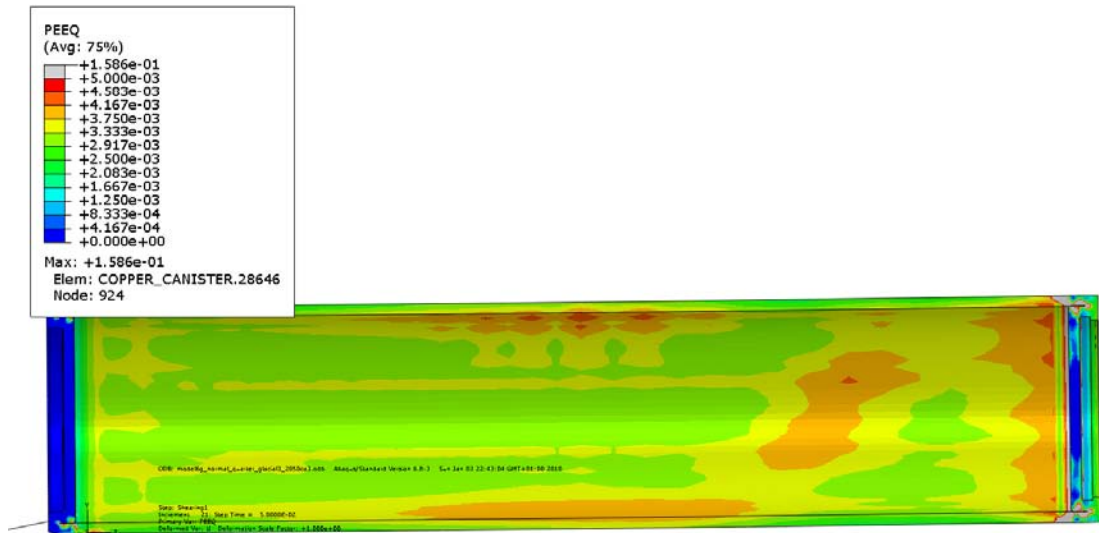


Figure A8-5. Plastic strain (PEEQ) for copper shell – 5 cm shearing magnitude.

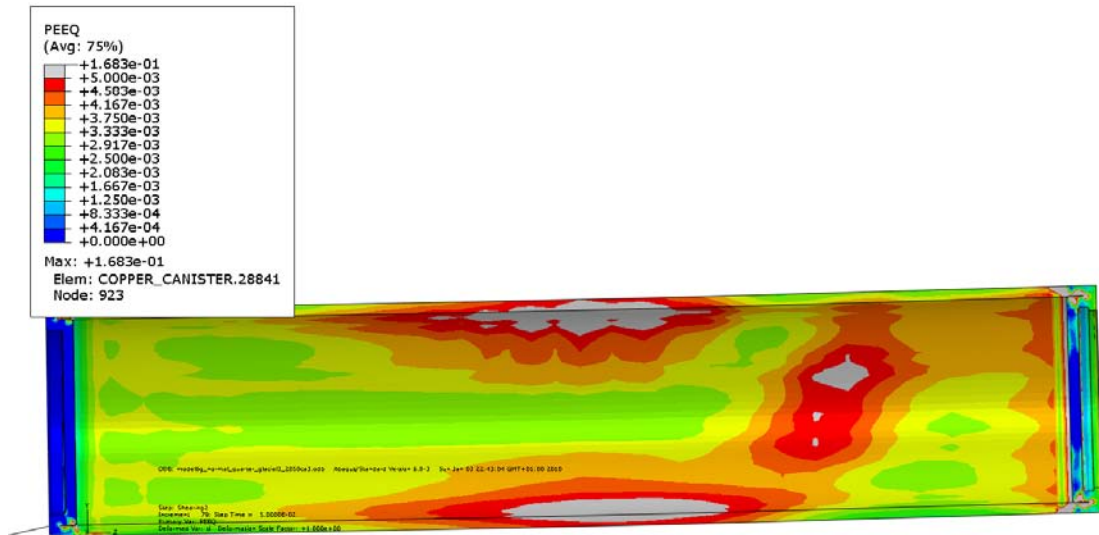


Figure A8-6. Plastic strain (PEEQ) for copper shell – 10 cm shearing magnitude.

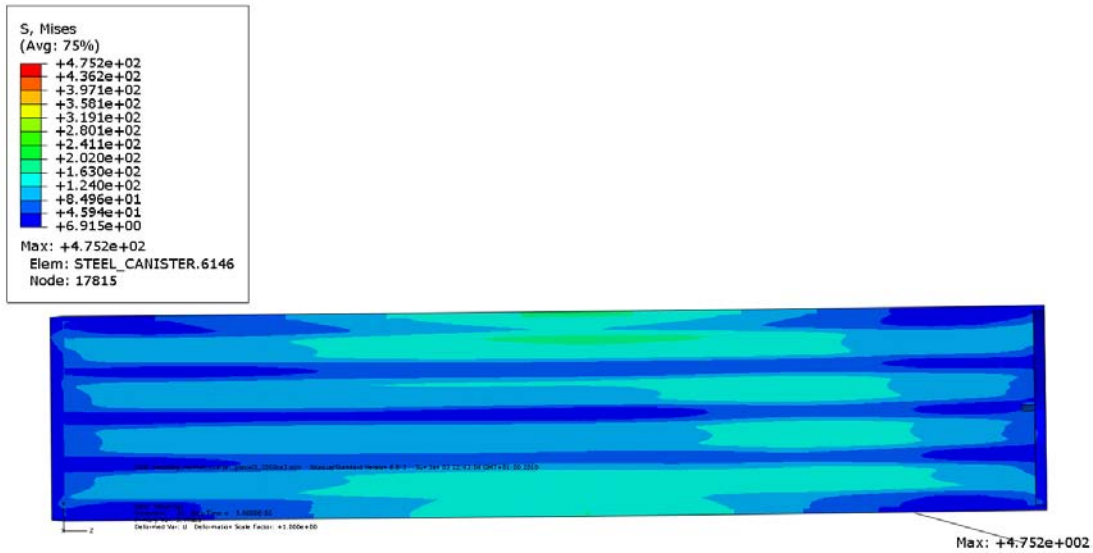


Figure A8-7. Mises stress for insert – 5 cm shearing magnitude.

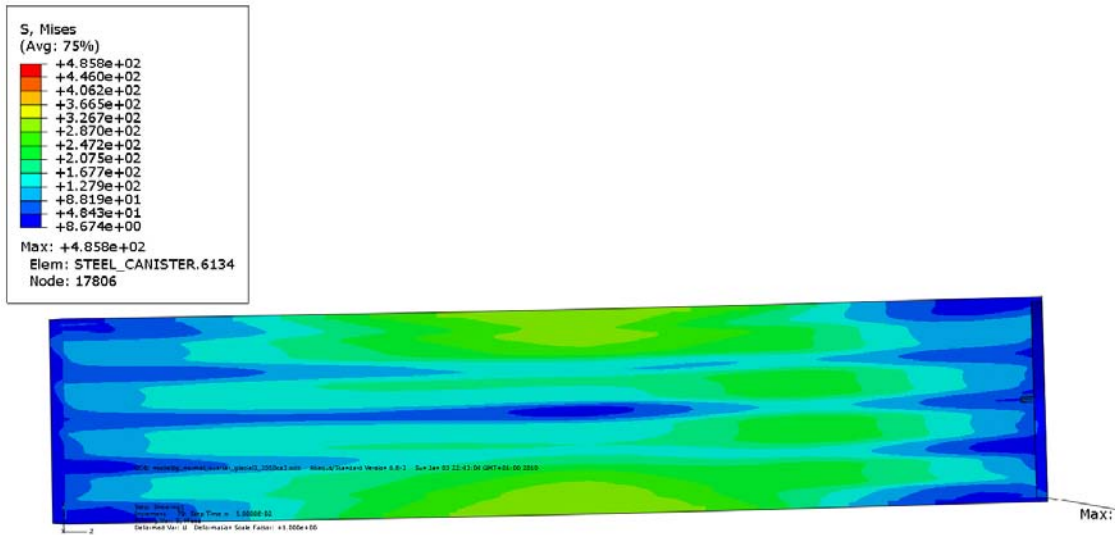


Figure A8-8. Mises stress for insert – 10 cm shearing magnitude.

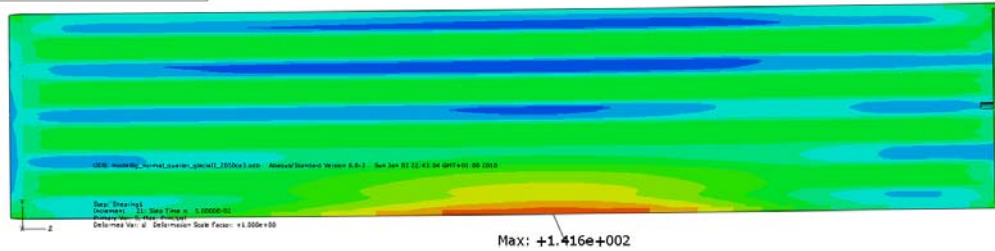
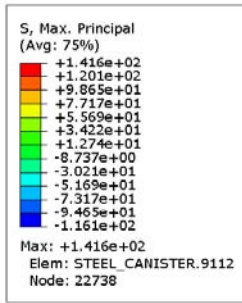


Figure A8-9. Max principal stress for insert – 5 cm shearing magnitude.

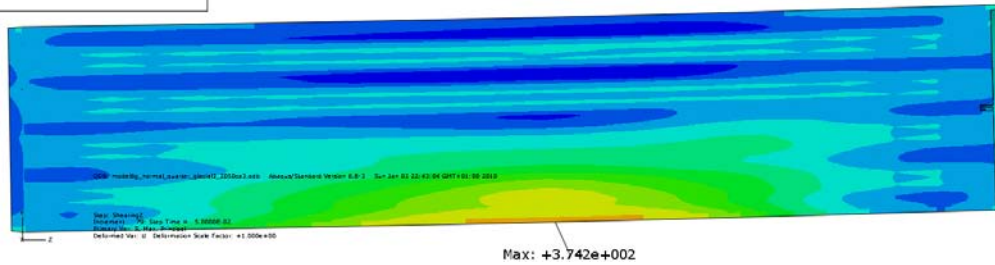
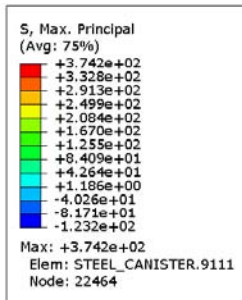


Figure A8-10. Max principal stress for insert – 10 cm shearing magnitude.

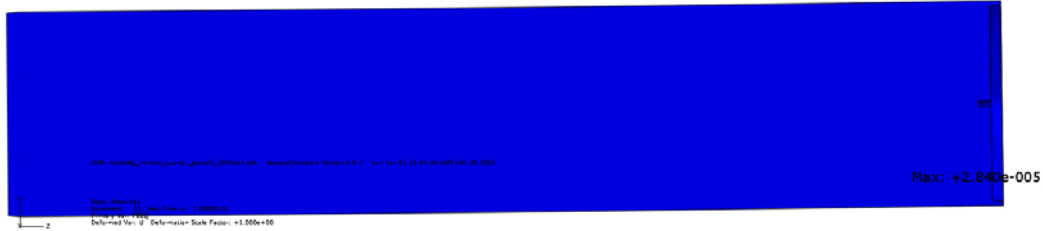
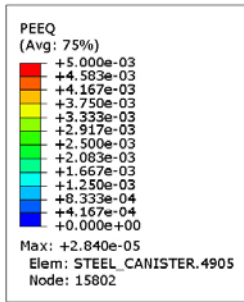


Figure A8-11. Plastic strain (PEEQ) for insert – 5 cm shearing magnitude.

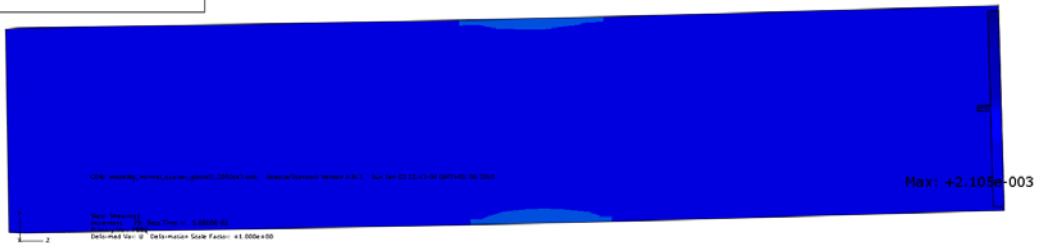
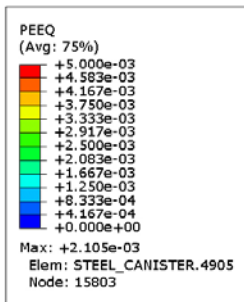


Figure A8-12. Plastic strain (PEEQ) for insert – 10 cm shearing magnitude.



Long term rock shear perpendicular to canister axis 2050ca3  
(quarter point)

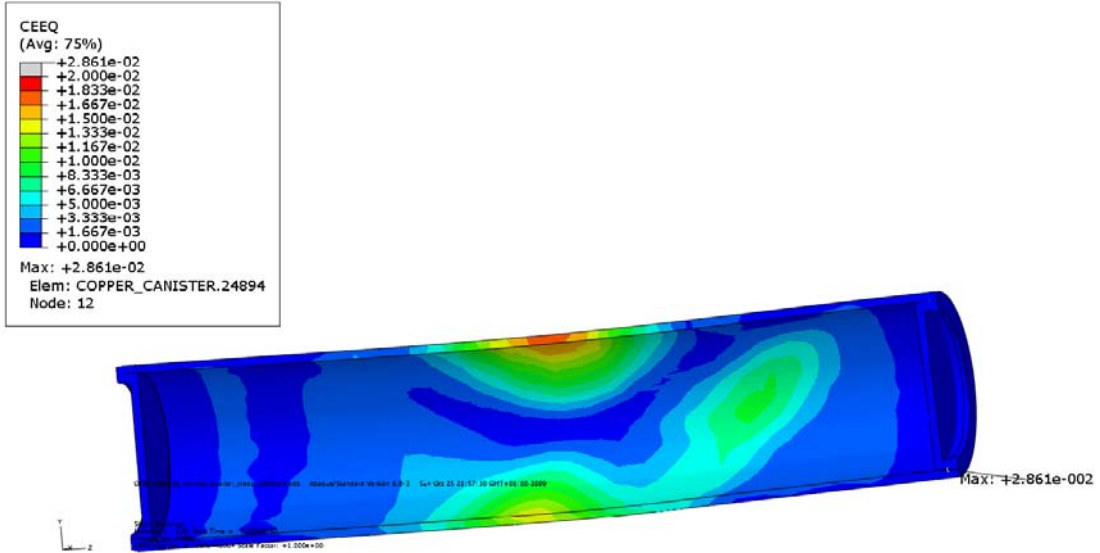


Figure A9-1. Plot of equivalent creep strain (CEEQ) after 10 cm shearing.

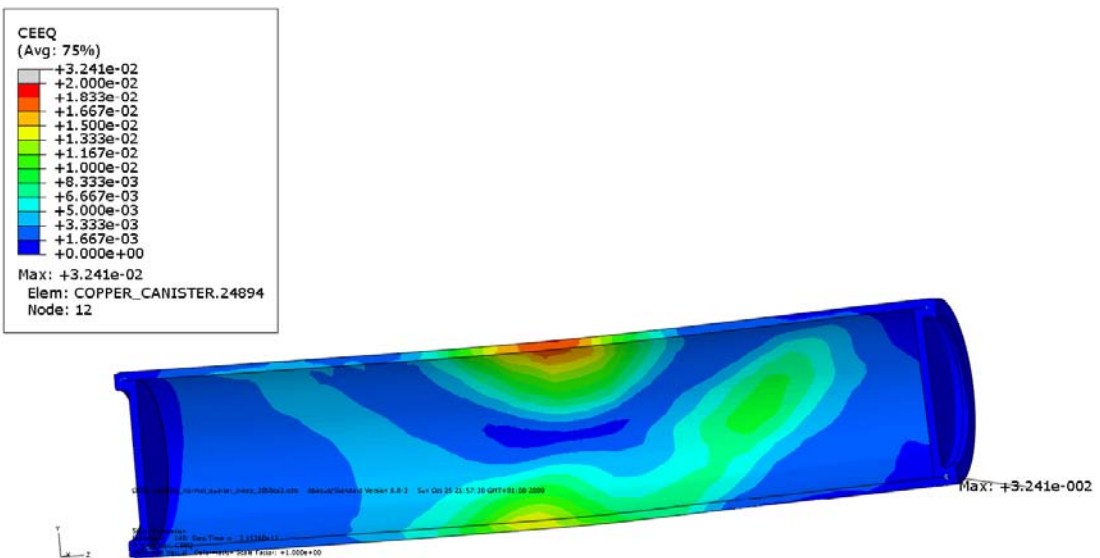
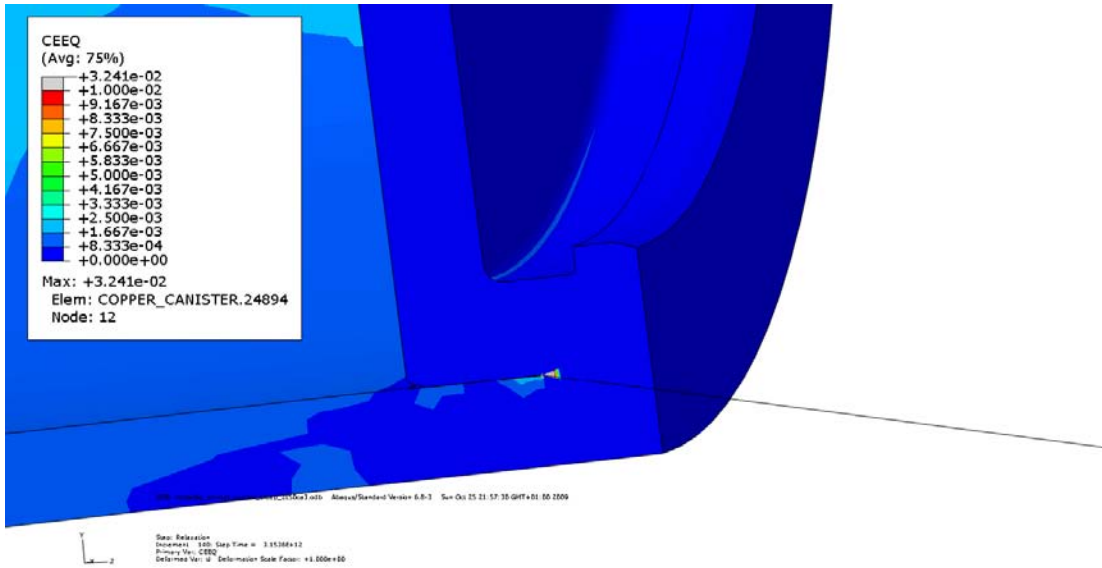
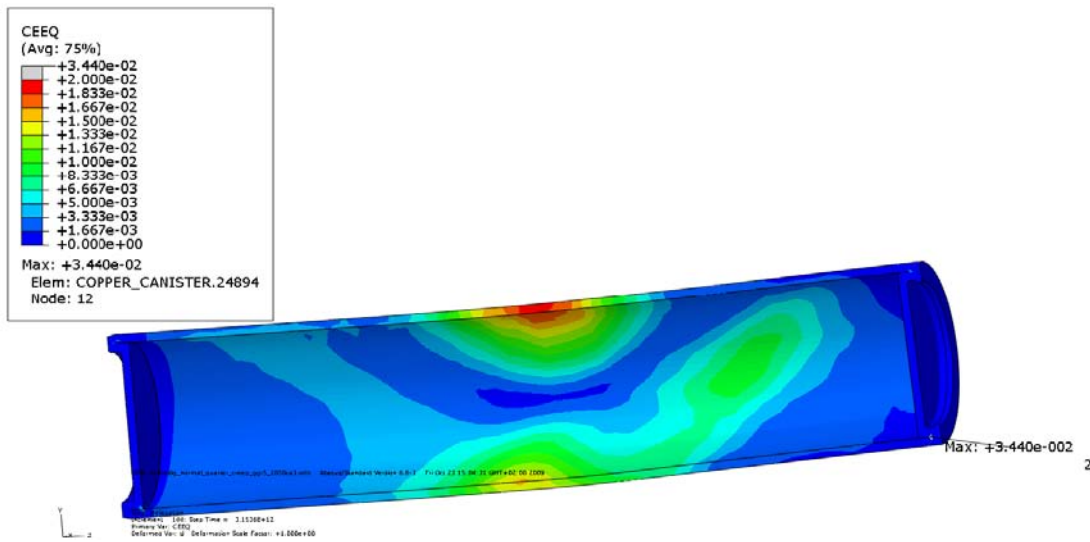


Figure A9-2. Plot of equivalent creep strain (CEEQ) after 10 cm shearing and relaxation for 100,000 years.



*Figure A9-3. Detailed plot of equivalent creep strain (CEEQ) after 10 cm shearing and relaxation for 100,000 years.*



*Figure A9-4. Plot of equivalent creep strain (CEEQ) after 10 cm shearing and relaxation for 100,000 years when the creep strain rate is multiplied by a factor of 5.*

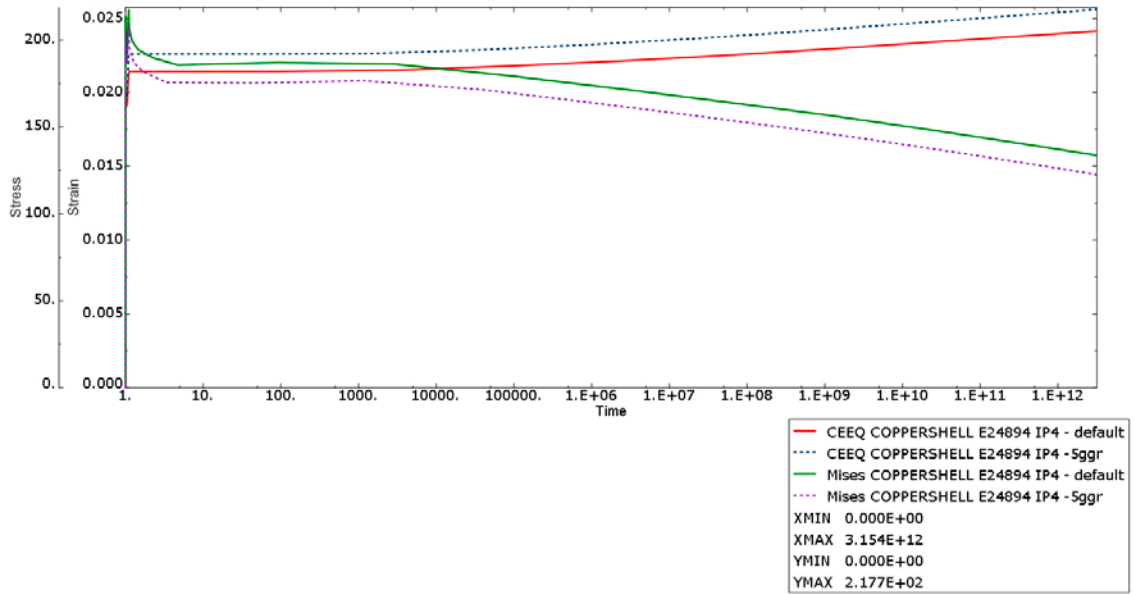


**Figure A9-5.** Equivalent creep strain (CEEQ) and Mises stress versus time. Solid lines when the default parameters are used inside the creep subroutine and dashed when the creep strain rate is magnified by a factor of 5.

### Storage of files

This report is based on the results from a lot of FE-simulations using Abaqus which is a commercial available code and is thus not stored as part of the work. Below is a short description of files used in the project and directories for storage of these. These files are also stored at SKBDoc 1258988.

The files are stored in directories as:

geometry  
 Input-files  
 plots  
 scripts  
 subroutines

### 1 – Plot-files used in the report

Contents in C:\Users\jhd\mappar\skb\kapsel\design\_report\_final\plots

model6g_normal-mesh.png	- Fig 1
model6g_22-mesh.png	- Fig 2
model6g_normal-corner_mesh.png	- Fig 3
model6g_BWR_mesh.png	- Fig 4
model6g_PWR_mesh.png	- Fig 5
model6g_lid_mesh.png	- Fig 6
model6g_copper_mesh.png	- Fig 7
model5_2_2050ca3_nobentonite-bc_xsymm.png	- Fig 11
model5_2_2050ca3_nobentonite-bc_rigid.png	- Fig 12
model6g_glacier_creep_2050ca3-normals.png	- Fig 13
model6g_copper_materials.png	- Fig 14
model6g_copper_output_regions.png	- Fig 15
model6g_normal_half_2050ca3-copper_peek_5cm_detailbot.png	- Fig 16
model6g_normal_half_2050ca3-peek_bot.png	- Fig 16
model6g_normal_half_2050ca3-copper_peek_5cm_detail.png	- Fig 17
model6g_normal_half_2050ca3-peek_top.png	- Fig 17
model6g_normal_half_2050ca3_copper_peek_5cm_detailbot2.png	- Fig 18
model6g_normal_half_2050ca3-peek_bot_fillet.png	- Fig 18
model6g_normal_half_2050ca3_copper_peek_5cm_detailtop2.png	- Fig 19
model6g_normal_half_2050ca3-peek_top_fillet.png	- Fig 19
model6g_normal_quarter_2050ca3-insert_iron-peek_5cm_detail.png	- Fig 20
model6g_normal_half_2050ca3-peek_iron_insert.png	- Fig 20
model6g_normal_half_2050ca3_channel_peek_5cm_detail.png	- Fig 21
model6g_normal_half_2050ca3-peek_steel_channel.png	- Fig 21
model6g_glacier_creep_2050ca3-peek_step1.png	- Fig 22
model6g_glacier_creep_2050ca3-peek_step2.png	- Fig 23
model6g_glacier_creep_2050ca3-insert-mises_step1.png	- Fig 24
model6g_glacier_creep_2050ca3-insert-mises_step2.png	- Fig 25
model6g_glacier_creep_2050ca3-peek_step1.png	- Fig 26
model6g_glacier_creep_2050ca3-peek_step2.png	- Fig 27
model6g_glacier_creep_2050ca3-peek_detail1.png	- Fig 28
model6g_glacier_creep_2050ca3-peek_detail2.png	- Fig 29
model6g_glacier_creep_2050ca3-copper-mises_step1.png	- Fig 30
model6g_glacier_creep_2050ca3-copper-mises_step2.png	- Fig 31
model6g_glacier_creep_2050ca3-peek_and_mises.png	- Fig 32
model6g_glacier_creep_2050ca3-deformed_step1.png	- Fig 33
model6g_glacier_creep_2050ca3-deformed_step2.png	- Fig 34
model6g_glacier_creep_2050ca3-u_mag.png	- Fig 35
model6g_glacier_creep_2050ca3-S33.png	- Fig 36

## Plot files used in the report

### Appendix 1

model6g\_normal\_quarter\_2050ca3- 5cm\_deformed.png  
model6g\_normal\_quarter\_2050ca3- 5cm\_maxPrin\_insert.png  
model6g\_normal\_quarter\_2050ca3- 5cm\_mises\_copper.png  
model6g\_normal\_quarter\_2050ca3- 5cm\_mises\_insert.png  
model6g\_normal\_quarter\_2050ca3- 5cm\_peek\_copper.png  
model6g\_normal\_quarter\_2050ca3- 5cm\_peek\_insert.png  
model6g\_normal\_quarter\_2050ca3-10cm\_deformed.png  
model6g\_normal\_quarter\_2050ca3-10cm\_maxPrin\_insert.png  
model6g\_normal\_quarter\_2050ca3-10cm\_mises\_copper.png  
model6g\_normal\_quarter\_2050ca3-10cm\_mises\_insert.png  
model6g\_normal\_quarter\_2050ca3-10cm\_peek\_copper.png  
model6g\_normal\_quarter\_2050ca3-10cm\_peek\_insert.png  
model6g\_normal\_quarter\_2050ca3-peek\_iron\_insert.png  
model6g\_normal\_quarter\_2050ca3-peek\_steel\_channel.png  
model6g\_normal\_quarter\_2050ca3-s33\_castiron.png  
model6g\_normal\_quarter\_2050ca3-s33\_steelchannels.png

### Appendix 2

model6g\_normal\_half\_2050ca3- 5cm\_deformed.png  
model6g\_normal\_half\_2050ca3- 5cm\_maxPrin\_insert.png  
model6g\_normal\_half\_2050ca3- 5cm\_mises\_copper.png  
model6g\_normal\_half\_2050ca3- 5cm\_mises\_insert.png  
model6g\_normal\_half\_2050ca3- 5cm\_peek\_copper.png  
model6g\_normal\_half\_2050ca3- 5cm\_peek\_insert.png  
model6g\_normal\_half\_2050ca3-10cm\_deformed.png  
model6g\_normal\_half\_2050ca3-10cm\_maxPrin\_insert.png  
model6g\_normal\_half\_2050ca3-10cm\_mises\_copper.png  
model6g\_normal\_half\_2050ca3-10cm\_mises\_insert.png  
model6g\_normal\_half\_2050ca3-10cm\_peek\_copper.png  
model6g\_normal\_half\_2050ca3-10cm\_peek\_insert.png

### Appendix 3

model6g\_22\_quarter\_tension\_2050ca3- 5cm\_deformed.png  
model6g\_22\_quarter\_tension\_2050ca3- 5cm\_maxPrin\_insert.png  
model6g\_22\_quarter\_tension\_2050ca3- 5cm\_mises\_copper.png  
model6g\_22\_quarter\_tension\_2050ca3- 5cm\_mises\_insert.png  
model6g\_22\_quarter\_tension\_2050ca3- 5cm\_peek\_copper.png  
model6g\_22\_quarter\_tension\_2050ca3- 5cm\_peek\_insert.png  
model6g\_22\_quarter\_tension\_2050ca3-10cm\_deformed.png  
model6g\_22\_quarter\_tension\_2050ca3-10cm\_maxPrin\_insert.png  
model6g\_22\_quarter\_tension\_2050ca3-10cm\_mises\_copper.png  
model6g\_22\_quarter\_tension\_2050ca3-10cm\_mises\_insert.png  
model6g\_22\_quarter\_tension\_2050ca3-10cm\_peek\_copper.png  
model6g\_22\_quarter\_tension\_2050ca3-10cm\_peek\_insert.png

## Plot files used in the report

### Appendix 4

model6g\_22\_mid\_tension\_2050ca3-5cm\_deformed.png  
model6g\_22\_mid\_tension\_2050ca3-5cm\_maxPrin\_insert.png  
model6g\_22\_mid\_tension\_2050ca3-5cm\_mises\_copper.png  
model6g\_22\_mid\_tension\_2050ca3-5cm\_mises\_insert.png  
model6g\_22\_mid\_tension\_2050ca3-5cm\_peek\_copper.png  
model6g\_22\_mid\_tension\_2050ca3-5cm\_peek\_insert.png  
model6g\_22\_mid\_tension\_2050ca3-10cm\_deformed.png  
model6g\_22\_mid\_tension\_2050ca3-10cm\_maxPrin\_insert.png  
model6g\_22\_mid\_tension\_2050ca3-10cm\_mises\_copper.png  
model6g\_22\_mid\_tension\_2050ca3-10cm\_mises\_insert.png  
model6g\_22\_mid\_tension\_2050ca3-10cm\_peek\_copper.png  
model6g\_22\_mid\_tension\_2050ca3-10cm\_peek\_insert.png

### Appendix 5

model6g\_full\_hori\_mid\_2050ca3-10cm\_deformed.png  
model6g\_full\_hori\_mid\_2050ca3-10cm\_maxPrin\_insert\_iron.png  
model6g\_full\_hori\_mid\_2050ca3-10cm\_minPrin\_insert\_iron.png  
model6g\_full\_hori\_mid\_2050ca3-10cm\_mises\_copper.png  
model6g\_full\_hori\_mid\_2050ca3-10cm\_mises\_insert.png  
model6g\_full\_hori\_mid\_2050ca3-10cm\_mises\_insert\_iron.png  
model6g\_full\_hori\_mid\_2050ca3-10cm\_peek\_copper.png  
model6g\_full\_hori\_mid\_2050ca3-10cm\_peek\_insert.png  
model6g\_full\_hori\_mid\_2050ca3-10cm\_peek\_insert\_iron.png  
model6g\_full\_hori\_mid\_2050ca3-10cm\_peek\_insert\_tubes.png  
model6g\_full\_hori\_mid\_2050ca3-5cm\_deformed.png  
model6g\_full\_hori\_mid\_2050ca3-5cm\_mises\_copper.png  
model6g\_full\_hori\_mid\_2050ca3-5cm\_mises\_insert.png  
model6g\_full\_hori\_mid\_2050ca3-5cm\_peek\_copper.png  
model6g\_full\_hori\_mid\_2050ca3-5cm\_peek\_insert.png

### Appendix 6

model6g\_full\_hori\_quarter\_2050ca3-10cm\_deformed.png  
model6g\_full\_hori\_quarter\_2050ca3-10cm\_maxPrin\_insert\_iron.png  
model6g\_full\_hori\_quarter\_2050ca3-10cm\_minPrin\_insert\_iron.png  
model6g\_full\_hori\_quarter\_2050ca3-10cm\_mises\_copper.png  
model6g\_full\_hori\_quarter\_2050ca3-10cm\_mises\_insert.png  
model6g\_full\_hori\_quarter\_2050ca3-10cm\_mises\_insert\_iron.png  
model6g\_full\_hori\_quarter\_2050ca3-10cm\_peek\_copper.png  
model6g\_full\_hori\_quarter\_2050ca3-10cm\_peek\_insert.png  
model6g\_full\_hori\_quarter\_2050ca3-10cm\_peek\_insert\_iron.png  
model6g\_full\_hori\_quarter\_2050ca3-10cm\_peek\_insert\_tubes.png  
model6g\_full\_hori\_quarter\_2050ca3-5cm\_deformed.png  
model6g\_full\_hori\_quarter\_2050ca3-5cm\_mises\_copper.png  
model6g\_full\_hori\_quarter\_2050ca3-5cm\_mises\_insert.png  
model6g\_full\_hori\_quarter\_2050ca3-5cm\_peek\_copper.png  
model6g\_full\_hori\_quarter\_2050ca3-5cm\_peek\_insert.png

## Plot files used in the report

### Appendix 7

model6g\_PWR\_normal\_quarter\_2050ca3-5cm\_deformed.png  
model6g\_PWR\_normal\_quarter\_2050ca3-5cm\_maxPrin\_insert.png  
model6g\_PWR\_normal\_quarter\_2050ca3-5cm\_mises\_copper.png  
model6g\_PWR\_normal\_quarter\_2050ca3-5cm\_mises\_insert.png  
model6g\_PWR\_normal\_quarter\_2050ca3-5cm\_peek\_copper.png  
model6g\_PWR\_normal\_quarter\_2050ca3-5cm\_peek\_insert.png  
model6g\_PWR\_normal\_quarter\_2050ca3-10cm\_deformed.png  
model6g\_PWR\_normal\_quarter\_2050ca3-10cm\_maxPrin\_insert.png  
model6g\_PWR\_normal\_quarter\_2050ca3-10cm\_mises\_copper.png  
model6g\_PWR\_normal\_quarter\_2050ca3-10cm\_mises\_insert.png  
model6g\_PWR\_normal\_quarter\_2050ca3-10cm\_peek\_copper.png  
model6g\_PWR\_normal\_quarter\_2050ca3-10cm\_peek\_insert.png

### Appendix 8

model6g\_normal\_quarter\_glacial3\_2050ca3-5cm\_deformed.png  
model6g\_normal\_quarter\_glacial3\_2050ca3-5cm\_maxPrin\_insert.png  
model6g\_normal\_quarter\_glacial3\_2050ca3-5cm\_mises\_copper.png  
model6g\_normal\_quarter\_glacial3\_2050ca3-5cm\_mises\_insert.png  
model6g\_normal\_quarter\_glacial3\_2050ca3-5cm\_peek\_copper.png  
model6g\_normal\_quarter\_glacial3\_2050ca3-5cm\_peek\_insert.png  
model6g\_normal\_quarter\_glacial3\_2050ca3-10cm\_deformed.png  
model6g\_normal\_quarter\_glacial3\_2050ca3-10cm\_maxPrin\_insert.png  
model6g\_normal\_quarter\_glacial3\_2050ca3-10cm\_mises\_copper.png  
model6g\_normal\_quarter\_glacial3\_2050ca3-10cm\_mises\_insert.png  
model6g\_normal\_quarter\_glacial3\_2050ca3-10cm\_peek\_copper.png  
model6g\_normal\_quarter\_glacial3\_2050ca3-10cm\_peek\_insert.png

### Appendix 9

model6g\_normal\_quarter\_creep\_2050ca3-copper\_peek-mises.png  
model6g\_normal\_quarter\_creep\_2050ca3-copper\_peek\_10cm.png  
model6g\_normal\_quarter\_creep\_2050ca3-copper\_peek\_relaxation.png  
model6g\_normal\_quarter\_creep\_2050ca3-copper\_peek\_relaxation\_detail.png  
model6g\_normal\_quarter\_creep\_5ggr\_2050ca3-copper\_peek-relaxation.png

## 2 – Input files used for the simulations

Each analysis is started by abaqus job = input-file (w/o .inp).

Creep analysis requires a user defined subroutine creep and the analysis is started by abaqus job = input-file user = creep\_subroutine.

Files with extension “incl” are referenced by some of the input-files (extension “inp”).

### Contents in C:\Users\jhd\mappar\skb\kapsel\design\_report\_final\Input-files

model6g\_22\_mid\_tension\_1950ca3.inp  
model6g\_22\_mid\_tension\_2000ca3.inp  
model6g\_22\_mid\_tension\_2050ca3.inp  
model6g\_22\_mid\_tension\_creep\_2050ca3.inp - requires user=creep\_rs\_march2009  
model6g\_22\_quarter\_tension\_1950ca3.inp  
model6g\_22\_quarter\_tension\_2000ca3.inp  
model6g\_22\_quarter\_tension\_2050ca3.inp  
model6g\_22\_quarter\_tension\_creep\_2050ca3.inp - requires user=creep\_rs\_march2009  
model6g\_axial\_mid\_2050ca3.inp  
model6g\_axial\_mid\_creep\_2050ca3.inp - requires user=creep\_rs\_march2009  
model6g\_axial\_quarter\_2050ca3.inp  
model6g\_axial\_quarter\_creep\_2050ca3.inp - requires user=creep\_rs\_march2009  
model6g\_full\_hori\_mid\_2050ca3.inp  
model6g\_full\_hori\_mid\_creep\_2050ca3.inp - requires user=creep\_rs\_march2009  
model6g\_full\_hori\_quarter\_2050ca3.inp  
model6g\_full\_hori\_quarter\_creep\_2050ca3.inp - requires user=creep\_rs\_march2009  
model6g\_glacier\_creep2\_2050ca3.inp - requires user=creep\_rs\_march2009  
model6g\_glacier\_creep3\_2050ca3.inp - requires user=creep\_rs\_march2009  
model6g\_glacier\_creep\_2050ca3.inp - requires user=creep\_rs\_march2009  
model6g\_hori\_2050ca3.inp  
model6g\_hori\_quarter\_2050ca3.inp  
model6g\_normal\_half\_2050ca3.inp  
model6g\_normal\_half\_creep\_2050ca3.inp - requires user=creep\_rs\_march2009  
model6g\_normal\_quarter\_1950ca3.inp - global model with density 1950  
model6g\_normal\_quarter\_2000ca3.inp - global model with density 2000  
model6g\_normal\_quarter\_2050ca3.inp - global model with density 2050  
model6g\_normal\_quarter\_creep\_2050ca3.inp - requires user=creep\_rs\_march2009  
model6g\_normal\_quarter\_creep\_glacial1b\_2050ca3.inp - requires user=creep\_rs\_march2009  
model6g\_normal\_quarter\_creep\_glacial1\_2050ca3.inp - requires user=creep\_rs\_march2009  
model6g\_normal\_quarter\_creep\_glacial2\_2050ca3.inp - requires user=creep\_rs\_march2009  
model6g\_normal\_quarter\_creep\_glacial3\_2050ca3.inp - requires user=creep\_rs\_march2009  
model6g\_normal\_quarter\_doublefrict\_2050ca3.inp  
model6g\_normal\_quarter\_glacial1\_2050ca3.inp - hydrostatic pressure  
model6g\_normal\_quarter\_glacial2\_2050ca3.inp - hydrostatic pressure  
model6g\_normal\_quarter\_glacial3\_2050ca3.inp - hydrostatic pressure  
model6g\_normal\_quarter\_halffrict\_2050ca3.inp  
model6g\_normal\_quarter\_pressure1\_2050ca3.inp  
model6g\_normal\_quarter\_pressure1b\_2050ca3.inp - uses load file below  
model6g\_normal\_quarter\_pressure2b\_2050ca3.inp - uses load file below  
model6g\_normal\_quarter\_pressure2\_2050ca3.inp  
model6g\_normal\_quarter\_slow\_2050ca3.inp  
model6g\_normal\_quarter\_steel\_2050ca3.inp  
model6g\_PWR\_normal\_quarter\_2050ca3.inp  
model6g\_PWR\_normal\_quarter\_creep\_2050ca3.inp  
model6g\_thick\_normal\_quarter\_2050ca3.inp  
model6f\_bentonite\_c3d6.incl - degenerated elements when pore pressure elements  
model6g\_material.incl - material definitions used by all input-files  
model6g\_normal\_quarter\_pressure1a\_2050ca3\_cload.incl - load definition used  
model6g\_normal\_quarter\_pressure2a\_2050ca3\_cload.incl



### **3 – Subroutines used in the analyses**

#### **Contents in C:\Users\jhd\mappar\skb\kapsel\design\_report\\_finalsubroutines**

creep\_rs\_march2009.f - default subroutine

creep\_rs\_march2009\_ggr5.f - used to increase creep rate by factor 5

### **4 – Scripts used for post-processing**

Used inside Abaqus/CAE or by abaqus cae startup = script.py after appropriate editing of job-name inside the script-file.

#### **Contents in C:\Users\jhd\mappar\skb\kapsel\design\_report\_final\scripts**

active\_elements.py

model6g\_copper\_material.py

model6g\_displaygroups.py

model6g\_full\_display.py

model6g\_full\_post.py

model6g\_geom.py

model6g\_special.py

model6\_nobentonite.py

model\_2step\_vp1.py

### **5 – Geometry definitions**

#### **Contents in C:\Users\jhd\mappar\skb\kapsel\design\_report\_final\geometry**

model6g.caemodel6g.jnl - Abaqus/CAE-database and journal files

CAD-geometries received from SKB:

IDE-00015-111-CALC\_plan\_top.igs

IDE-00015-111-CALC\_plan\_top.stp

IDE-00015-111-CALC\_plan\_top\_R02.igs

IDE-00015-111-CALC\_plan\_top\_R02.stp

IDE-00015-111-CALC\_R03.stp

PWR\_INSATS\_CALC.stp

Ritningar\_kapsel.pdf

sammanställning svetsad kopparcylinder\_mått från IDE-00015\_sheet 1.pdf

sammanställning svetsad kopparcylinder\_mått från IDE-00015\_sheet 2.pdf

sammanställning svetsad kopparcylinder\_mått från IDE-00015\_sheet 3.pdf

SKB00-IDE-00015-CALC.igs

SKB00-IDE-00015-CALC.stp

SKB00-IDE-00015-CALC\_02.stp

SKB00-IDE-00015-CALC\_old.stp

SKB00-IDE-00015.igs

SKB00-IDE-00015.stp

\_0816123248\_001.pdf

\_0903090815\_001.pdf